Lawrence Berkeley National Laboratory
LBL Dissertations

Title

THE COUPLED CLUSTER SINGLE AND DOUBLE EXCITATION (CCSD) METHOD IN QUANTUM CHEMISTRY: AN EFFICIENT FORMULATION OF THE THEORY AND APPLICATION TO CLOSED SHELL MOLECULAR SYSTEMS

Permalink

https://escholarship.org/uc/item/3k38j9rp

Author

Scheiner, A.C.

Publication Date

1987-08-01

Thesis/dissertation

eScholarship.org Powered by the California Digital Library
University of California

LBL-23923

Lawrence Berkeley Laboratory
UNIVERSITY OF CALIFORNIA

Materials & Chemical Sciences Division

RECEIVED
LAWRENCE
BERKELEY LABORATORY
OCT 19 1987
LIBRARY AND
DOCUMENTS SECTION

The Coupled Cluster Single and Double Excitation (CCSD) Method in Quantum Chemistry: An Efficient Formulation of the Theory and Application to Closed Shell Molecular Systems

A.C. Scheiner
(Ph.D. Thesis)

August 1987

TWO-WEEK LOAN COPY
This is a Library Circulating Copy
which may be borrowed for two weeks.

Prepared for the U.S. Department of Energy under Contract DE-AC03-76SF00098

LBL-23923

DISCLAIMER

This document was prepared as an account of work sponsored by the United States Government. While this document is believed to contain correct information, neither the United States Government nor any agency thereof, nor the Regents of the University of California, nor any of their employees, makes any warranty, express or implied, or assumes any legal responsibility for the accuracy, completeness, or usefulness of any information, apparatus, product, or process disclosed, or represents that its use would not infringe privately owned rights. Reference herein to any specific commercial product, process, or service by its trade name, trademark, manufacturer, or otherwise, does not necessarily constitute or imply its endorsement, recommendation, or favoring by the United States Government or any agency thereof, or the Regents of the University of California. The views and opinions of authors expressed herein do not necessarily state or reflect those of the United States Government or any agency thereof or the Regents of the University of California.

The Coupled Cluster Single and Double Excitation (CCSD) Method in Quantum Chemistry: An Efficient Formulation of the Theory and Application to Closed Shell Molecular Systems

Andrew Carl Scheiner

Ph.D. Thesis

Lawrence Berkeley Laboratory
University of California
Berkeley, California 94720

August 1987

This work was supported by the U.S. Department of Energy under Contract Number DE-AC03-76SF00098.

Table of Contents

Acknowledgements

First, I would like to acknowledge Professor H. F. Schaefer. His sincere enthusiasm for science and personal encouragement have meant a great deal to me throughout my course of studies at Berkeley. Especially appreciated was that this encouragement and interest extended well beyond my scientific work and into my personal goals and interests as well.

I have developed far too many valuable friendships and scientific relationships over the past four years for each of them to be individually listed here. However, I wish to acknowledge those who have been especially helpful to me. First, Drs. Mark Hoffmann, Tim Lee, Julia Rice, and Gustavo Scuseria have each been very good teachers of the science/art known as quantum chemistry. Their help and encouragement have been invaluable to me. Secondly, all the other members of the Schaefer research group from 1983-1987 have each been a source of help, encouragement, information, and humor at one time or another. Finally, my friend Vickie DeRose has shared the good and not-so-good aspects of graduate school and the entire Berkeley/Bay Area experience with me. Because of our friendship the good aspects have been that much more enjoyable and the not-so-good have not seemed so bad.

Last but not least, I should acknoweldge the 1986 Self-Consistent Fielders. Our clutch hitting and sparkling defense made for a championship season that will long be remembered.

Introduction

1.1 Quantum Chemistry: Successes and Outstanding Problems

One of the great successes of physical science in the 20th century has been the development of methods which make possible the application of the basic laws of quantum physics to a wide variety of chemical problems. In particular, the solution of the electronic structure problem has spawned a new and vital field of predictive and quantitative chemistry known as quantum chemistry.[1-3] Today the computational power available to quantum chemists has made possible the reliable prediction of many molecular properties such as equilibrium molecular structure, electrostatic potential, electronic, photoelectric, and vibrational spectra along with thermochemical data. Such predictions can serve as (1) an independent source of chemical information in cases where experimental studies are rendered difficult such as identification of reaction intermediates and transition states and (2) a guide to the interpretation of experimental results in cases where these results are ambiguous.

The electronic structure problem is compactly expressed by the electronic Schrödinger equation, Eq. (1.1).

$$\hat{H}|\Psi\rangle = E|\Psi\rangle \tag{1.1}$$

Here $\hat{H}$ is the time-independent, non-relativistic,[4] electronic Hamiltonian operator. In atomic units this operator is written

$$\hat{H} = -\frac{1}{2}\sum_i \nabla_i^2 + \sum_{i<j} \frac{1}{|\mathbf{r}_i - \mathbf{r}_j|} - \sum_{i,A} \frac{Z_A}{|\mathbf{r}_i - \mathbf{R}_A|} . \tag{1.2}$$

The electronic wavefunction $|\Psi\rangle$ is an explicit function of the spatial and spin coordinates of each of the electrons, $\mathbf{r}_i$ and σ_i, and depends parametrically (by application

of the Born-Oppenheimer separation of nuclear and electronic coordinates)[5,6] on the spatial coordinates of each of the nuclear centers, $\mathbf{R}_A$.

By proceeding from the general understanding expressed by the electronic Schrödinger equation to the specific application of this understanding, quantum chemistry has been able to address and provide quantitative predictions for particular questions of chemical interest, and, perhaps of even greater significance, the systematic analysis and review of the body of quantum chemical results has increased our general qualitative understanding in broad areas of chemistry.

In addressing the many fermion problem expressed by Eq. (1.1), we will take as our independent-particle reference wavefunction, $|\Psi_0\rangle$, a self-consistent field (SCF) or Hartree-Fock (HF) wavefunction expressed as a Slater determinant of orthonormal one-electron orbitals, ψ_I. Each ψ_I is a function of the space and spin coordinates of a single electron with the index I labeling these spin-orbitals. (The spatial and spin coordinates of electron i will be compactly expressed as $\mathbf{x}_i \equiv \mathbf{r}_i \bigcup \sigma_i$).

$$|\Psi_0\rangle = \hat{A}\psi_1(\mathbf{x}_1)\psi_2(\mathbf{x}_2) \cdots \psi_n(\mathbf{x}_n) \tag{1.3}$$

In Eq. (1.3) $\hat{A}$ represents the antisymmetrizing operator appropriate for an n fermion system. Following Roothan,[7] each of these one-electron spin orbitals is constructed as a linear expansion of basis functions, ϕ_μ,

$$\psi_I(\mathbf{x}) = \sum_\mu c_{\mu I}\, \phi_\mu(\mathbf{x}) \tag{1.4}$$

and the independent-particle reference is variationally optimized with respect to the expansion coefficients, $c_{\mu I}$, until a self-consistent solution is reached.

Having defined the independent-particle reference, the many-electron wavefunction $|\Psi\rangle$ is constructed as an expansion in terms of this reference. This expansion

may be a linear expansion (configuration interaction),[8] an exponential expansion (coupled cluster),[9] a perturbative expansion (many-body perturbation theory),[9] or other similar construction.[10]

Given this approach to the electronic structure problem, one must address three practical limitations of *ab initio* quantum chemistry which are the focus of ongoing research.

[1] The limitation to an incomplete one-electron basis, $\phi_\mu(x)$.

[2] The limitation to an incomplete expansion in the many-electron space.

[3] The number of nuclear degrees of freedom in large molecular systems.

While much research has been focused on the formulation of well described (in the sense of an accurate expansion of Eq. (1.4)) yet practical-sized basis sets,[11–17] in terms of absolute energies, the limitation to an incomplete basis generally represents the largest source of error in standard *ab initio* theory. While it is often possible to saturate the basis set in the Hartree-Fock space, convergence of the total energy with respect to basis set within a many-electron scheme requires massive one-particle bases.[18] On the other hand, for most chemical systems, equilibrium molecular structures, vibrational spectra, and relative energies can be accurately predicted using moderate-sized basis sets which are able to treat a variety of chemical species and bond types consistently.[19] For accurate theoretical predictions of electrical moments and for properties of systems with diffuse electronic distributions (e.g. anions and highly excited electronic states) however, larger basis sets are generally required.[19,20]

Several alternatives to the one-electron basis set approach have been proposed, however, none has yet proven to be of general utility. Numerical Hartree-Fock calculations have been carried out for small diatomic systems.[21] Also, with the goal of

reducing the number of basis functions required for heavy nuclei, effective potentials have been substituted for the *ab initio* treatment of the inner core electrons.[22–26] Two other methods which are currently of interest are (1) the use of Gaussian geminals which directly include many-electron effects within the basis set[27] and (2) floating orbital methods in which the basis functions are not fixed at the atomic centers.[28]

Regarding the many-electron (or electron correlation) problem, much study has been directed at the development of methods which accurately and consistently approximate the complete many-electron expansion while remaining tractable and efficient for a wide range of chemical systems.[8–10,29–45] The areas where electron correlation has been found to be most important are for the quantitative predictions of relative energies at different points on a potential surface and relative energies of one electronic state vs another.[46,47] Additionally, electron correlation is generally necessary for quantitative predictions of electrical moments and the prediction of equilibrium structures and vibrational spectra of excited electronic states.[19]

The desirable features of an approximate many-electron theory or "theoretical model chemistry" have been concisely presented by Pople.[48]

[1] It should be well defined, leading to a unique energy for any nuclear configuration and a continuous potential surface.

[2] It should be size-extensive, so that the energy scales properly with the size of the system.

[2'] It should be able to correctly separate a molecule into its fragments.

[3] It should be exact (equivalent to a complete expansion in the many-electron space) when applied to a two-electron system.

[4] It should be efficient, so that application is possible for large basis sets.

[5] It should be accurate enough to give an adequate approximation to the exact result.

[6] It should be variational, so that the computed energy is an upper bound to the correct energy.

A major topic of discussion herein will be the problem of electron correlation, and in particular, Chapter 2 details the development of an efficient formulation of coupled cluster theory for closed-shell molecular systems along with several molecular applications. Chapter 3 then describes a detailed study of the *s*–tetrazine molecule for which the coupled cluster approach to electron correlation resolves a long standing question regarding the photochemical dissociation of this molecule.

The third limitation mentioned above, that of many nuclear degrees of freeedom, arises from the application of the Born-Oppenheimer approximation to molecular systems. Within this approximation scheme, the electronic energy becomes a parametric function of the $3N_A' - 6$ nuclear degrees of freedom, where N_A represents the total number of nuclear centers being considered. In order to describe the potential in which these nuclei move, and, in particular, to locate critical points and to describe the energetics of chemical reactions, many points on this multidimensional energy surface must be searched. However, with the efficient implementation of analytic energy derivative methods for both Hartree-Fock and many-body energies, the characterization of these potential surfaces has become a much less arduous task. Recently, two detailed accounts of the advances in analytical derivative theories have been presented by Gaw & Handy and by Schaefer & Yamaguchi.[49] The latter authors summarize the dramatic impact of such advances on the field of quantum

chemistry:

> Even more important than enhancements in computer technology has been the theoretical development of analytical derivative methods. It may be realistically stated that such analytic derivative methods provide a new dimension to molecular electronic structure theory.

For this reason, it is of the utmost importance to develop efficient derivative methods for many-electron wavefunctions, and in Chapter 4 a tractable gradient theory for the coupled cluster energy is presented along with initial results.

1.2 The Electron Correlation Problem

As noted above, one of the principle topics of study in the present work is the many-electron or electron correlation problem. Below, the configuration interaction and coupled cluster theories of electron correlation are introduced and compared. First, however, it is timely here to define a useful quantity, the electron correlation energy ΔE. ΔE is defined as the difference between the exact energy (for a given one-electron basis) and the energy obtained from the independent-electron reference. Thus $\Delta E = E - E_{HF}$ using a Hartree-Fock reference.

1.2.1 The Configuration Interaction (CI) Approach

For a given one-particle basis set, the exact, full CI wavefunction $|\Psi\rangle$ can be written as the complete expansion of independent-particle states $|\Psi_\lambda\rangle$.

$$|\Psi\rangle = \sum_{\lambda} C_\lambda |\Psi_\lambda\rangle \tag{1.5}$$

Each of these independent-particle states may be expressed relative to the reference wavefunction $|\Psi_0\rangle$ so that Eq. (1.5) may be rewritten as

$$|\Psi\rangle = \left(C_0 + \sum_{I,A} C_I^A \, A^\dagger I + \sum_{\substack{I<J \\ A<B}} C_{IJ}^{AB} \, A^\dagger I B^\dagger J + \cdots \right) |\Psi_0\rangle \tag{1.6}$$

where $P^\dagger$ (P) represents the standard creation (annihilation) operator for spin-orbital ψ_P as expressed in the language of second quantization,[50] and the $C^{'s}$ are the CI expansion coefficients. Note that in Eq. (1.6) and all that follow, the indices I,J,K,L are reserved for orbitals occupied in the reference; A,B,C,D for unoccupied orbitals; while P,Q,R,S are used for general orbital indices.

From the action of the creation and annihilation operators on the independent-particle reference, excitations relative to this reference are defined

$$A^\dagger I|\Psi_0\rangle = |\Psi_I^A\rangle \qquad A^\dagger I B^\dagger J|\Psi_0\rangle = |\Psi_{IJ}^{AB}\rangle \qquad \cdots \tag{1.7}$$

where $|\Psi_I^A\rangle$ represents the Hartree-Fock determinant with spin-orbital I replaced by spin orbital A, and similarly for the higher excitations. We thus refer to C_I^A, C_{IJ}^{AB}, $\cdots$ as the CI singles, doubles, $\cdots$ coefficients.

The CI energy can be evaluated by diagonalization of the CI Hamiltonian matrix (in the basis of independent-particle determinants)

$$E = \frac{\langle\Psi|\hat{H}|\Psi\rangle}{\langle\Psi|\Psi\rangle} \tag{1.8}$$

thus variationally optimizing the energy with respect to the CI coefficients.

1.2.2 The Coupled Cluster (CC) Approach

An alternative, yet equivalent, expression for the exact many-electron wavefunction is based on the exponential ansatz

$$|\Psi\rangle = e^{\hat{T}}|\Psi_0\rangle \tag{1.9}$$

where the cluster operator $\hat{T}$ is defined as

$$\hat{T} = \hat{T}_1 + \hat{T}_2 + \hat{T}_3 + \cdots \tag{1.10}$$

and

$$\hat{T}_1 = \sum_{I,A} t_I^A \, A^\dagger I \qquad \hat{T}_2 = \sum_{\substack{I<J \\ A<B}} t_{IJ}^{AB} \, A^\dagger I B^\dagger J \qquad \cdots \tag{1.11}$$

This cluster expansion of the wavefunction was first introduced in the context of nuclear physics by Coester and Kümmel in 1958-1961.[51] Subsequent to this, Cizek and Paldus formulated a coupled cluster theory for atomic and molecular physics.[32,52–54] Since these early developments, the CC method has been applied to a variety of problems in physics, and in a recent review of the method, Bishop and Kümmel state[55]

> Clearly the coupled cluster method works for systems of both bosons and fermions quite regardless of the type and range of interaction, and yields high precision results for the ground state as well as low-energy excited states. We regard it therefore as the "universal" method of theoretical many body physics.

The cluster operator as defined by Eq. (1.10) is a sum of one, two, three, $\cdots$ -body terms, and each of these is defined by Eq. (1.11). Thus t_I^A, t_{IJ}^{AB}, $\cdots$ are referred to as the one, two, $\cdots$ -body cluster coefficients.

1.2.3 The Correspondence between CI and CC

Expanding the exponential of Eq. (1.9) and using Eq. (1.10), one may write

$$|\Psi\rangle = \left\{ 1 + \hat{T}_1 + (\frac{1}{2!}\hat{T}_1^2 + \hat{T}_2) + (\frac{1}{3!}\hat{T}_1^3 + \hat{T}_2\hat{T}_1 + \hat{T}_3) \right. \tag{1.12}$$

$$\left. + (\frac{1}{4!}\hat{T}_1^4 + \frac{1}{2!}\hat{T}_2^2 + \frac{1}{2!}\hat{T}_2\hat{T}_1^2 + \hat{T}_3\hat{T}_1 + \hat{T}_4) + \cdots \right\} |\Psi_0\rangle$$

Comparing this to the equivalent CI description

$$|\Psi\rangle = \left\{ \hat{C}_0 + \hat{C}_1 + \hat{C}_2 + \hat{C}_3 + \hat{C}_4 + \cdots \right\} |\Psi_0\rangle \tag{1.13}$$

where from Eq. (1.6)

$$\hat{C}_0 = C_0 \qquad \hat{C}_1 = \sum_{I,A} C_I^A \, A^\dagger I \qquad \hat{C}_2 = \sum_{\substack{I<J \\ A<B}} C_{IJ}^{AB} A^\dagger I B^\dagger J \qquad \cdots \tag{1.14}$$

a direct correspondence between the full CI and the complete cluster expansion becomes evident. The singly excited determinants generated by $\hat{C}_1$ correspond simply to the action of the one-body cluster operator on the reference determinant. The doubly excited configurations generated by $\hat{C}_2$ correspond to the action of the two-body cluster operator plus the product of two one-body terms. Similarly triply, quadruply, $\cdots$ excited determinants contain a contribution from the three, four, $\cdots$ -body cluster operator (the so-called "connected" terms in the cluster expansion) along with products of lower order terms (the so-called "disconnected" terms). The exact relationship between the cluster coefficients and the CI coefficients after rescaling the intermediate normalized cluster expansion by C_0 is

$$\frac{C_I^A}{C_0} = t_I^A \tag{1.15}$$

$$\frac{C_{IJ}^{AB}}{C_0} = t_{IJ}^{AB} + \frac{1}{2} t_I^A t_J^B \tag{1.16}$$

$$\frac{C_{IJK}^{ABC}}{C_0} = t_{IJK}^{ABC} + t_{IJ}^{AB} t_K^C + \frac{1}{6} t_I^A t_J^B t_K^C \tag{1.17}$$

$$\frac{C_{IJKL}^{ABCD}}{C_0} = t_{IJKL}^{ABCD} + t_{IJK}^{ABC} t_L^D + \frac{1}{2} t_{IJ}^{AB} t_{KL}^{CD} + \frac{1}{2} t_{IJ}^{AB} t_K^C t_L^D + \frac{1}{24} t_I^A t_J^B t_K^C t_L^D \tag{1.18}$$

and so on. Note that this relationship holds only for a complete expansion in the many-electron space. There is no such correspondence for the coefficients of a truncated CI wavefunction with those of a truncated CC wavefunction.

1.3 Truncation of the Many-Electron Expansion

In order to satisfy feature [4] of Pople's theoretical model chemistry, this complete expansion in the many-electron space must be truncated; however, in so doing, one (or more) of the other desirable features must be sacrificed. Truncated CI, which retains the property of variationality (feature [6]) but is no longer size-extensive (feature [2]), has been used extensively, and the method has been well studied and optimized.[8,33,37,38,43] More recently, truncated coupled cluster theory, which yields an energy that is no longer guaranteed to be an upper bound to the full CI result but which is size-extensive, has received much attention as a means to accurately determine the electron correlation energy in molecular systems.[9,42,45,56–80]

1.3.1 Size-Extensivity

The property of size-extensivity, which is retained at all levels of truncation within the exponential ansatz of coupled cluster theory but sacrificed by truncation of the linear CI expansion, is of great importance if a method is to be applied to a wide variety of molecular systems and at many points on a given electronic energy hypersurface. Simply stated, the electronic energy predicted by a method which is size-extensive scales properly as the size of the system (where size refers to the number of elecrons being correlated).[67,81,82] A desirable feature of this property is that the electronic energy of non-interacting fragments A and B is (correctly) given as $E_A + E_B$, and thus size-extensive methods are clearly preferred for a study of bond breaking/bond forming processes. It should be noted that in order for a method to properly describe such a fragmentation process, the wavefunction must properly dissociate (feature [2′] of the theoretical model chemistry). This is an additional

requirement on the wavefunction, and, in general, a spin-unrestricted or multideterminant reference must be employed to satisfy [2']. A wavefunction which is both size-extensive and dissociates properly is termed size-consistent.[67,82] A second clear advantage is that heats of formation predicted by size-extensive methods are additive (as are experimental values), and thus, the heat of formation of an aggregate "super molecule" can be determined as the sum of its parts. Conversely, non size-extensive methods would require a super molecule calculation to provide this quantity. Ahlrichs has studied just this and has found non-additivity errors for CI truncated at $\hat{C} = \hat{C}_0 + \hat{C}_2$ of ≈ 9 kcal/mole for $2BH_3 \rightarrow B_2H_6$ [83] and ≈ 15 kcal/mole for $CH_3F + F^- \rightarrow CH_3F_2^-$. [84]

An additional conspicuous advantage of coupled cluster when compared to truncated CI is that as the number of electrons increases, truncated CI methods account for an increasingly smaller fraction of the electron correlation energy. Only approximation schemes which possess this property of proper scaling are suitable for application to large molecules such as those of biological interest. This situation is illustrated in Figure 1.

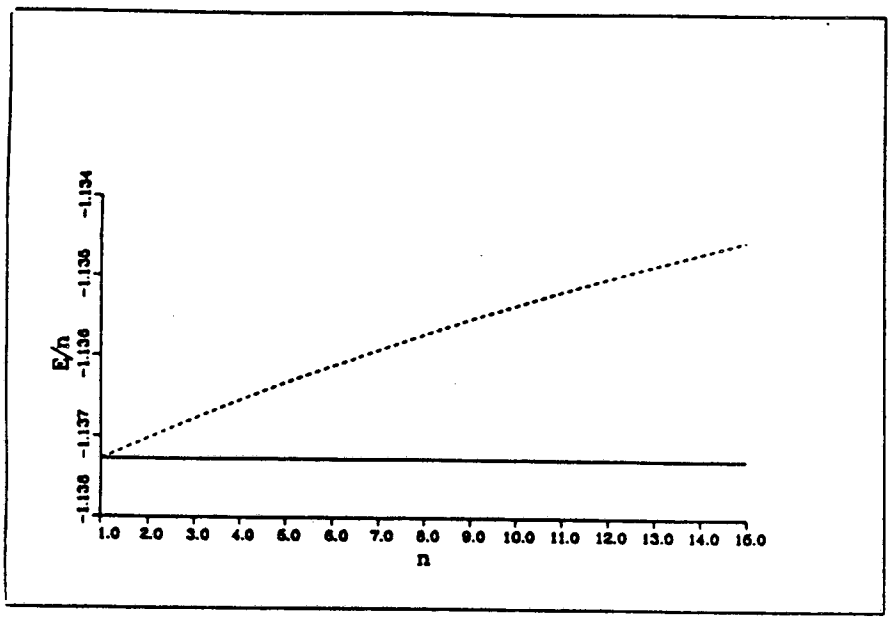

Figure 1: Comparison of the CISD (dashed line) and CCSD (solid line) (= full CI) electron correlation energies for a system of non-interacting H_2 molecules. The energy per molecule ($\frac{E}{n}$) is plotted as a function of the number of H_2 molecules being addressed (n).

Here the electronic energies for a lattice of non-interacting H_2 molecules are compared for two different many-electron methods. The energy per molecule ($\frac{E}{n}$) is plotted as a function of the number of non-interacting molecules being considered (n). The results using a coupled cluster wavefunction truncated at $\hat{T}_1 + \hat{T}_2$ (CCSD), which, for this system, gives the exact full CI result, are given by the horizontal line. Additionally, the $\frac{E}{n}$ vs n curve for CI truncated at $\hat{C}_1 + \hat{C}_2$ (CISD) is illustrated.

Before proceeding with a discussion of this illustration, note [from the comparison of Eqs. (1.12) and (1.13)] that a truncated CC expansion contains disconnected terms corresponding to all levels of excitation for a given molecular system. For example, truncation of the cluster expansion at CCSD results in a many-electron wavefunction of the form

$$|\Psi_{CCSD}\rangle = \left\{1 + \hat{T}_1 + (\frac{1}{2!}\hat{T}_1^2 + \hat{T}_2) + (\frac{1}{3!}\hat{T}_1^3 + \hat{T}_2\hat{T}_1)\right. \tag{1.19}$$

$$\left. + (\frac{1}{4!}\hat{T}_1^4 + \frac{1}{2!}\hat{T}_2^2 + \frac{1}{2!}\hat{T}_2\hat{T}_1^2) + \cdots \right\} |\Psi_0\rangle.$$

The disconnected excitations are able to fully correlate this lattice of non-interacting electron pairs (Figure 1) for arbitrary n.

Returning to Figure 1, first note that both methods satisfy feature [3] of the theoretical model chemistry in that they are exact for a system of two electrons, $n = 1$. The non size-extensive CI method accounts for an increasingly smaller fraction of the correlation energy as n increases. In fact as $n \rightarrow \infty$ the correlation energy per electron pair accounted for by CISD (and all truncated CI methods) goes to zero ($E_{CI} \rightarrow E_{Hartree-Fock}$). This is a particularly simple example, but the same result will hold for an arbitrary system of interacting electrons. That is, the correlation energy accounted for by a truncated CI method will go to zero as the number of electrons becomes large.

An interesting result of the above discussion is that while higher excitation CI methods which additionally include, for example, $\hat{C}_4$ or $\hat{C}_3 + \hat{C}_4$ (CISDQ, CISDTQ, respectively) may be more accurate than CCSD for a moderate number of electrons, as one applies electron correlation methods to increasingly larger systems, a greater fraction of the correlation energy will eventually be accounted for by CCSD than by such higher excitation CI methods. More precisely, the errors associated with the *complete* neglect of the contribution of determinants above a certain level of CI truncation will eventually become greater than the errors associated with the *partial* neglect of contributions to determinants which are at least triply excited.

1.3.2 Variationality

As mentioned above, due to the non-variational character of the truncated CC method, the total electronic energy of any state predicted by this method is no longer guaranteed to be an upper bound to the true electronic energy of this state. In this sense CI methods are preferable to CC methods. However, in practice one is generally not interested in total electronic energies of chemical systems, but in relative energies of one state and/or structure vs another; these differences of total energies are of course non-variational irrespective of the method used. In any event, according to recent studies one can expect CCSD and approximate CCSDT ($\hat{T} = \hat{T}_1 + \hat{T}_2 + \hat{T}_3$) calculations to predict a major portion (96-102%) of the correlation energy with a given one-particle basis.[82] Assuming these methods achieve such accuracy in all cases, then non-variationality should not be a serious liability of truncated CC theory. The one foreseeable problem with a non-variational method such as truncated coupled cluster is that, unlike truncated CI, it is not guaranteed that one is improving the description of the chemical system by including more terms in the expansion. In other words, there may be pathological cases where the CC expansion does not converge smoothly, and that, for example, a particular CCSD energy may be closer to the true energy than the analogous CCSDT energy.

1.3.3 Accuracy vs Efficiency

Clearly as one makes more drastic approximations to the exact many-electron wavefunction, one gains with regard to feature [4] of the theoretical model chemistry while sacrificing accuracy, feature [5]. Therefore, one would like to find an approximation scheme which takes the middle ground and supplies both efficiency and accuracy. With the present state of computational technology, methods which scale as

N^6, where N represents the number of basis functions in the one-particle expansion, are tractable for systems where N is as large as 150. At present this is considered "large" in the sense of feature [4]. Methods which scale as N^7 are not yet as widely applicable but are becoming increasingly routine.[41,45]

With regards to this N^6 scaling limit, both the CI expansion and the cluster expansion must be truncated at singles and doubles, CISD and CCSD. As discussed above, CCSD will, in general, be a more accurate method than CISD due to the higher order, disconnected terms included in the cluster expansion. In fact, it is believed that, with the contribution of $\frac{1}{2}\hat{T}_2^2$, the CCSD wavefunction includes the major contribution due to $\hat{C}_4$. Complete treatment of these quadruples through a CI scheme requires work which is proportional to N^{10}, and thus full quadruples CI is limited in application to only the simplest of molecular systems.

Several questions regarding the trade off of accuracy vs efficiency have been addressed in the present study. First of all, what are the additional computational requirements for CCSD vs CISD? More precisely, since it is theoretically known that CCSD scales as $\alpha_{CCSD}N^6$ and CISD as $\alpha_{CISD}N^6$ with $\alpha_{CCSD} > \alpha_{CISD}$, what is the $\frac{\alpha_{CCSD}}{\alpha_{CISD}}$ ratio in practice, and on what parameters does this ratio depend? Secondly, how do the additional terms included in the CCSD expansion (relative to truncated CI) translate into chemical energetics, structures, and spectroscopic properties, and how do such results compare to CI? Eventually, one would like to investigate the size-extensivity errors associated with higher excitation CI methods for several molecular systems, and perhaps determine the point at which CCSD becomes a better approximation to the full CI energy than CISDTQ, however, at present the CISDTQ calculations needed-to-investigate this question remain prohibitive. Finally,

it is of interest to compare the CCSD energetic predictions to those predicted by Davidson corrected CISD,[85] denoted herein as CISD(+Q). The Davidson correction, which is defined as

$$E_{\mathrm{CISD(+Q)}} = E_{\mathrm{CISD}} + E_{\mathrm{CISD}}(1 - C_0^2)\,, \tag{1.20}$$

was formulated as an approximate, inexpensive scheme to account for the disconnected quadruple excitations which are rigorously treated by CCSD.

An Efficient Formulation of the Closed-Shell CCSD Equations

2.1 Derivation of CCSD Equations

As outlined in 1.2.2, the coupled cluster method is based on the exponential ansatz, i.e. the exact wavefunction may be written as

$$|\Psi\rangle = e^{\hat{T}}|\Psi_0\rangle. \tag{2.1}$$

The exact wavefunction is approximated to the CCSD wavefunction by truncating the cluster operator at $\hat{T}_1 + \hat{T}_2$.

$$|\Psi\rangle \approx |\Psi_{CCSD}\rangle = e^{(\hat{T}_1 + \hat{T}_2)}|\Psi_0\rangle \tag{2.2}$$

Substituting Eq. (2.1) into the electronic Schrödinger equation, the electronic structure problem may be expressed as

$$\hat{H}e^{(\hat{T}_1 + \hat{T}_2)}|\Psi_0\rangle = E_{CCSD}e^{(\hat{T}_1 + \hat{T}_2)}|\Psi_0\rangle. \tag{2.3}$$

The Hamiltonian is most conveniently expressed in normal product, second-quantized form

$$\hat{H} = \hat{H}_2 + \hat{H}_1 + \hat{H}_0 \tag{2.4}$$

with

$$\hat{H}_2 = \frac{1}{4}\sum_{\substack{P,Q \\ R,S}} \langle PQ||RS\rangle\, N\,[P^\dagger Q^\dagger SR]\,, \tag{2.5}$$

$$\hat{H}_1 = \sum_{P,Q} f_Q^P\, N\,[P^\dagger Q]\,, \tag{2.6}$$

and

$$\hat{H}_0 = E_0 = \sum_I f_I^I \equiv \sum_I h_{II} + \frac{1}{2}\sum_{IJ}\langle IJ||IJ\rangle. \tag{2.7}$$

Here the standard notation for one- and two-electron integrals is used,

$$\langle PQ||RS\rangle \equiv v_{RS}^{PQ} - v_{SR}^{PQ} \tag{2.8}$$

$$v_{RS}^{PQ} \equiv \int d\mathbf{x}_1\, d\mathbf{x}_2\, \psi_P^*(\mathbf{x}_1)\, \psi_Q^*(\mathbf{x}_2)\, \frac{1}{|\mathbf{r}_1 - \mathbf{r}_2|}\, \psi_R(\mathbf{x}_1)\, \psi_S(\mathbf{x}_2) \tag{2.9}$$

$$h_{PQ} \equiv \int d\mathbf{x}_1\, \psi_P^*(\mathbf{x}_1) \left\{ -\frac{1}{2}\nabla_1^2 - \sum_A \frac{Z_A}{|\mathbf{r}_1 - \mathbf{R}_A|} \right\} \psi_Q(\mathbf{x}_1)\,, \tag{2.10}$$

and the Fock matrix, f_Q^P is defined by Eq. (2.7). The notation $N[\ \cdots\ ]$ is used to indicate that the creation/annihilation operators enclosed within the brackets are in normal product order.[32,52–54]

Next the Schrödinger equation is renormalized by subtracting the reference energy from both sides of Eq. (2.3) as follows. From the definition of the correlation energy,

$$E_{\mathrm{CCSD}} = \Delta E_{\mathrm{CCSD}} + \hat{H}_0 \tag{2.11}$$

and Eq. (2.4), one may write

$$(\hat{H}_2 + \hat{H}_1 + \hat{H}_0)\, e^{(\hat{T}_1 + \hat{T}_2)}|\Psi_0\rangle = (\Delta E_{\mathrm{CCSD}} + \hat{H}_0) e^{(\hat{T}_1 + \hat{T}_2)}|\Psi_0\rangle\,. \tag{2.12}$$

Thus, the renormalized Schrödinger equation becomes

$$\hat{H}_N\, e^{(\hat{T}_1 + \hat{T}_2)}|\Psi_0\rangle = \Delta E_{\mathrm{CCSD}}\, e^{(\hat{T}_1 + \hat{T}_2)}|\Psi_0\rangle \tag{2.13}$$

where

$$\hat{H}_N \equiv \hat{H}_1 + \hat{H}_2\,. \tag{2.14}$$

Left-multiplying by $e^{-(\hat{T}_1 + \hat{T}_2)}$ yields

$$e^{-(\hat{T}_1 + \hat{T}_2)}\, \hat{H}_N\, e^{(\hat{T}_1 + \hat{T}_2)}\, |\Psi_0\rangle = \Delta E_{\mathrm{CCSD}}|\Psi_0\rangle\,. \tag{2.15}$$

Finally, by applying the connected cluster theorem of Cizek,[32] the Schrödinger

equation can be written

$$\left\{\hat{H}_N\, e^{(\hat{T}_1 + \hat{T}_2)}\right\}_C |\Psi_0\rangle = \Delta E_{CCSD} |\Psi_0\rangle \tag{2.16}$$

where $\left\{ \cdots \right\}_C$ denotes that only size-extensive terms generated by the operator $\cdots$ are considered. In the language of diagrammatic many-body theory, these size-extensive terms correspond to diagrams which are "linked" or "connected".

In order to solve Eq. (2.16) explicitly for the CCSD energy and wavefunction, one simply projects this equation onto the set of determinants, $\langle\Psi_0|$, $\{ \langle\Psi_I^A| \}$, and $\{ \langle\Psi_{IJ}^{AB}| \}$, yielding

$$\Delta E_{CCSD} = \langle\Psi_0| \left\{\hat{H}_N\, e^{(\hat{T}_1 + \hat{T}_2)}\right\}_C |\Psi_0\rangle \,, \tag{2.17}$$

$$0 = \langle\Psi_I^A| \left\{\hat{H}_N\, e^{(\hat{T}_1 + \hat{T}_2)}\right\}_C |\Psi_0\rangle \,, \tag{2.18}$$

$$0 = \langle\Psi_{IJ}^{AB}| \left\{\hat{H}_N\, e^{(\hat{T}_1 + \hat{T}_2)}\right\}_C |\Psi_0\rangle \,. \tag{2.19}$$

By applying the rules of diagrammatic many-body theory, the detailed algebraic expressions for this set of non-linear, coupled CCSD equations have been formulated by Purvis and Bartlett.[42]

$$\Delta E_{CCSD} = \sum_{I,A} t_I^A\, f_A^I + \sum_{\substack{I>J \\ A>B}} \langle IJ||AB\rangle\, \kappa_{IJ}^{AB} \,, \tag{2.17a}$$

$$0 = f_D^L + \sum_A t_L^A f_A^D - \sum_I t_I^D f_L^I + \sum_{I,A} \langle DI||LA\rangle\, t_I^A - \sum_{I,A} f_A^I\, \kappa_{LI}^{AD} \qquad (2.18a)$$

$$+ \sum_{\substack{I \\ A>B}} \langle ID||AB\rangle\, \kappa_{IL}^{AB} - \sum_{\substack{I>J \\ A}} \langle IJ||AL\rangle\, \kappa_{IJ}^{AD} - \sum_{\substack{I,K \\ A>B}} \langle IK||AB\rangle\, t_K^D\, t_{IL}^{AB}$$

$$- \sum_{\substack{I>J \\ C,A}} \langle IJ||CA\rangle\, t_L^C\, t_{IJ}^{DA} + \sum_{\substack{J,K \\ B,C}} \langle JK||CB\rangle\, t_K^C\, \tilde{\kappa}_{JL}^{DB} \,,$$

$$0 = \langle AB||IJ\rangle - \sum_L \left(f_J^L\, t_{IL}^{AB} + f_I^L\, t_{LJ}^{AB} \right) + \sum_D \left(f_D^B\, t_{IJ}^{AD} + f_A^D\, t_{IJ}^{DB} \right) \qquad (2.19a)$$

$$- \sum_K \left(\langle AK||IJ\rangle\, t_K^B + \langle KB||IJ\rangle\, t_K^A \right) + \sum_C \left(\langle AB||CJ\rangle\, t_I^C + \langle AB||IC\rangle\, t_J^C \right)$$

$$+ \sum_{C>D} \langle AB||CD\rangle\, \kappa_{IJ}^{CD} + \sum_{K>L} \langle IJ||KL\rangle\, \kappa_{KL}^{AB} + \sum_D \left(\eta^{BD}\, t_{IJ}^{AD} - \eta^{AD}\, t_{IJ}^{BD} \right)$$

$$- \sum_{K,D} \left(\langle BK||ID\rangle\, \tilde{\kappa}_{KJ}^{AD} - \langle BK||JD\rangle\, \tilde{\kappa}_{KI}^{AD} - \langle AK||ID\rangle\, \tilde{\kappa}_{JK}^{DB} + \langle AK||JD\rangle\, \tilde{\kappa}_{IK}^{DB} \right)$$

$$- \sum_{K,C} f_C^K \left(t_K^A\, t_{IJ}^{CB} + t_K^B\, t_{IJ}^{AC} + t_I^C\, t_{KJ}^{AB} + t_J^C\, t_{IK}^{AB} \right)$$

$$- \sum_L \left(\eta_{LJ}\, t_{IL}^{AB} + \eta_{LI}\, t_{JL}^{AB} \right) + \sum_C \left(t_I^C\, \alpha_{ABCJ} - t_J^C\, \alpha_{ABCI} \right)$$

$$+ \sum_L \left(t_L^A\, \tilde{\alpha}_{IJLB} - t_L^B\, \tilde{\alpha}_{IJLA} \right)$$

$$+ \frac{1}{4} \sum_{\substack{K,L \\ C,D}} \langle KL||CD\rangle \left[\kappa_{IJ}^{CD}\, \kappa_{KL}^{AB} - 2 \left(t_{IJ}^{AC}\, \kappa_{KL}^{BD} + t_{IJ}^{BD}\, \kappa_{KL}^{AC} \right) - 8\, t_I^D\, t_K^B\, t_L^A\, t_J^C \right.$$

$$\left. - 2 \left(t_{IK}^{AB}\, \kappa_{JL}^{CD} + t_{JL}^{AB}\, \kappa_{IK}^{CD} \right) + 4 \left(\tilde{\kappa}_{KI}^{AC}\, \tilde{\kappa}_{LJ}^{BD} + \tilde{\kappa}_{KI}^{BD}\, \tilde{\kappa}_{LJ}^{AC} \right) \right] .$$

where

$$\kappa_{IJ}^{AB} \equiv t_{IJ}^{AB} + t_I^A\, t_J^B - t_J^A\, t_I^B$$

$$\tilde{\kappa}_{IJ}^{AB} \equiv t_{IJ}^{AB} + t_I^A\, t_J^B$$

$$\eta^{AB} \equiv \sum_{K,C} \langle BK||DC\rangle \, t_K^C$$

$$\eta_{LJ} \equiv \sum_{K,C} \langle KL||CJ\rangle \, t_K^C$$

$$\alpha_{ABCJ} \equiv \sum_{K,D} \langle BK||CD\rangle \, \zeta 2_{KJ}^{AD} - \sum_{K,D} \langle AK||CD\rangle \, \zeta 2_{KJ}^{BD} + \sum_{K>L} \langle LK||UC\rangle \, \zeta 1_{KL}^{AB}$$

$$\alpha_{IJLB} \equiv \sum_{K,C} \langle LK||CJ\rangle \, \zeta 2_{IK}^{CB} - \sum_{K,C} \langle LK||CI\rangle \, \zeta 2_{JK}^{CB} + \sum_{C>D} \langle BL||CD\rangle \, \zeta 1_{IJ}^{CD}$$

$$\zeta 1_{IJ}^{AB} \equiv t_{IJ}^{AB} + \frac{1}{3} \left(t_I^A \, t_J^B - t_J^A \, t_I^B \right)$$

$$\zeta 2_{IJ}^{AB} \equiv t_{IJ}^{AB} + \frac{1}{3} \, t_I^A \, t_J^B$$

2.2 Spin Restriction to Closed-Shell Systems

Up to this point, no restrictions on the electronic spin coordinates have been considered, and, thus, Eqs. (2.17a)-(2.19a) are applicable to a general single-determinant based molecular system. More precisely, the spatial part of a molecular orbital occupied by an electron with spin up (α) is allowed to be different from that occupied by an electron with spin down (β). Eqs. (2.17a)-(2.19a) therefore decribe a spin-unrestricted CCSD theory (UCCSD). By imposing the approriate closed-shell, spin-restricted symmetry constraints to the cluster coefficients (RCCSD), significant reductions in computational cost and storage requirements can be realized. In so doing, one loses the spin-flexibility that is contained within the UCCSD formalism, however, many interesting chemical problems can be addressed with a closed-shell theory, and the savings achieved will certainly allow the RCCSD method to be applied to larger scale problems. Additionally, it is likely that the RCC theory for open-shell systems will soon be available thus superceding UCC methods for most

open-shell problems.

By explicitly considering the definitions of the antisymmetrized cluster coefficients,[53] and imposing the restriction to closed-shell molecular orbitals, the set of independent closed-shell cluster coefficients can be obtained as follows. Throughout this discourse, the lower case indices *i,j,k,l* will label doubly occupied, closed-shell spatial molecular orbitals, *a,b,c,d* unoccupied spatial molecular orbitals, and *p,q,r,s* are used for general spatial MO indices. Additionally, these one-electron spatial molecular orbitals will be denoted by $\chi_p(\mathbf{r})$, and the corresponding one-electron spin function as $\sigma_p(\xi)$. Considering first the one-electron cluster coefficients

$$t_I^A = \langle\psi_A(\mathbf{x}_1)|\hat{T}_1|\psi_I(\mathbf{x}_1)\rangle = \langle\chi_a(\mathbf{r}_1)\,\sigma_a(\xi_1)|\hat{T}_1|\chi_i(\mathbf{r}_1)\,\sigma_i(\xi_1)\rangle \tag{2.20}$$

$$= \langle\chi_a(\mathbf{r}_1)|\hat{T}_1|\chi_i(\mathbf{r}_1)\rangle\,\langle\sigma_a(\xi_1)|\sigma_i(\xi_1)\rangle = t_i^a\,\langle\sigma_a(\xi_1)|\sigma_i(\xi_1)\rangle \equiv t_{i_{\sigma_i}}^{a_{\sigma_a}}$$

Since $\langle\sigma_p(\xi_1)|\sigma_q(\xi_1)\rangle = \delta_{\sigma_p\sigma_q}$, it follows that

$$t_{i_\alpha}^{a_\alpha} = t_{i_\beta}^{a_\beta} \equiv \tilde{t}_i^a \tag{2.21}$$

with the other two possible spin couplings yielding zero-valued one-electron cluster coefficients.

Similarly, for the two-electron cluster coefficients

$$t_{IJ}^{AB} = \langle\psi_A(\mathbf{x}_1)\psi_B(\mathbf{x}_2)|\hat{T}_2|\psi_I(\mathbf{x}_1)\psi_J(\mathbf{x}_2)\rangle - \langle\psi_A(\mathbf{x}_1)\psi_B(\mathbf{x}_2)|\hat{T}_2|\psi_J(\mathbf{x}_1)\psi_I(\mathbf{x}_2)\rangle \tag{2.22}$$

$$= t_{ij}^{ab}\,\delta_{\sigma_i\sigma_a}\,\delta_{\sigma_j\sigma_b} - t_{ji}^{ab}\,\delta_{\sigma_i\sigma_b}\,\delta_{\sigma_j\sigma_a}\,.$$

From Eq. (2.22), it follows that there are only six non-zero t_2 spin combinations out of which there are three equivalent pairs:

$$t_{i_\alpha j_\alpha}^{a_\alpha b_\alpha} = t_{i_\beta j_\beta}^{a_\beta b_\beta} \equiv \hat{t}_{ij}^{ab} \tag{2.23}$$

$$t_{i_\alpha j_\beta}^{a_\alpha b_\beta} = t_{i_\beta j_\alpha}^{a_\beta b_\alpha} \equiv \tilde{t}_{ij}^{ab} \tag{2.24}$$

$$t_{i_\alpha j_\beta}^{a_\beta b_\alpha} = t_{i_\beta j_\alpha}^{a_\alpha b_\beta} \equiv \bar{t}_{ij}^{ab} \tag{2.25}$$

Finally, it is possible to eliminate two of these three remaining spin reduced t_2 coefficients by making use of the following two interdependencies. First, from Eq. (2.22)

$$\hat{t}_{ij}^{ab} = \tilde{t}_{ij}^{ab} + \bar{t}_{ij}^{ab} \,, \tag{2.26}$$

and from the antisymmetry of the $\hat{T}_2$ matrix elements

$$\tilde{t}_{ij}^{ab} = -\bar{t}_{ji}^{ab} = -\bar{t}_{ij}^{ba} = \tilde{t}_{ji}^{ba} \,. \tag{2.27}$$

Thus, there is only one independent set of spin restricted, closed-shell coefficients for each of t_1 and t_2. Choosing $\tilde{t}_i^a$ and $\tilde{t}_{ij}^{ab}$ ($\equiv t_i^a$ and t_{ij}^{ab} in all that follows, i.e. the ~ superscript will be dropped) as the independent set, there are a total of $\frac{1}{2}\, NM \times (NM + 1)$ t_2 coefficients and NM t_1 coefficients, where $NM = NO \times NV$ and NO (NV) is the number of occupied (unoccupied) spatial molecular orbitals in the closed-shell reference determinant. It must be stressed that NO is one half the number of electrons and NV is one half the number of virtual (unoccupied) orbitals in the corresponding UCCSD formulation. The total number of unknown cluster coefficients in this closed-shell CCSD model is equal to the total number of single and double excitation coefficients in a closed-shell CISD calculation using a spin-adapted basis as in the unitary group approach.[86] The number of unique unknowns in the closed-shell case is approximately a factor of four smaller than the number resulting from the simple use of Slater determinants which are not spin-restricted and is a direct consequence of the symmetry relations, Eqs. (2.21) and (2.23)-(2.25)

which are only valid for the closed-shell case. It should be mentioned that the selection of $\tilde{t}_{ij}^{ab}$ as the independent set of t_2 amplitudes is obviously not unique. However, it has been found that this selection yields the most symmetrical and computationally simplified CCSD equations. Recently, Pulay and co-workers[87] made a similar choice for an efficient reformulation of the closed-shell CCD theory. Geertsen and Oddershede[76] used a different basis when formulating a spin-adapted CCD theory.

Making use of this closed-shell adaptation desribed above, the energy becomes

$$\Delta E_{\mathrm{CCSD}} = 2 \sum_{i,a} f_a^i \, t_i^a + \sum_{\substack{i,j \\ a,b}} v_{ab}^{ij} \, (2\tau_{ij}^{ab} - \tau_{ji}^{ab}) \, , \tag{2.28}$$

where

$$\tau_{ij}^{ab} \equiv t_{ij}^{ab} + t_i^a \, t_j^b \, , \tag{2.29}$$

$$v_{pq}^{rs} = (pr|qs) \tag{2.30}$$

$$= \int d\mathbf{r}_1 \, d\mathbf{r}_2 \, \chi_p^*(\mathbf{r}_1)\chi_r(\mathbf{r}_1)\frac{1}{|\mathbf{r}_1 - \mathbf{r}_2|}\chi_q^*(\mathbf{r}_2)\chi_s(\mathbf{r}_2) \, ,$$

and

$$f_q^p = h_{pq} + \sum_j (2v_{qj}^{pj} - v_{jj}^{pq}) \tag{2.31}$$

is the Fock matrix in the MO basis.

The resulting equation for the t_u^β amplitudes is

$$0 = -f_u^\beta + \sum_i f_u^i\, t_i^\beta - \sum_a f_a^\beta\, t_u^a - \sum_{i,a} (2v_{au}^{i\beta} - v_{ua}^{i\beta})\, t_i^a \tag{2.32}$$

$$+ \sum_{\substack{i,j\\a,b}} (2v_{ab}^{ij} - v_{ba}^{ij})\, [t_{ij}^{\beta b}\, t_u^a + t_{uj}^{ab}\, t_i^\beta - (2t_{uj}^{\beta b} - \tau_{uj}^{b\beta})\, t_i^a]$$

$$+ \sum_{\substack{i,j\\a}} (2v_{au}^{ij} - v_{ua}^{ij})\, \tau_{ij}^{a\beta} - \sum_{\substack{i\\a,b}} (2v_{ab}^{i\beta} - v_{ba}^{i\beta})\, \tau_{iu}^{ab}$$

and for the $t_{uv}^{\beta\gamma}$ amplitudes

$$0 = \hat{P}\Bigg[\frac{1}{2}\Bigg\{v_{uv}^{\beta\gamma} + \sum_{k,l} v_{uv}^{kl}\, \tau_{kl}^{\beta\gamma} + \sum_{c,d} v_{cd}^{\beta\gamma}\, \tau_{uv}^{cd} + \sum_{\substack{k,l\\c,d}} v_{cd}^{kl}\, \tau_{kl}^{\beta\gamma}\, \tau_{uv}^{cd}\Bigg\} \tag{2.33}$$

$$+ \sum_c f_c^\beta\, t_{uv}^{c\gamma} - \sum_k f_u^k\, t_{kv}^{\beta\gamma} - \sum_{k,c} f_c^k\, (t_{uv}^{c\gamma}\, t_k^\beta + t_{uk}^{\beta\gamma}\, t_v^c) + \sum_c v_{uc}^{\beta\gamma}\, t_v^c - \sum_k v_{uv}^{\beta k}\, t_k^\gamma$$

$$+ \sum_{k,c} [(2v_{cu}^{k\beta} - v_{uc}^{k\beta})\, t_{vk}^{\gamma c} - v_{uc}^{k\gamma}\, \tau_{kv}^{\beta c} - v_{cu}^{k\beta}\, \tau_{vk}^{c\gamma}]$$

$$+ \sum_{\substack{k,l\\c,d}}\Bigg\{(2v_{cd}^{kl} - v_{dc}^{kl})\, [t_{vl}^{\gamma d}(t_{uk}^{\beta c} - \tau_{uk}^{c\beta}) - \tau_{kl}^{\gamma d}\, t_{uv}^{\beta c} - \tau_{vl}^{cd}\, t_{uk}^{\beta\gamma}] + v_{cd}^{kl}(t_{vl}^{d\gamma}\, T_{uk}^{c\beta} + t_{ul}^{c\gamma}\, T_{vk}^{d\beta})\Bigg\}$$

$$- \sum_{\substack{k,l\\c}}\Bigg\{(2v_{uc}^{kl} - v_{cu}^{kl})\, (t_{kj}^{\beta\gamma}\, t_l^c + t_{lv}^{c\gamma}\, t_k^\beta) - v_{uc}^{kl}\, (t_{vl}^{c\gamma}\, t_k^\beta + t_{vk}^{c\beta}\, t_l^\gamma + \tau_{kl}^{\beta\gamma}\, t_v^c)\Bigg\}$$

$$+ \sum_{\substack{k\\c,d}}\Bigg\{(2v_{cd}^{\beta k} - v_{dc}^{\beta k})\, (t_{uv}^{c\gamma}\, t_k^d + t_{kv}^{d\gamma}\, t_u^c) - v_{cd}^{\beta k}\, (t_{kv}^{\gamma d}\, t_u^c + t_{ku}^{\gamma c}\, t_v^d + \tau_{uv}^{cd} t_k^\gamma)\Bigg\}\Bigg]$$

where τ is defined in Eq. (2.29),

$$T_{ij}^{ab} \equiv \frac{1}{2} t_{ij}^{ab} + t_i^a\, t_j^b\,, \tag{2.34}$$

and $\hat{P}$ represents a permutation operator which acts only over the set of external indices labeling the $\frac{1}{2}\, NM \times (NM + 1)$ t_2 equations distinguished by the letters u,v

(occupied) and β,γ (virtual), and when acting on a function $f(u,v,\beta,\gamma)$ has the action

$$\hat{P} f(u,v,\beta,\gamma) = f(u,v,\beta,\gamma) + f(v,u,\gamma,\beta) \tag{2.35}$$

Basically, $\hat{P}$ generates a new term by interchanging u with v, β with γ, and leaving all the other contracted indices unchanged. All t_2 coefficients in Eqs. (2.32) and (2.33) refer to the arrangement of spin indices defined as t_2 in Eq. (2.24) which is a set sufficient [together with t_1 of Eq. (2.21)] to obtain the energy, solve the non-linear coupled algebraic equations (2.32) and (2.33), and if desired, obtain any of the other possible non-zero spin combinations of t_2 coefficients defined through Eqs. (2.23)-(2.27). It must be pointed out that this simplification is only pertinent to the closed-shell case and is no longer valid either for the UCCSD or open-shell cases based on an RHF reference determinant. The permutation operator $\hat{P}$ appearing in Eq. (2.33) greatly simplifies the algebraic expression of Eq. (2.33) by roughly reducing the number of terms by a factor of two, but, unfortunately, this symmetry property is of little help computationally since most intermediate products (except the first four terms with a factor of $\frac{1}{2}$ in front which can be easily taken out of $\hat{P}$) have no symmetry and require evaluation for all possible values of their respective indices. A detailed discussion of the computational implementation of the present closed-shell CCSD method is presented in Section 2.3.

It should be noted that owing to the symmetry properties of the t_2 amplitudes, loops over the indices labeling the CCSD equations run over $\beta>\gamma$ for all u,v and only $u\geq v$ for $\beta=\gamma$. The t_1 coefficients must be evaluated for all u,β. This results in the $\frac{1}{2}\,NM\times(NM+1)$ and NM number of independent equations for t_2 and t_1, respectively.

As mentioned above, the general CCSD model scales as N^6 ($N = NO + NV$). A detailed analysis of the loop structure of the closed-shell CCSD equations presented in the following section yields a computational factor of $\frac{1}{2} NO^2 NV^4 + 12 NO^3 NV^3 + \frac{13}{2} NO^4 NV^2$ if N^5 and N^4 loops are neglected. The corresponding factor for the general UCCSD formalism can be roughly obtained from Eqs. (2.18a) and (2.19a) as $\frac{5}{2} (2NO)^2 (2NV)^4 + 6 (2NO)^3(2NV)^3 + \frac{9}{2} (2NO)^4(2NV)^2$. It has been asserted, however, that a major part of the reduction in computational time in going from UCCSD to closed-shell RCCSD could be taken into account by inserting adequate factors of two and skipping loops when coding the UCCSD equations to benefit from the closed-shell symmetry.[42]

If all t_1 amplitudes are neglected, the CCD model is obtained. In this case, Eq. (2.32) (which has a computational cost proportional to N^5) does not appear, and all contributions to Eq. (2.33) coming from E- and F-type integrals (see Section 2.3) vanish. Further simplification in D-type terms (see Section 2.3) reduces the scaling factor to $\frac{1}{2} NO^2 NV^4 + 8 NO^3 NV^3 + \frac{7}{2} NO^4NV^2$ which is essentially the same as obtained by Pulay using the generator state formalism.[87] If non-linear t_2 terms are neglected at the CCD level (LCCD) this factor is finally reduced to $\frac{1}{2} NO^2 NV^4 + 3 NO^3 NV^3 + \frac{1}{2} NO^4 NV^2$. It is interesting to note that an identical factor results for the linearized CCSD model (LCCSD) where all terms involving any combination of products of t_1 and t_2 are neglected. These results which can be easily verified from Eqs. (2.32) and (2.33) by appropriately neglecting nonlinear terms or zeroing t_1 amplitudes show two important results. First, the cost of solving the t_1 equation is marginal (i.e. proportional to N^5) if t_2 amplitudes are already present in

the model. However, t_1 couples with t_2 giving a non-negligible contribution in the t_2 equation. Secondly, the eventual high price of the CC model comes from the non-linear terms (especially $\hat{T}_2^2$ in CCSD) which are not present in the CI formulation. The effect of including these quadruple excitations in CCSD is reflected by 6 NO^3 NV^3 loops (see D_{2a}, D_{2b}, D_{2c} and their products with t_2 in Section 2.3), two additional NO^3 NV^3 loops are already present in the linear model and the remaining four appear from the inclusion of the t_1 amplitudes through the F-type integrals (see F_2, F_{11}, and F_{12} products with t_2 in Section 2.3).

The molecular point group symmetry may be used to further reduce the computational requirements. This is done in two different steps in the present research. First, since the t_1 (t_2) amplitudes are zero unless the direct product of the irreducible representations of the two (four) indices contains the totally symmetric representation, loops over the external u,v,β,γ indices are restricted such that only non-vanishing elements are calculated. Once this condition is satisfied, the inner loops are performed only over the irreducible representations that yield a non-zero contribution. This means that only products of two-electron integrals, t_2, and t_1 amplitudes where the direct product of the symmetries of the indices of the individual terms are totally symmetric need be performed. In the present work, the spatial symmetry implementation has been limited to the point group D_{2h} and its subgroups. Results presented in Section 2.4 indicate the importance of using molecular symmetry.

Finally, the option of using frozen core and deleted virtual orbitals throughout the CCSD energy calculation has been included. This may be easily accomplished by deleting from the t_1 and t_2 lists those coefficients whose indices correspond to one or more frozen orbitals and simply restricting all the sums to run over only active

orbitals. Results obtained within this approximation will be presented in Section 2.4.

2.3 Implementational Details

Equation (2.32) for the t_1 coefficients can be cast into the following form:

$$(f_\beta^\beta - f_u^u)\, t_u^\beta = -f_u^\beta + \sum_{i\neq u} f_u^i\, t_i^\beta - \sum_{a\neq\beta} f_a^\beta\, t_u^a + \sum_{i,a} f_a^i\,(2t_{ui}^{\beta a} - \tau_{ui}^{a\beta}) \tag{2.36}$$

$$- \sum_a g_a^\beta\, t_u^a - \sum_{\substack{i,j\\ a}} (2[D_1]_{ju}^{ai} - [D_1]_{iu}^{aj})\, t_j^a\, t_i^\beta - \sum_{i,a} [2(D_{2a} - D_{2b}) + D_{2c}]_{au}^{i\beta}\, t_i^a$$

$$- \sum_a [F_{2a}]_{au}^{\beta a} + \sum_i \left\{ [\frac{1}{2}(E_{2a} - E_{2b}) + E_{2c} + C_1]_{ui}^{i\beta} - 2[D_1]_{ui}^{\beta i} \right\} + \sum_i g_u^i\, t_i^\beta$$

and Eq. (2.33) for the t_2 amplitudes can be cast into

$$(f_u^u + f_v^v - f_\beta^\beta - f_\gamma^\gamma)\, t_{uv}^{\beta\gamma} = v_{uv}^{\beta\gamma} + J_{uv}^{\beta\gamma} + J_{vu}^{\gamma\beta} + S_{uv}^{\beta\gamma} + S_{vu}^{\gamma\beta}\,, \tag{2.37}$$

where the occupied and virtual indices labeling the equations are u,v and β,γ, respectively. With

$$J_{uv}^{\beta\gamma} = \sum_{a\neq\beta} f_a^\beta\, t_{uv}^{a\gamma} - \sum_{i\neq u} f_u^i t_{iv}^{\beta\gamma} - \sum_{i,a} f_a^i\,(t_{uv}^{a\gamma}\, t_i^\beta + t_{ui}^{\beta\gamma}\, t_v^a) + \sum_a g_a^\gamma\, t_{uv}^{\beta a} - \sum_i g_v^i\, t_{ui}^{\beta\gamma}\,, \tag{2.38}$$

$$S_{u\nu}^{\beta\gamma} = [\frac{1}{2} A_{2'} + \frac{1}{2} B_{2'} - E_1^*]_{u\nu}^{\beta\gamma} - [C_2 + C_{2'} - D_{2a} - F_{12}]_{\beta\nu}^{u\gamma} \tag{2.39}$$

$$+ \sum_{i,a} \left\{ [D_{2a} - D_{2b}]_{av}^{i\gamma} (t_{ui}^{\beta a} - T_{ui}^{a\beta}) + \frac{1}{2} [D_{2c}]_{av}^{i\gamma} t_{ui}^{\beta a} + [D_{2c}]_{au}^{i\gamma} T_{vi}^{a\beta} \right\}$$

$$+ \sum_{ij} [\frac{1}{2} D_{2'} + E_1]_{u\nu}^{ij} \tau_{ij}^{\beta\gamma} - \sum_{i} [D_1 + F_{2'}]_{u\nu}^{\beta i} t_i^{\gamma} - \sum_{i} ([E_{2a} - E_{2b}]_{u\nu}^{i\gamma} - [E_{2c}]_{vu}^{i\gamma}) t_i^{\beta}$$

$$- \sum_{i,a} \left\{ [F_{11}]_{av}^{\gamma i} t_{ui}^{\beta a} + [F_{11}]_{av}^{\beta i} t_{ui}^{a\gamma} - [F_{12}]_{av}^{i\gamma} (2t_{ui}^{\beta a} - t_{ui}^{a\beta}) \right\},$$

$$g_u^i = \sum_j \left\{ 2[E_1 + D_{2'}]_{uj}^{ij} - [E_1 + D_{2'}]_{uj}^{ji} \right\}, \tag{2.40}$$

$$g_a^{\beta} = \sum_b \left\{ 2[F_1^* + D_{2'}^*]_{ab}^{\beta b} - [F_1^* + D_{2'}^*]_{ba}^{\beta b} \right\}. \tag{2.41}$$

In Eqs. (2.36)-(2.41), the following intermediate products have been defined:

$$[A_{2'}]_{u\nu}^{\beta\gamma} = \sum_{i,j} v_{u\nu}^{ij} \tau_{ij}^{\beta\gamma}, \tag{2.42}$$

$$[B_{2'}]_{u\nu}^{\beta\gamma} = \sum_{a,b} v_{ab}^{\beta\gamma} \tau_{u\nu}^{ab}, \tag{2.43}$$

$$[C_1]_{ui}^{i\beta} = \sum_{a} v_{ua}^{i\beta} t_i^a, \tag{2.44}$$

$$[C_2]_{\beta\nu}^{u\gamma} = \sum_{i,a} v_{au}^{\beta i} t_{vi}^{\gamma a}, \tag{2.45}$$

$$[C_{2'}]_{\beta\nu}^{u\gamma} = \sum_{i,a} v_{ia}^{u\gamma} \tau_{iv}^{\beta a}, \tag{2.46}$$

$$[D_1]_{u\nu}^{\beta i} = \sum_{a} v_{ua}^{\beta i} t_v^a, \tag{2.47}$$

$$[D_{2'}]_{u\nu}^{ij} = \sum_{a,b} v_{ab}^{ij} \tau_{u\nu}^{ab}, \tag{2.48}$$

$$[D^{*}_{2'}]^{\beta b}_{ac} = \sum_{i,j} v^{ij}_{ac}\, \tau^{\beta b}_{ij} \,, \tag{2.49}$$

$$[D_{2a}]^{i\gamma}_{av} = \sum_{j,b} v^{ji}_{ba}\, (2t^{\gamma b}_{vj} - t^{b\gamma}_{vj}) \,, \tag{2.50}$$

$$[D_{2b}]^{i\gamma}_{av} = \sum_{j,b} v^{ij}_{ba}\, t^{\gamma b}_{vj} \,, \tag{2.51}$$

$$[D_{2c}]^{i\gamma}_{av} = \sum_{j,b} v^{ij}_{ba}\, t^{b\gamma}_{vj} \,, \tag{2.52}$$

$$[E^{*}_{1}]^{\beta\gamma}_{uv} = \sum_{i} v^{\beta i}_{uv}\, t^{\gamma}_{i} \,, \tag{2.53}$$

$$[E_{1}]^{ij}_{uv} = \sum_{a} v^{ij}_{ua}\, t^{a}_{v} \,, \tag{2.54}$$

$$[E_{2a}]^{i\gamma}_{uv} = \sum_{j,b} v^{ji}_{bu}\, (2t^{\gamma b}_{vj} - t^{b\gamma}_{vj}) \,, \tag{2.55}$$

$$[E_{2b}]^{i\gamma}_{uv} = \sum_{j,b} v^{ij}_{bu}\, t^{\gamma b}_{vj} \,, \tag{2.56}$$

$$[E_{2c}]^{i\gamma}_{uv} = \sum_{j,b} v^{ij}_{bu}\, t^{b\gamma}_{vj} \,, \tag{2.57}$$

$$[F_{11}]^{\beta i}_{bv} = \sum_{a} v^{\beta i}_{ba}\, t^{a}_{v} \,, \tag{2.58}$$

$$[F_{12}]^{i\beta}_{bv} = \sum_{a} v^{i\beta}_{ba}\, t^{a}_{v} \,, \tag{2.59}$$

$$[F^{*}_{1}]^{\beta b}_{ac} = \sum_{i} v^{\beta i}_{ac}\, t^{b}_{i} \,, \tag{2.60}$$

$$[F_{2a}]^{\beta a}_{au} = \sum_{i,b} v^{\beta i}_{ab}\, (2t^{ab}_{ui} - t^{ba}_{ui}) \,, \tag{2.61}$$

$$[F_{2'}]^{\beta i}_{uv} = \sum_{a,b} v^{\beta i}_{ab}\, \tau^{ab}_{uv} \,. \tag{2.62}$$

The notation used for these intermediate products requires explanation. First, each letter (*A* through *F*) refers to a specific block of two-electron integrals in the MO

basis. Thus, $A = \{(ooloo)\}$, $B = \{(vvlvv)\}$, $C = \{(oolvv)\}$, $D = \{(ovlov)\}$, $E = \{(oolov)\}$, and $F = \{(ovlvv)\}$, where o and v represent occupied and unoccupied MOs, respectively. Secondly, the first subindex specifies the set of t coefficients contracting the particular group of integrals: 1 refers to t_1, 2 to t_2, and 2′ to τ. If different contraction schemes occur for any group of integrals with the same set of t coefficients, then a second subindex (a, b, or c) specifies each of them. Finally, a * superscript indicates a replacement of the contracted variable (always occupied for virtual) in the same contraction scheme.

It should be mentioned that this is neither the most elegant nor compact form of presenting the closed-shell CCSD equations. However, they have been formulated in an attempt to achieve maximum computational efficiency, and the computer code was written employing the above development.

In defining the intermediate products, all possible contraction schemes have been investigated and the most efficient one selected. For example, the term

$$\sum_{\substack{i \\ a,b}} v_{ab}^{i\gamma}\, t_{uv}^{\beta a}\, t_i^b \tag{2.63}$$

may be evaluated either as

$$\sum_a \left[\sum_{i,b} v_{ab}^{i\gamma}\, t_i^b\right] t_{uv}^{\beta a} = \sum_a \left[\sum_i [F]_{bi}^{\gamma i}\right] t_{uv}^{\beta a} \tag{2.64}$$

or

$$\sum_{i,b} \left[\sum_a v_{ab}^{i\gamma}\, t_{uv}^{\beta a}\right] t_i^b \,. \tag{2.65}$$

The first is an $NO\,NV^3 + NO^2\,NV^3$ procedure, whereas the latter is $NO^3\,NV^4 + NO^3\,NV^3$. Obviously, Eq. (2.64) should be chosen over Eq. (2.65).

The construction of the intermediate products (2.42)-(2.62) may be properly set up inside the loops where each is needed, and thus they are not held permanently in core memory. A small number of arrays of maximum length *NO×NV* is sufficient for this purpose.

2.4 Application to Molecular Systems

2.4.1 Diatomic Nitrogen Molecule

Table I summarizes the present results for the N_2 molecule in its electronic ground state. The first basis set employed was the standard Huzinaga-Dunning double-ζ plus polarization (DZ+P) set,[12,15] with the nitrogen polarization exponent, α_d (N) = 0.8. The second set was of triple-ζ plus double polarization (TZ+2P) quality, with polarization function orbital exponents, α_d = 0.5, 1.5. A third basis set was of quadruple-ζ plus triple polarization (QZ+3P) quality, with polarization function orbital exponents α_d = 0.25, 0.75, and 2.25. In addition to the SCF, CISD, and CCSD energies, included in Table I are the Davidson corrected[85] CISD energies. To the extent that the Davidson correction is quantitatively reliable, one would expect

$$E_{\mathrm{CISD(+Q)}} - E_{\mathrm{CISD}} \simeq E_{\mathrm{CCSD}} - E_{\mathrm{CISD}} \tag{2.66}$$

to be approximately true. That is, one would hope that the Davidson correction for disconnected higher excitations would be comparable to the predictions made by CCSD. Note, however, that recent large CI studies have shown that in some cases (e.g., the Ne atom[88] and the BH molecule[89]), the Davidson correction, designed to incorporate the effects of disconnected quadruple excitations only, can overshoot the importance of *all* triples and quadruples.

Table I. Coupled Cluster (CCSD) and configuration interaction (CISD) energies for the nitrogen molecule. A standard bond distance r_{N-N} = 2.068 a.u. was used. Total energies are given at the SCF level; correlation energies are given for correlated levels of theory. Timings refer to an IBM 3081K computer.

	DZ+P (9*s*5*p*1*d*/4*s*2*p*1*d*)		TZ+2P (9*s*5*p*2*d*/5*s*3*p*2*d*)		QZ+3P (11*s*7*p*3*d*/6*s*4*p*3*d*)	
	Energy (hartrees)	Time (min)	Energy (hartrees)	Time (min)	Energy (hartrees)	Time (min)
SCF	− 108.958 506	···	− 108.975 879	···	− 108.987 357	···
CISD	− 0.312 747	0.3	− 0.360 375	0.9	− 0.376 889	2.5
CISD(+Q)	− 0.340 052	···	− 0.392 445	···	− 0.410 652	···
CCSD	− 0.336 449	1.2	− 0.387 925	7.2	− 0.406 157	20.0

Given the above examples, it is not suprising to find that the Davidson correction gives lower energies for N_2 than the theoretically rigorous CCSD method. The computation times for the CCSD approach are four times greater than CISD with the DZ+P basis set and eight times greater with the TZ+2P and QZ+3P basis sets. The CISD wavefunctions were determined via the shape-driven graphical unitary group approach (GUGA)[90] which evolved from the earlier loop-driven GUGA.[38] It has been previously claimed in the literature[9,42] that since both CISD and CCSD (or CCD) are essentially N^6 procedures they should have very similar computational requirements. This statement, which was never supported with actual calculations, was made when CISD codes were probably one or two orders of magnitude slower than the present state of the art CI codes. It is now evident that the higher order disconnected terms accounted for by CCSD represent an additional and inherent cost when compared to CISD.

Table II illustrates the effectiveness of introducing symmetry into the solution of the CCSD equations. In Table II are given CISD and CCSD timings for the DZ+P

treatment of N_2 in the four point groups D_{2h}, C_{2v}, C_s, and C_1. The CISD timings in Table II illustrate the typical result that adding an element of symmetry reduces the overall computation time by roughly a factor of two. Interestingly, much greater computation reductions are observed for the CCSD method, when compared to CISD, with the addition of symmetry. Thus it would appear that the present implementation of symmetry (see discussion in Section 2.2) in the CCSD method is rather effective and is certainly arising from the non-linearity of the algebraic equations.

Table II. The use of symmetry in CCSD and CISD treatments of the nitrogen molecule. All theoretical methods employed a DZ+P basis set (32 contracted Gaussian basis functions) and the standard geometry, r_{N-N} = 2.068 a.u. The timings refer to an IBM 3081K computer

Symmetry exploited	Number of configurations in CISD	CISD time (s)	CCSD time (s)	Timing ratio (CCSD/CISD)
C_1	15 576	107	2030	19.0
C_s	7 848	46	493	10.7
C_{2v}	4 360	24	178	7.4
D_{2h}	2 436	17	70	4.1

2.4.2 Water, Hydronium Ion, and Hydrated Hydronium Ion

Table III summarizes the present results for H_2O, H_3O^+, and $H_5O_2^+$. Again, the standard Huzinaga-Dunning DZ+P basis set [12,15] was used with polarization function orbital exponents $\alpha_d(O) = 0.8$, $\alpha_p(H) = 1.0$ and hydrogen s function scale factor 1.2. The geometries used were the DZ+P CISD stationary point geometries determined by Remington.[91]

For H_2O and H_3O^+, the Davidson corrected CISD energies are again below the CCSD results, by 0.002-0.003 hartrees. The predicted proton affinity of water is 177.3 kcal/mol at the DZ+P SCF level of theory. Correction for zero-point vibrational energies reduces the predicted DZ+P SCF proton affinity to 168.8 kcal/mol.[91] The effect of electron correlation is to slightly increase the predicted proton affinity, by 0.53 kcal/mol (CISD), 0.31 kcal/mol (Davidson corrected CISD), and 0.22 kcal/mol (CCSD). It is apparent that correlation has only a minor effect on the water proton affinity, for which Moylan and Brauman[92] recommend an experimental value of 165.13 kcal/mol.

Also included in Table III are results from theoretical treatments in which the oxygen 1*s*-like molecular orbital has been frozen, i.e. held doubly occupied. This restriction has a negligible effect (0.1 kcal/mol) on the predicted proton affinities but reduces the computation times by a factor of two. The timing ratios CCSD/CISD range from four (water) to eight (H_3O^+ with all orbitals included).

Table III. Comparison of coupled cluster (CCSD) and configuration interaction (CISD) energies for H_2O, H_3O^+, and $H_5O_2^+$. Total energies are given at the SCF level of theory and correlation energies for the correlated levels of theory. A DZ+P basis set was used with geometries taken from CISD optimizations with oxygen core orbital(s) frozen. Timings refer to an IBM 3081K computer.

	H_2O		H_3O^+		Centrosymmetric $H_5O_2^+$		Asymmetric $H_5O_2^+$	
	Energy (hartrees)	Time (min)	Energy (hartrees)	Time (min)	Energy (hartrees)	Time (min)	Energy (hartrees)	Time (min)
SCF	− 76.046 282	···	− 76.328 876	···	− 152.426 888	···	− 152.427 306	···
Correlated methods with oxygen frozen core								
CISD	− 0.195 632	0.1	− 0.196 259	0.4	− 0.378 911	11	− 0.378 327	12
CISD(+Q)	− 0.205 747	···	− 0.206 026	···	− 0.412 072	···	− 0.411 358	···
CCSD	− 0.203 786	0.4	− 0.203 948	2.0	− 0.412 897	96	− 0.412 185	105
Correlated methods with all orbitals included								
CISD	− 0.209 475	0.2	− 0.210 318	0.5	− 0.405 706	15	− 0.405 133	18
CISD(+Q)	− 0.220 233	···	− 0.220 720	···	− 0.440 799	···	− 0.440 086	···
CCSD	− 0.218 354	0.8	− 0.218 712	4.0	− 0.442 238	181	− 0.441 539	200

The CCSD treatment of $H_5O_2^+$ was of interest because CISD reverses the energetic ordering of the centrosymmetric (point group C_2) and asymmetric (point group C_s) stationary points.[91] At the DZ+P SCF level, the C_s structure of $H_5O_2^+$ is the absolute minimum; the C_2 structure is a transition state lying 0.27 kcal/mol higher in energy. However, Remington has shown[91] that reoptimization at the DZ+P CISD level predicts the centrosymmetric C_2 structure to lie lowest, with the C_s structure lying 0.10 kcal/mol higher. When the Davidson correction is appended this energy difference increases to 0.19 kcal/mol.

It is apparent that the energy difference between the C_2 and C_s stationary points of $H_5O_2^+$ is quite sensitive to the level of theory applied. Table III shows that the

CCSD method predicts a somewhat greater contribution (≈0.001 hartree) to the correlation energy than does CISD(+Q). However, the energy separation between the C_2 and C_s stationary points is 0.19 kcal/mol with two frozen core MOs and 0.18 kcal/mol with all electrons explicitly correlated. Although the results for this energy difference now appear converged with respect to electron correlation, it must be emphasized that significantly larger basis sets will be required for a reliable theoretical prediction of the ordering of the $H_5O_2^+$ stationary points.

Another problem of interest concerning hydrated hydronium is the dissociation energy for the process

$$H_5O_2^+ \rightarrow H_3O^+ + H_2O \ .$$

At the DZ+P SCF level this dissociation energy D_0 is predicted to be 31.3 kcal/mol. CISD(+Q) predicts 34.5 kcal/mol with the oxygen core orbitals frozen. Since CISD is not size-extensive, a supermolecule CISD (with frozen core orbitals) was performed on $H_3O^+ \cdots H_2O$ seperated by 1000 bohr. The CISD optimum geometries were used for the H_3O^+ and H_2O fragments. The CISD and CISD(+Q) energies are − 152.749 069 and − 152.781 686 hartrees, respectively. A somewhat smaller dissociation energy is predicted with the CCSD method, namely 33.2 kcal/mol with or without frozen core orbitals. An experimental value for D_0 is that of Cunningham, Payzant, and Kebarle,[94] namely 31.6 kcal/mol.

The computation times for $H_5O_2^+$ show that the use of even one element of symmetry is important. When the C_2 structure was treated ignoring symmetry, the CCSD calculation with all electrons explicitly correlated required 616 minutes of IBM 3081K cpu time. With the inclusion of the proper C_2 symmetry (which contains only a single twofold rotation), the CCSD time was reduced to 181 minutes.

Given the relatively low point group symmetry, the ratio of CCSD to CISD times for $H_5O_2^+$ are among the highest reported here, namely about eight.

2.4.3 Hydrogen Thioperoxide (HSOH)

This molecule provides a good test of the CCSD method because its equilibrium geometry includes no elements of symmetry, i.e. point group C_1. As such it puts the present CCSD method in the worst possible light compared to CISD in terms of computation times. The equilibrium geometry was recently predicted by Lee, Handy, Rice, Scheiner, and Schaefer[94] in the course of their research on analytic CI energy second derivatives. Those authors used a DZ+P basis set and explicitly correlated all electrons, including a total of 50 basis functions and 116 403 configurations.

The present results for hydrogen thioperoxide are summarized in Table IV. With both the DZ and DZ+P basis sets the CCSD energy lies about 0.01 hartree below the Davidson corrected CISD result. Thus, the Davidson correction, a very simple and transparent procedure, is doing an excellent job here of reproducing the higher level CCSD results. For the larger DZ+P basis set, the present CCSD implementation requires about ten times more computation than the shape driven graphical unitary group approach.[90]

Table IV. Comparison between CCSD and CISD energies for hydrogen thioperoxide, HSOH. The geometry is the DZ+P CISD structure from reference 94. Total SCF energies are given; correlation energies are given for correlated theories. Timings refer to an IBM 3081K computer.

	DZ basis set		DZ+P basis set	
	Energy (hartrees)	Time (min)	Energy (hartrees)	Time (min)
SCF	− 473.433 887	···	− 473.517 003	···
CISD	− 0.257 712	11	− 0.391 023	67
CISD(+Q)	− 0.275 240	···	− 0.427 401	···
CCSD	− 0.276 503	83	− 0.428 584	683

2.4.4 *s*-Tetrazine ($C_2N_4H_2$)

The largest molecule examined in this CCSD study was *s*–tetrazine which is isoelectronic with benzene. A detailed account of a study of the ground and excited electronic states of *s*–tetrazine will be presented in Chapter 3. Here, the total energies of this molecule are compared using CCSD, CISD, and CISD(+Q) methods. Initially, a standard DZ basis set of 64 basis functions was employed, but additional work included polarization functions for a total of 106 contracted Gaussian functions. Polarization function orbital exponents for the latter basis set were α_d(N) = 0.8, α_d(C) = 0.75, and α_p(H) = 1.0. In all theoretical procedures including correlation effects, the six core-like (N 1*s*, C 1*s*) MOs were frozen (doubly occupied) and the six highest virtual orbitals (core counterparts) were deleted.

Table V summarizes the CISD and CCSD results for *s*–tetrazine. Note first that the magnitude of the correlation energies for *s*–tetrazine is significantly greater than

for the previous cases. Not anticipated, however, is the fact that the Davidson correction falls significantly short of the CCSD correlation energy. Specifically, the left side of Eq. (2.66) is 0.123 hartree with the DZ+P basis set, while the right side is 0.164 hartree. As mentioned in the above discussion of HSOH, the Davidson correction does an excellent job for the other molecules studied herein. However, the opposite finding for *s*–tetrazine should not be too suprising, since the Davidson correction formula includes only a fraction of the higher excitation effects incorporated by CCSD.

Table V. Theoretical results for *s*–tetrazine at SCF equilibrium geometries. Total SCF energies are given; correlation energies are given for correlated theories. Timings refer to an IBM 3081K computer.

	DZ basis set		DZ+P basis set	
	Energy (hartrees)	Time (min)	Energy (hartrees)	Time (min)
SCF	– 294.456 829	· · ·	– 294.647 387	· · ·
CISD	– 0.503 599	11	– 0.733 073	57
CISD(+Q)	– 0.583 024	· · ·	– 0.856 089	· · ·
CCSD	– 0.607 673	25	– 0.897 068	222

The comparison between computation times in Table V shows the CCSD method to be relatively efficient compared to CISD. This of course is due to the high point group symmetry (D_{2h}) of *s*–tetrazine. The CCSD method takes 2.3 times longer with the DZ basis set and 4.2 times longer with the larger DZ+P basis. These ratios confirm a point which may be seen in Tables I, III and IV as well. Namely, for a given molecule and number of electrons correlated, the CISD time scales with

basis set expansion at a slower rate than does the CCSD computational time. This result is due to the shape driven algorithm of the SDGUGA program,[90] which is designed specifically to handle the external space of the CISD procedure in a very efficient manner. There should be a point (when the external space dominates the CI procedure) beyond which the ratio of the CCSD to CISD cpu times remains constant.

A Theoretical Study of *s*-Tetrazine

3.1 Introduction

The symmetric tetra-aza substituted benzene, *s*-tetrazine (Figure 2), has been of great interest to chemists for eighty years, with the original studies of this red crystalline heterocycle carried out by Curtius, Darapsky, & Muller[95] in 1907 and Koenigsberger & Vogt[96] in 1913. Since that time much effort has been devoted to the characterization of the ground and excited electronic states of *s*-tetrazine. Three especially interesting areas which have recently been investigated are (1) the high resolution characterization of the S_0 and S_1 states using rovibronic absorption and emission spectroscopy; (2) the dynamics and dissociative photochemistry of electronically excited *s*–tetrazine; and (3) the chemistry and physics of van der Waals complexes involving *s*–tetrazine. Additionally, several methods of electronic structure theory have been applied to this system.

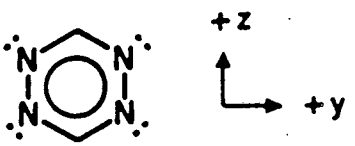

Figure 2: Conventional cartesian axis designations for *s*–tetrazine (the $+x$ axis is directed out of the page).

3.1.1 $S_1 \leftarrow S_0$ Spectroscopy

The bulk of the high resolution spectroscopic studies have focused on the series of visible rovibronic transitions with origin at 18 128 cm^{-1}. This series corresponds to the lowest spin and orbitally allowed $n \rightarrow \pi^*$ electronic transition which in the D_{2h} symmetry group (with axes as defined in Figure 2) is the $^1B_{3u} \leftarrow {}^1A_g$ transition. The

papers of Mason[97] (1958) and Spencer, Cross, and Wiberg[98] (SCW, 1961) report vibronic spectral data for this transition series along with infrared spectra for the ^1A_g state. Based on this data in conjunction with spectral data for benzene and other aza-benzenes, SCW made initial assignments of several of the *s*–tetrazine fundamental frequencies. This data was given a second interpretation by Berezin in 1964 based on his calculations of and modifications to the force constants of pyridine.[99] Innes, Byrne, and Ross[100] collected and reviewed this data (along with previously unpublished results) in 1967.

Further progress was made toward the assignment of all 18 fundamental frequencies of the ground state with the combined vapor phase IR - solid state Raman study of Franks, Merer, and Innes[101] (1968). Based on their data 17 of these 18 ground state fundamentals were assigned (10 vapor phase assignments and 7 solid state assignments). Additionally, the frequencies assigned to the two b_{3u} modes along with the low frequency b_{1u} mode by SCW were revised.

The vibronic absorption study of Innes, Franks, Merer, Vemulapalli, Cassen, and Lowry[102] (1977) enabled vapor phase frequency assignments to be made for three ground state *gerade* modes which could previously only be observed by Raman spectra of the solid state. Furthermore, six fundamentals of the $^1B_{3u}$ state were assigned. One difficulty which arose from this study was the observation of an anomalously large intensity for a band assigned as a $^1B_{3u} \leftarrow {}^1A_g$ vibronic absorption overtone at 18 913 cm^{-1}. The authors proposed an intensity borrowing mechanism through either a Fermi resonance with a nearby fundamental level within the same electronic surface or a coupling to a fundamental vibration on a second excited singlet electronic surface. The 1981 work of Brumbaugh and Innes[103] showed that this intensity borrowing was the result of Fermi resonance within the $^1B_{3u}$ state through the study

of the single vibronic level (SVL) fluoresence from several excitations to the $^1B_{3u}$ state. Additionally, from this study, seven vapor phase fundamental frequencies of ground state *gerade* modes were newly assigned or revised.

Further SVL fluorescence work was carried out by Brumbaugh, Haynam, and Levy[104] in 1982. This study employed a supersonic expansion of *s*–tetrazine vapor in order to observe spectra originating from conditions of extreme vibrational and rotational cooling. New frequency assignments for two excited state ($\tilde{A}\ ^1B_{3u}$) modes (b_{2g} and a_g) were made. A study of the lifetimes of several excited state vibronic levels was also presented (see dynamics discussion below). Most recently, two detailed infrared studies of the rotational profiles of two ground state vibrations by Thakur, Job, and Kartha[105] have resulted in a reassignment of the 882 cm^{-1} band from b_{1u} symmetry (*z*-polarized) to b_{2u} symmetry (*y*-polarized).

Spectroscopic studies of the $^1B_{3u} \leftarrow {}^1A_g$ transition have also led to the characterization of the equilibrium geometries of these two states. In 1959 Mason[106] analyzed the *J*-rotational structure (the *K*-rotational quantization was neglected) of the 0-0 vibronic absorption band using equations appropriate for an oblate symmetric top (*s*–tetrazine is actually a slighty assymetric top). From this analysis the in-plane rotational constant $\frac{1}{2}(A + B)$ was determined for both the ground and excited states. Additionally, based on an a qualitative analysis of the HOMO and LUMO of the ground state, Mason concluded that the change in geometry upon $S_1 \leftarrow S_0$ excitation was small.

The first published vapor phase geometries of these two electronic states were from Merer and Innes[107] in 1968. These geometries were deduced from an analysis of rotational contours of two vibronic absorption bands (the 0-0 band and the 0-0 +

780 cm^{-1} band) in the $S_1 \leftarrow S_0$ transition for six isotopically substituted *s*–tetrazine frameworks. In contrast to Mason's prediction, Merer and Innes found the geometry change upon excitation to be quite large (particularly in the N-N bond distance and NCN bond angle). Brown[108] (1969) also analyzed a high resolution photograph of the ^qQ branch ($\Delta J = 0$, $\Delta K = 0$) of the 0-0 vibronic band and obtained results in agreement with Merer and Innes for the change in the rotational constant C (*x*-axis inertial constant) upon excitation. A computer simulation was used by Innes, Khan, and Livak[109] (1971) to match the observed rotational contour of the 18 913 cm^{-1} band and from this the three distinct moments of inertia for the S_0 and S_1 states were determined. However, the validity of this analysis was questioned due to the possibilty of coupling between S_1 and a second excited singlet state.[110]

As an alternative method for the evaluation of the change in geometry upon $^1B_{3u} \leftarrow {}^1A_g$ excitation, Meyling, van der Werf, and Wiersma[111] (1974) applied a one-dimensional Franck-Condon analysis to the intensity profile of a vibrational progession within this transition. Their results differed significantly from those obtained from rotational analyses. This Franck-Condon calculation predicted, in agreement with the qualitative molecular orbital arguments of Mason,[107] that the geometry change is rather small.

In 1977 Smalley, Wharton, Levy, and Chandler[112] studied the fluorescence of *s*–tetrazine in a supersonic expansion and resolved the geometry conflict by revealing an axis interchange involving the nearly degenerate A and B (in plane) inertial axes upon excitation from ^1A_g to $^1B_{3u}$. This interchange results in an altered set of rotational selection rules (relative to those which apply when no interchange occurs) which when applied to the analysis of the rotational structure of the 0-0 band of this transition[112,113] gave results for the change in geometry upon excitation that were in

agreement with the Franck-Condon analyses of vibronic intensity profiles;[111,114] that is, the change upon electronic excitation is relatively small. Finally, the recent work of Thakur, Job, and Kartha[105] has yielded very precise values for the three rotational constants of the ground state.

3.1.2 $T_1 \leftarrow S_0$ Spectroscopy

The lowest energy ground state electronic transition is the spin-forbidden $^3B_{3u} \leftarrow {}^1A_g$ transition with origin at 13 608 cm^{-1}. While this transition involves the same n (HOMO) $\rightarrow \pi^*$ (LUMO) spatial molecular orbitals as the $S_1 \leftarrow S_0$ transition, the electronic spin coordinates are coupled as triplet rather than singlet. Only one rovibronic study of this transition has been reported. Livak and Innes[115] (1971) collected absorption data, and from this, assigned five fundamental vibrational frequencies. Additionally, the geometry change upon excitation was determined by means of a Franck-Condon analysis. This analysis predicted a rather small $\Delta_{geometry}$ with the exception of the N-N bond distance which was predicted to contract significantly relative to the ground state equilibrium N-N bond distance.

3.1.3 Excited State Dynamics and Photochemistry

While the mechanisms for the relaxation of electronically excited *s*–tetrazine have been well studied experimentally, there is still no consensus as to the details of these mechanisms. As with the spectroscopic studies, the majority of the mechanistic studies have focused on the $^1B_{3u} \leftarrow {}^1A_g$ transition (i.e. relaxation from the first excited singlet state). Chowdhury and Goodman[116] (CG, 1962) first reported fluorescence from this state of *s*–tetrazine in a hydrocarbon glass. At that time, theirs was

the first reported fluorescence from an $n \rightarrow \pi^*$ state of an aza-substituted benzene. In a second more detailed paper,[117] CG reported a very short radiative lifetime for this fluorescence process, thus indicating that the majority of relaxation occurs through one or more non-radiative pathways. Vemulapalli and Cassen[118] (VC) subsequently reported fluorescence data from this same transition in the vapor phase. Again a short fluorescence lifetime was measured resulting in a quantum yield of 0.01-0.05 for fluorescence. VC proposed a statistical limit, unimolecular, non-radiative relaxation to a state of lower energy as the major dynamic pathway because no collisional quenching of the fluorescence was observed upon addition of several inert gases.

Further investigations of the relaxation from the $^1B_{3u}$ state, as well as the $^3B_{3u}$ state, were reported by McDonald and Brus (MB) in 1973.[119] They concluded, based on the densities of vibrational levels for possible relaxation pathways and the absence of phosphorescence after $^1B_{3u} \leftarrow {}^1A_g$ excitation, that the state of lower energy into which the first excited singlet relaxed was most probably the ground state. Furthermore, MB observed weak phosphorescence after the $^3B_{3u} \leftarrow {}^1A_g$ transition. This phosphorescence also displayed a negligible quantum yield (≤ 0.01) and thus a non-radiative relaxation pathway was proposed here as well. However, at that time, it was not clear whether the $^3B_{3u}$ state was relaxing directly into the ground state or into a proposed lower triplet state.

Hochstrasser and King[120] (1974) reported studies of the dynamics of the $^1B_{3u}$ and $^3B_{3u}$ states in the crystalline state. The conclusion of MB that the $^1B_{3u}$ state relaxes via a statistical limit process into the ^1A_g state was confirmed. Additionally, it was concluded that the $^3B_{3u}$ state is the lowest triplet state, and it too undergoes a

statistical limit, radiationless transition into the ground state. The most significant result to come out of this study was the observation of decomposition of *s*–tetrazine upon photoirradiation. It was proposed that the photodecomposition may be an important relaxation pathway. Meyling *et. al.*[111] measured a photodecomposition quantum yield of 1.3 ± 0.3 for the $^1B_{3u}$ state. It was concluded that the ultimate fate of a $^1B_{3u}$ excited *s*–tetrazine molecule was dissociation. However, the lifetime of this state may be determined by either the dissociation process itself or internal conversion to the ground state prior to dissociation.

Based on infrared spectra used to follow the photoreaction in molecular crystals, Hochstrasser and King[121] (1975) suggested that the observed photoprocess was

$$s\text{–tetrazine} \xrightarrow{h\nu} N_2 + 2\,HCN \qquad (3.1)$$

Furthermore, it was reported that the rate of relaxation from S_1 was 10^5 times that from T_1, implying that the reaction proceeds along a spin singlet reaction path. Additionally, HK were successful in selectively promoting the photochemical process for *s*–tetrazine isotopes containing ^{13}C, ^{15}N, and deuterium, thus revealing an elegant and effective method for the enrichment of carbon, nitrogen, and hydrogen isotopes in both the reactant and product molecules. Karl and Innes[122] (1975) also reported a highly effective laser induced isotope separation scheme using gaseous *s*–tetrazine.

Hochstrasser and coworkers published more detailed reports of their isotope enrichment experiments on *s*–tetrazine in mixed crystals with benzene[123] and in an argon matrix.[124] In these reports the enthalpy change for the ground state dissociation, Eq. (3.1), was estimated at approximately 1 kcal/mol exothermic based on an extrapolation of available combustion data for other azines. It was also pointed out

that the dissociation of the $^1B_{3u}$ state could yield neither electronically excited HCN nor electronically excited N_2 because both of these would lie well above the energy available to the zero point level of the S_1 state. Therefore, at some point along the reaction path prior to dissociation, relaxation to the ground electronic state must take place. Additionally, HK[123] concluded that the presence of a bi-radical intermediate is unlikely based on comparison of the $^1B_{3u}$ vs $^3B_{3u}$ dynamic data. Further elucidation of the relaxation process was provided by King, Denny, Hochstrasser, and Smith[125] in 1977. It was demonstrated, by selectively promoting the photoreaction for 1,4-*s*–tetrazine-$^{15}N_2$, that no 1 to 4 nitrogen bonding (i.e. no cross ring bonding) occurs to form the product N_2.

Hochstrasser, King, and Smith[126] (1977) proposed the following process as a likely dissociation scenario

$$\text{cold } {}^1A_g \text{ } s\text{–tetrazine} \xrightarrow{h\nu} \text{rovib. manifold of } {}^1B_{3u} \text{ } s\text{–tetrazine} \rightarrow$$

$$\text{vib. \& rot. hot } {}^1A_g \text{ } s\text{–tetrazine} \rightarrow \underset{\text{rovib. manifold}}{\text{ground state}} \text{ of } [2HCN + N_2]. \qquad (3.2)$$

They also concluded, based on symmetry and density of states arguments, that the C-H stretching modes are important in coupling the nonradiative transition from S_1 to S_0.

In 1978 Coulter, Dows, Reisler, and Wittig studied the vibrational energy distribution in the product molecules, $2HCN + N_2$.[127] First, they estimated the ground state $\Delta H_{\text{dissociation}} \approx -51$ kcal/mol (this estimate differed markedly from that of

Hochstrasser and King[123] ≈ −1 kcal/mol). This estimate yields a $\Delta H_{photodiss.} \approx -108$ kcal/mol. It was then found that ≤ 2% of this $\Delta H_{photodiss.}$ occupies the stretching vibrations of HCN and N_2. Therefore, it was concluded that the majority of the relaxation energy is distributed among the HCN bending mode and rotational/translational motion.

Burland, Carmona, and Pacansky (BCP)[128] (1978) demonstrated that both substituent effects and the bulk chemical environment are crucial in determining the relaxation process for electronically excited *s*-tetrazines. They found, contrary to the results of previous experiments,[126] that di-methyl-*s*–tetrazine (DMT) exhibits no photodissociation in either a room temperature hexane solution or in a low temperature argon matrix. Furthermore, it was shown that, in organic mixed crystals, the photodissociation of both *s*–tetrazine and DMT occurs via a two photon process. It had been previously concluded that the dissociation of all tetrazines occured via one photon processes with a quantum yield of near unity. Glownia and Riley[129] (1980) also found no evidence for the previously suggested one-step unimolecular dissociation process of vapor phase *s*–tetrazine [124,125] and proposed a two step/two photon dissociation.

The vibrational relaxation time for a single quantum of the 703 cm^{-1} a_g mode in the $^1B_{3u}$ state was determined to be ≤ 8 ps by Barbara, Brus, and Rentzepis[130] in 1980. This demonstrated that vibrational relaxation within the S_1 state is most likely not a rate determining step for the excited state dynamic process (and it is certainly not rate determining with regard to this particular a_g mode). Also in 1980, Aartsma, Hesselink, and Wiersma[131] reported the analysis of a resonant CARS spectrum of *s*–tetrazine vapor and proposed that the photochemical reaction rate is enhanced by

increasing the principle rotational quantum number for a given vibronic level in the S_1 state.

Paczkowski, Pierce, Smith, and Hochstrasser[132] (1980) reported a detailed study of the relative quantum yields of fluorescence vs non-radiative/non-dissociative relaxation vs photodissociation of DMT in the vapor phase as a function of excitation wavelength. They found, first of all, that the dominant process at all wavelengths was non-radiative/non-dissociative relaxation. Secondly, they proposed a "bottleneck state" along the tetrazine relaxation pathway from which either photodissociation or non-radiative/non-dissociative relaxation could result depending on the stability of the proposed bottleneck. It was further proposed that the stability of this bottleneck may be greatly influenced by substituent and environmental effects, thus rationalizing the observations of BCP[128] discussed above. This bottleneck state could also be used to rationalize the two photon dependence observed by BCP[128] and Glownia and Riley.[129]

Brumbaugh, Haynam, and Levy[104] have found that the $^1B_{3u}$ fluorescence lifetime depends on the single vibronic level from which relaxation originates; however, there was no evidence for the dependence of this lifetime on the excess vibrational energy in the excited state (i.e. mode dependence was observed, but not energy dependence).

Very recently Kiermeier, Dietrich, Riedle, and Neusser[133] (1986) analyzed the homogeneous linewidths of two vibronic bands within the $^1B_{3u} \leftarrow {}^1A_g$ electronic transition in the vapor phase and concluded, contrary to the proposal of Glownia and Riley,[129] that the dynamics of the S_1 state was dominated by a primary, nonradiative electronic process. These authors suggested a statistical process of internal

conversion to the ground state followed by dissociation (as originally proposed in reference 126, see Eq. (3.2)).

3.1.4 *s*-Tetrazine van der Waals Systems

The spectroscopic studies of *s*–tetrazine and its methyl and dimethyl substituted analogues in supersonic expansions with argon, helium, and H_2 carrier gases have yielded both absorption and fluorescence bands which can not be assigned to the isolated tetrazine framework.[104,112,134] These bands have been assigned to vibronic transitions involving van der Waals complexes of tetrazine-Ar,He,H_2 and tetrazine dimers, thus comprising the first studies of rare gas-polyatomic and polyatomic-polyatomic van der Waals molecules. Further experiments have led to the characterization of these weakly bound systems[134–141] with particular emphasis on structures, binding energies, vibrational energies of the van der Waals bond, and the dynamics and possible mode specificity of energy transfer between the tetrazine unit and the van der Waals bond.

3.1.5 Previous Theoretical Studies

The *s*–tetrazine molecule has been studied using several different methods of electronic structure theory. The earliest molecular orbital approaches applied to this system were based on Pariser-Parr-Pople (PPP) type π electron theory. Both Paoloni[142] (1956) and Mataga[143] (1958) used this approach to calculate $\pi \rightarrow \pi^*$ excitation energies along with the oscillator strengths associated with these transitions. Flurry, Stout, and Bell[144] (1967) extended the earlier PPP calculations by including all of the off-diagonal core Hamiltonian matrix elements in their π electron

calculations. In this study $\pi \rightarrow \pi^*$ excitation energies and π orbital ionization potentials were reported. In 1968 a PPP + 4 electron/4 orbital configuration interaction calculation including single excitations from the one-particle reference configuration was carried out by Pukanic, Forshey, Wegener, and Greenshields.[145] $\pi \rightarrow \pi^*$ excitation energies and π orbital ionization potentials were reported there as well.

The first attempt at including the nitrogen lone-pair orbitals in an electronic structure calculation was reported in 1971 by Sundbom.[146] A modified PPP scheme was employed, and results for the excitation energies of both $n \rightarrow \pi^*$ and $\pi \rightarrow \pi^*$ transitions were reported along with ionization potentials. Ridley and Zerner[147] went beyond the PPP method and calculated orbital energies, excitation energies, and oscillator strengths based on an INDO theory. In 1975 Dewar employed a MINDO theory to calculate the heats of formation and dissocation for the ground state of *s*–tetrazine.[148]

Three *ab initio* studies of the electronic structure of *s*–tetrazine have also been reported. Almlöf, Roos, Wahlgren, and Johansen[149] (1973) have used Hartree-Fock theory with a double-ζ like basis set to calculate the ionization potentials for the ground state and compared their results with photoelectron spectra. A similar study using both a minimum basis set and a double-ζ basis set has been carried out by Palmer, Gaskell, and Findlay[150] (1974). T. K. Ha reported a study of the electronic states of *s*–tetrazine in 1975.[151] Two small basis sets were employed for Hartree-Fock + limited multi-step configuration interaction (18 electrons/16 orbitals) calculations. The vertical excitation energies of the 22 lowest electronic states were reported.

Finally, four more recent papers have reported results for (1) radiative triplet lifetimes using an INDO method,[152] (2) excited triplet energies employing a CNDO + 2nd order perturbation calculation,[153] (3) ionization potentials using a Green's function approach,[154] and (4) excitation energies for the first excited singlet, triplet, and quintet states employing an INDO + configuration interaction method.[155]

3.1.6 Goals of the Present Study

In spite of the long and abundant history of research, both experimental and theoretical, focused on this molecule, there still remain many questions which have not yet been addressed or are not yet unambiguously resolved. In this study the standard methods of *ab initio* electronic structure theory have been employed to characterize the ground and excited electronic states of *s*–tetrazine. In particular, the equilibrium geometries and harmonic vibrational frequencies (along with infrared absorption intensities) for the S_0, S_1, and T_1 states have been predicted theoretically. In order to critically evaluate both the experimental data and the theoretical predictions, the results of the present work are compared to the spectroscopic results. Additionally, excitation energies, D_{2h} stationary point geometries and harmonic vibrational frequencies + infrared absorption intensities for several other low-lying electronic states are reported. Again these results are compared to the experimental spectral assignments where available. One point of particular interest here is the possble interaction between two electronic states which are proximate in energy. This interstate vibronic coupling has been proposed by several authors.[102,110,156] An additional goal of the present study is to elucidate the thermochemistry and possible mechanisms associated with the photodissociation of *s*–tetrazine.

In what follows is presented (1) a discussion of the theoretical methods employed for this study; (2) the results of the present study including a discussion of electronic excitation energies, the structures, energetics, and harmonic vibrational frequencies + infrared absorption intensities of the S_0, T_1, and S_1 states, and a discussion of higher excited states; and (3) a review of the present theoretical predictions for the mechanism and thermochemistry of the photodissociation of *s*–tetrazine.

3.2 Theoretical Method

This is the first theoretical study of *s*–tetrazine in which full geometry optimizations have been carried out. To this end the methods of restricted Hartree-Fock (RHF) theory have been employed to obtain energies[7] and analytic energy first and second derivatives[157] for the low-lying electronic surfaces of *s*–tetrazine. All structures were precisely optimized such that no energy gradient was greater than 10^{-7} hartrees / bohr.

For these self-consistent field (SCF) RHF calculations, two atomic orbital bases were utilized: (1) the standard Huzinaga-Dunning double-ζ (DZ) basis set[12,15] designated C,N (9s 5p/4s 2p), H (4s/2s) consisting of 64 contracted Gaussian functions, and (2) basis set 1 augmented with a set of polarization functions at all atomic centers. This DZ+P basis consisted of 106 contracted Gaussian functions. The polarization functions consisted of six primitive d-like functions per carbon and nitrogen center with Gaussian exponents $\alpha_C = 0.75$, $\alpha_N = 0.80$ along with a set of p-functions at each hydrogen center with $\alpha_H = 0.75$. For all theoretical treatments the hydrogen s-functions were scaled by a factor of 1.2.

In order to characterize all SCF stationary points, analytic energy second derivatives[157] were evaluated with respect to cartesian displacements; harmonic vibrational frequencies were obtained, and assignments of the normal modes were made based on a well chosen set of symmetrized internal coordinates. All optimizations initially restricted the molecular framework to D_{2h} symmetry; however, based on the second derivative calculations, only the S_0, T_1, and T_5 states were found to be genuine minima within this restriction. In the case of the S_1 state, this restriction could be relaxed without collapse of the single determinant excited state wavefunction to the ground state. Thus the equilibrium geometry for this state was also located.

In addition to the standard SCF second derivative method, the excited state second derivative method of Fitzgerald and Schaefer[158] was employed to predict the harmonic vibrational frequencies on the S_1 surface. This technique, based on the theory of Davidson and Stenkamp,[159] eliminates the non-variational collapse of the excited state wavefunction for displacements which lower the symmetry of the nuclear framework such that the excited state wavefunction is no longer orthogonal to that of the ground state.

Before presentation of the present theoretical results, the method used in assigning the theoretical vibrational frequencies warrants further discussion here. The majority of experimental assignments for the vibrational motions of *s*–tetrazine have been based on Wilson's nomenclature for the normal modes of benzene.[160] During the course of the present study, it became clear that in many cases (excited electronic states in particular) there is no clear analogue between the *s*–tetrazine motions and any of the benzene normal modes. As Innes and co-authors stated in their review,[100]

> A further difficulty ... resides in correlating the azine frequencies with particular benzene frequencies. With each nitrogen substituent, three degrees of freedom are lost, and it is not always evident which of two benzene modes most nearly approximates the motion in an azine.

Consequently, in the present work, the Wilson scheme has not been utilized in labeling the normal modes of *s*–tetrazine; rather, these assignments have been based on the symmetry of the motion and the potential energy distributions arising from contributions of each of the defined symmetrized internal coordinates (Figure 4) to the total potential for the displacement of a given mode.

Finally, in order to predict electronic excitation energies more accurately, single point configuration interaction energy wavefunctions including all single and double excitations out of the RHF reference configuration (CISD) were determined at the RHF stationary points. For all of these CISD wavefunctions, the molecular orbitals corresponding to the carbon and nitrogen 1s atomic orbitals were held inactive along with the six highest lying virtual orbitals. Davidson's correction for unlinked clusters,[92] designated herein as CISD(+Q), was also used to predict electronic excitation energies. In addition single point coupled cluster energies (with the cluster operator truncated at $T_1 + T_2$), CCSD, were obtained for the closed-shell structures investigated. Again the same six core and six virtual orbitals from the RHF reference determinant were held inactive within the CCSD approach.

3.3 Results and Discussion

The ground state electron configuration for *s*–tetrazine is as follows.

$$1b_{2u}^2\ 1a_g^2\ 1b_{3g}^2\ 1b_{1u}^2\ 2a_g^2\ 2b_{1u}^2\ 3a_g^2\ 2b_{2u}^2\ 3b_{1u}^2\ 2b_{3g}^2\ 4a_g^2\ 3b_{2u}^2\ 5a_g^2\ 4b_{1u}^2\ 1b_{3u}^2\ 4b_{2u}^2\ 6a_g^2\ 5b_{1u}^2\ 1b_{1g}^2\ 1b_{2g}^2\ 3b_{3g}^2$$

Among the six highest occupied molecular orbitals, the $4b_{2u}$, $6a_g$, $5b_{1u}$, and $3b_{3g}$ are the in plane nitrogen lone-pair orbitals, while the $1b_{1g}$ and $1b_{2g}$ are the two highest energy occupied π orbitals. The two LUMOs, $1a_u$ and $2b_{3u}$, are both of type π^*. These eight valence orbitals are illustrated qualitatively in Figure 3.

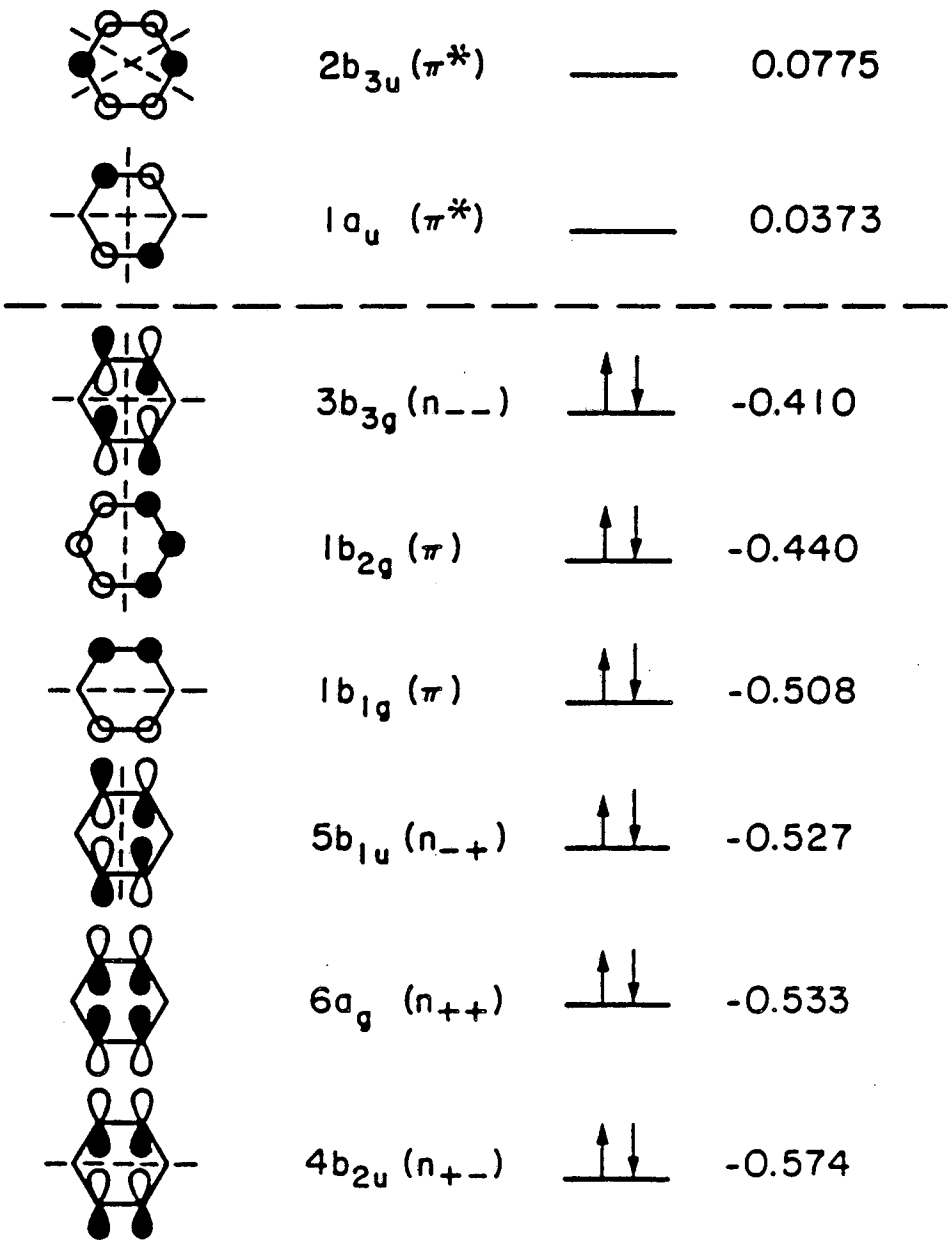

Figure 3: The six HOMOs and two LUMOs for the $\tilde{X}\ ^1A_g$ state of *s*–tetrazine. Orbital energies are expressed in hartrees. The signs associated with the lone-pair orbitals denote their symmetry with respect to reflection in the xy and xz planes, respectively.

3.3.1 Electronic Excitation Energies

Table VI lists the thirteen lowest electronic states of *s*–tetrazine predicted by this theoretical study. The SCF, single point CISD and Davidson corrected CISD energies using the DZ and DZ+P basis sets are listed here (in eV), and are expressed relative to the corresponding energy calculations at the ground state surface SCF equilibrium geometry. As indicated in Table VI, only the S_0 (^1A_g), T_1 ($^3B_{3u}$), and T_5 ($^3B_{1g}$) states are minima in D_{2h} symmetry at the DZ SCF level. The DZ SCF surfaces for the remaining ten states are characterized by at least one imaginary vibrational frequency at their respective D_{2h} stationary points. The calculated excitation energies for nine of these ten electronic states are thus not true 0-0 excitation energies, but most likely are not considerably greater than $\Delta E_{0\text{-}0}$. In the case of the S_1 (^1A_u C_{2h} symmetry / $^1B_{3u}$ D_{2h} symmetry) state, the C_{2h} equilibrium lies only 534 cm^{-1} below the D_{2h} supertransition state on the DZ SCF S_1 surface. The difference shrinks to 132 cm^{-1} on the DZ+P SCF surface.

Table VI. Electronic excitation energies for low lying states of *s*-tetrazine.

Electronic State (Orbital Excitation)	Vertical Excitation Energy (eV)						Adiabatic Excitation Energy (eV)						Expt. (eV)
	DZ Basis			DZ+P Basis			DZ Basis			DZ+P Basis			
	SCF	CISD[a]	CISD(+Q)[a]	SCF	CISD[a]	CISD(+Q)[a]	SCF	CISD[a]	CISD(+Q)[a]	SCF	CISD[a]	CISD(+Q)[a]	
^1A_g	0.00	0.00	0.00	0.00	0.00	0.00	0.00	0.00	0.00	0.00	0.00	0.00	0.00
$^3B_{3u}$ $(3b_{3g} \rightarrow 1a_u)$	2.65	1.98	1.80	3.09	2.44	2.23	2.65	1.98	1.81	2.94	2.34	2.15	1.69[d]
S_1[h] $(3b_{3g} \rightarrow 1a_u)$	3.53	2.81	2.60	3.78	3.11	2.89	3.32	2.67	2.49	3.61	3.00	2.80	2.25[e]
^3A_u $(3b_{3g} \rightarrow 2b_{3u})$	4.78	3.80	3.50	5.11	4.21	3.89	3.54[b]	2.89	2.71	3.92[c]	3.23	2.98	—
^1A_u $(3b_{3g} \rightarrow 2b_{3u})$	5.05	4.03	3.72	5.40	4.46	4.13	3.78[b]	3.10	2.90	4.16[c]	3.45	3.18	—
$^3B_{1u}$ $(1b_{2g} \rightarrow 2b_{3u})$	4.85	5.15	5.15	4.82	5.10	5.14	3.47[b]	3.77	3.78	3.63[c]	3.96	3.95	—
$^3B_{2u}$ $(1b_{2g} \rightarrow 1a_u)$	4.47	5.05	5.19	4.20	4.69	4.86	4.16[b]	4.43	4.46	4.10[c]	4.34	4.34	—
$^3B_{1g}$ $(5b_{1u} \rightarrow 1a_u)$	6.17	5.11	4.75	6.35	5.43	5.08	6.13	5.10	4.76	6.41[c]	5.42	5.02	—
$^3B_{2g}$ $(4b_{2u} \rightarrow 1a_u)$	6.87	6.01	5.73	7.33	6.55	6.25	5.84[b]	4.79	4.41	6.39[c]	5.49	5.06	—
$^1B_{2g}$ $(4b_{2u} \rightarrow 1a_u)$	7.47	6.55	6.18	7.89	7.06	6.72	6.41[b]	5.31	4.86	6.93[c]	6.00	5.54	3.88, 4.06[f]
$^1B_{1g}$ $(5b_{1u} \rightarrow 1a_u)$	7.15	6.04	5.63	7.21	6.24	5.85	7.12[b]	6.02	5.61	7.29[c]	6.23	5.78	—
$^1B_{2u}$ $(1b_{2g} \rightarrow 1a_u)$	7.30	6.63	6.22	7.25	6.71	6.38	6.98[b]	6.02	5.49	7.25[c]	6.71	6.38	4.43-5.40[g]
$^1B_{1u}$ $(1b_{2g} \rightarrow 2b_{3u})$	8.90	8.52	8.35	8.64	8.27	8.10	8.08[b]	7.48	7.23	8.03[c]	7.49	7.17	—

[a] Single point energy calculation at corresponding SCF stationary point.

[b] This excitation is to a non-equilibrium structure on the DZ SCF excited state surface

[c] Single point DZ+P SCF energy calculation at corresponding DZ SCF stationary point.

[d] 0-0 excitation band; Reference 21.

[e] 0-0 excitation band; Reference 3.

[f] See text and Reference 3.

[g] Broad band with maximum at 5.01 eV; Reference 4.

[h] ^1A_u within C_{2h} symmetry; $^1B_{3u}$ within D_{2h} symmetry.

There are several points to be noted regarding the results in Table VI. First, in comparing the theoretical "adiabatic" excitation energies with those measured spectroscopically, single point DZ CISD(+Q) theory overestimates the experiments[97,115] by 7.1% for the first excited triplet and by 10.7% for the first excited singlet while the corresponding DZ+P predictions overestimate the experiments by 27.2% and 24.4%, respectively. Using this as a guide, I concur with Ha[151] that the broad band observed by SCW[98] at 4.43-5.40 eV (with maximum at 5.01 eV) is the first $\pi \rightarrow \pi^*$ excited singlet state, $^1B_{2u}$. If one takes the band maximum at 5.01 eV as the band origin (this has not been determined spectroscopically), then DZ CISD(+Q) overshoots the experimental excitation energy by 9.5% and DZ+P by 27.3%. This seems consistent with the discrepancies exhibited by T_1 and S_1.

A second point of interest is the location of S_2, the ^1A_u state. The results of Ha[151] predicted a vertical excitation energy of 4.78 eV, and consequently, the $n \rightarrow \pi^*$ transition observed by Mason[97] at 3.88 eV in cyclohexane and at 4.06 eV in water, was assigned to the $^1A_u \leftarrow {}^1A_g$ transition.[151] The present study predicts a vertical excitation energy significantly smaller than that determined by Ha, namely 3.72 eV DZ CISD(+Q) and 4.13 eV DZ+P CISD(+Q). Furthermore the difference between the vertical and adiabatic excitation energies is quite large for this state with the present theoretical adiabatic predictions being 2.90 eV and 3.18 eV for DZ and DZ+P CISD(+Q), respectively. It it thus suggested that the previous assignment[151] of the bands observed by Mason[97] be revised.

The most likely candidates for the Mason bands appear to be either (1) the $n \rightarrow \pi^*$ $^1B_{2g}$ state which DZ and DZ+P CISD(+Q) results predict to lie at 4.86 eV and 5.54 eV, respectively. This assignment results in rather large discrepancies with experiment of 19.7% (DZ) and 36.5% (DZ+P); or (2) a second $n \rightarrow \pi^*$ $^1B_{3u}$ state.

Although the second $^1B_{3u}$ surface is not accessible using a single determinant theory, Ghosh and Chowdhury have recently identified the analogous state for 3,6-diphenyl-*s*-tetrazine with band origin at 3.25 eV.[161] Additionally, Ha has predicted a vertical excitation energy of 5.10 eV for this state.

If the electronic states are listed in ascending energetic order for the different levels of theory applied in the present study, one finds for the vertical order,

DZ SCF

$$^1A_g < {}^3B_{3u} < {}^1A_u / {}^1B_{3u} < {}^3B_{2u} < {}^3A_u < {}^3B_{1u} < {}^1A_u < {}^3B_{1g} < {}^3B_{2g} < {}^1B_{1g} < {}^1B_{2u} < {}^1B_{2g} < {}^1B_{1u}$$

DZ CISD

$$^1A_g < {}^3B_{3u} < {}^1A_u / {}^1B_{3u} < {}^3A_u < {}^1A_u < {}^3B_{2u} < {}^3B_{1g} < {}^3B_{1u} < {}^3B_{2g} < {}^1B_{1g} < {}^1B_{2g} < {}^1B_{2u} < {}^1B_{1u}$$

DZ CISD(+Q)

$$^1A_g < {}^3B_{3u} < {}^1A_u / {}^1B_{3u} < {}^3A_u < {}^1A_u < {}^3B_{1g} < {}^3B_{1u} < {}^3B_{2u} < {}^1B_{1g} < {}^3B_{2g} < {}^1B_{2g} < {}^1B_{2u} < {}^1B_{1u}$$

DZ+P SCF and CISD

$$^1A_g < {}^3B_{3u} < {}^1A_u / {}^1B_{3u} < {}^3A_u < {}^1A_u < {}^3B_{2u} < {}^3B_{1u} < {}^3B_{1g} < {}^1B_{1g} < {}^3B_{2g} < {}^1B_{2u} < {}^1B_{2g} < {}^1B_{1u}$$

DZ+P CISD(+Q)

$$^1A_g < {}^3B_{3u} < {}^1A_u / {}^1B_{3u} < {}^3A_u < {}^1A_u < {}^3B_{2u} < {}^3B_{1g} < {}^3B_{1u} < {}^1B_{1g} < {}^3B_{2g} < {}^1B_{2u} < {}^1B_{2g} < {}^1B_{1u}$$

and for the adiabatic order,

DZ SCF

$$^1A_g < {}^3B_{3u} < {}^1A_u / {}^1B_{3u} < {}^3B_{1u} < {}^3A_u < {}^1A_u < {}^3B_{2u} < {}^3B_{2g} < {}^3B_{1g} < {}^1B_{2g} < {}^1B_{2u} < {}^1B_{1g} < {}^1B_{1u}$$

DZ CISD

$$^1A_g < {}^3B_{3u} < {}^1A_u / {}^1B_{3u} < {}^3A_u < {}^1A_u < {}^3B_{1u} < {}^3B_{2u} < {}^3B_{2g} < {}^3B_{1g} < {}^1B_{2g} < {}^1B_{2u} \leq {}^1B_{1g} < {}^1B_{1u}$$

DZ CISD(+Q)

$$^1A_g < {}^3B_{3u} < {}^1A_u / {}^1B_{3u} < {}^3A_u < {}^1A_u < {}^3B_{1u} < {}^3B_{2g} < {}^3B_{2u} < {}^3B_{1g} < {}^1B_{2g} < {}^1B_{2u} < {}^1B_{1g} < {}^1B_{1u}$$

DZ+P SCF

$$^1A_g < {}^3B_{3u} < {}^1A_u / {}^1B_{3u} < {}^3B_{1u} < {}^3A_u < {}^3B_{2u} < {}^1A_u < {}^3B_{2g} < {}^3B_{1g} < {}^1B_{2g} < {}^1B_{2u} < {}^1B_{1g} < {}^1B_{1u}$$

DZ+P CISD and CISD(+Q)

$$^1A_g < {}^3B_{3u} < {}^1A_u / {}^1B_{3u} < {}^3A_u < {}^1A_u < {}^3B_{1u} < {}^3B_{2u} < {}^3B_{1g} < {}^3B_{2g} < {}^1B_{2g} < {}^1B_{1g} < {}^1B_{2u} < {}^1B_{1u}$$

Considering both the vertical and adiabatic order of states, it is clear that the closed-shell ^1A_g state is the electronic ground state, $^3B_{3u}$ is T_1, ^1A_u [C_{2h}] / $^1B_{3u}$ [D_{2h}] is S_1, and the $^1B_{1u}$ state is the highest energy state found here. It is also evident (with the exception of the the DZ SCF results) that the ^3A_u state is T_2 and the ^1A_u state is S_2. Conversely, the qualitative picture of states $T_3 - T_6$ and $S_3 - S_5$ is not so clear at present.

In progressing SCF → CISD → CISD(+Q) the $^3B_{1g}$ and $^3B_{2g}$ states exhibit a significant decrease in ΔE, both adiabatic and vertical. This trend was found to hold for all of the states investigated in the present study with the exception of the $^3B_{1u}$ and $^3B_{2u}$ states which exhibit an increase (or no change) in ΔE with the inclusion of electron correlation. Thus the relative order of these four triplet states varies with the level of theory. Additionally, while the $^3B_{2u}$ and $^3B_{1g}$ energies do not decrease greatly in relaxing from the ground state equilibrium geometry to their adiabatic geometries, the $^3B_{1u}$ and $^3B_{2g}$ states exhibit a rather large energy lowering. Thus, the vertical vs adiabatic order of these four states shows significant variation as well. As

pointed out by Hochstrasser and King,[120] the location of the $^3B_{2g}$ state is of great interest because this state would provide a pathway (through vibronic mixing with $\tilde{a}\ ^3B_{3u}$) for the rapid intersystem crossing of T_1 to S_0.

Variation is also observed within the states $S_3 - S_5$ ($^1B_{2u}$, $^1B_{2g}$, $^1B_{1g}$). Here, all three singlets exhibit a significant decrease in ΔE with the inclusion of electron correlation; however, the relative increase in ΔE with the addition of polarization functions is much greater for the $^1B_{2g}$ state than for the other two.

In general it is found here that (1) if the effect of electron correlation in the form of the CISD approximation is to decrease (increase) the SCF electronic excitation energy, then the Davidson correction decreases (increases) ΔE further but by a smaller amount; however, the correlation energy is not yet converged. In fact as discussed in Section 2.2.4, the Davidson correction greatly underestimates the effect of unlinked quadruple excitations in the ground state equilibrium of *s*–tetrazine; (2) the electronic excitation energies are sensitive to the basis set, and although the changes observed in ΔE in going from DZ to DZ+P are in general not as large as those associated with correlating the electrons, the theoretical results are not yet converged with respect to basis set. In order to obtain a truly accurate description of the energetics and order of the low-lying electronic states of *s*–tetrazine, it seems one would need to apply well correlated wavefunctions constructed from large basis sets. It remains to be seen how much correlation (both dynamic and non-dynamic) and how large a basis will be required.

3.3.2 $\tilde{X}\ ^1A_g$ State

As discussed in Section 3.1.1, the ground state of *s*–tetrazine has been extensively studied spectroscopically. This is the first report in which the properties of the ground state have been predicted independent of experiment. To calibrate the various relative energies quoted herein, Table VII lists the ground state absolute electronic energies obtained with the various basis sets and levels of theory. The results of Almlöf and coworkers,[149] Palmer and coworkers,[150] and Ha[151] are also included.

Table VII. Total electronic energies of the ground state of *s*–tetrazine. The correlated energies were calculated at the SCF stationary points

	Energy (hartrees)
DZ SCF	– 294.456 83
DZ CISD	– 294.960 43
DZ CISD(+Q)	– 295.039 85
DZ CCSD	– 295.064 50
DZ+P SCF	– 294.647 39
DZ+P CISD	– 295.380 46
DZ+P CISD(+Q)	– 295.503 48
DZ+P CCSD	– 295.544 46
Reference 150	– 293.474 8
Reference 149	– 294.150
Reference 151	– 294.229 4

The DZ SCF, DZ+P SCF, and experimentally determined (Job and Innes, 1978)[113] geometries are compared in Table VIII. As has been found for the ground states of smaller molecular systems,[19] DZ SCF theory is able to predict bond distances to an accuracy of 0.1%-0.8% (with the theoretical distances being shorter than the experimentally determined quantities). The addition of polarization functions in the present theoretical SCF procedures also follows the trends established for smaller molecular systems[19] in that the prediction for the NCN angle is greatly improved from 1.8% to 0.9% in error, and the predicted bond distances (with the exception of

the C-H bond) are now shorter still with errors in the range of 1%-2%. It should be noted that the DZ+P SCF N-N bond distance is 2.5% shorter that that determined by Job and Innes.[113] This error is somewhat larger than expected but not alarmingly so.

Table VIII. Comparison of equilibrium theoretical geometries of the ground state of *s*–tetrazine with the experimentally determined ground state geometry. Refer to Figure 4 for definition of internal coordinates. The experimental values are from reference 113.

	$\tilde{X}\ ^1A_g$ Geometry (bond distances in angstroms)		
	DZ SCF	DZ+P SCF	Expt.[a]
r_1	1.3392	1.3215	1.3405
s_1	1.3189	1.2923	1.3256
t_1	1.0643	1.0743	1.0726
α_1	124.03°	125.19°	126.36°

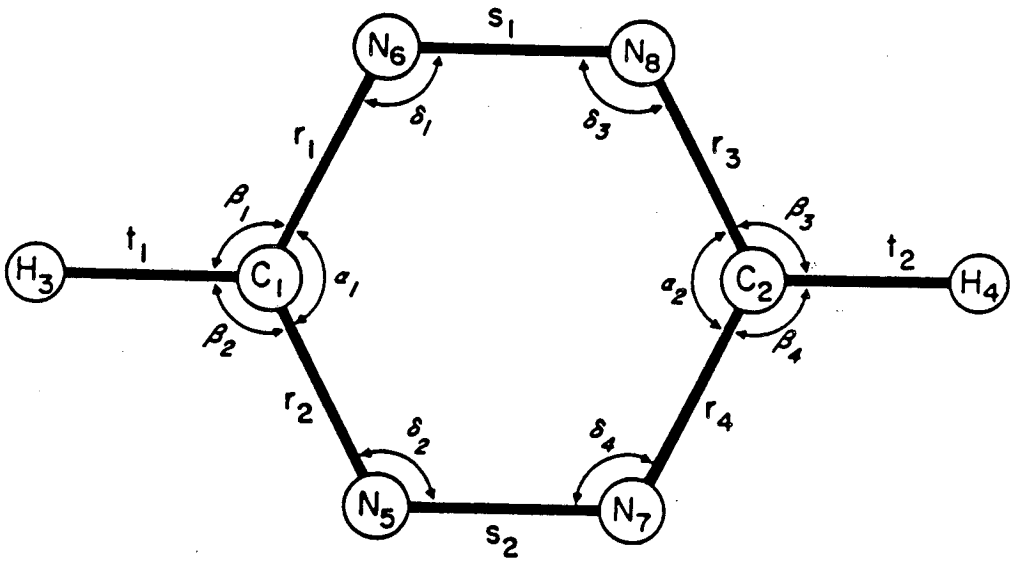

Figure 4: Definition of the simple internal coordinates for the *s*–tetrazine framework.

The DZ+P SCF harmonic vibrational frequencies are compared with the experimental assignments[101,103,105] in Table X. As mentioned above, the modes have been characterized by the percentage of the total potential involved in an infinitesimal displacement along a normal mode k from a symmetrized internal coordinate S_n. This percentage is given by

$$F_n(\%) \equiv \frac{\frac{1}{2}[\delta S_n^k]^2 F_{nn}}{\frac{1}{2}\sum_{i=1}^{3N-6}[\delta S_i^k]^2 F_{ii}} \times 100 \tag{3.3}$$

where F_{ij} is the force constant matrix under which the nuclei move. Figure 4 illustrates the set of internal coordinates which were used to construct the $3N-6 = 18$ orthonormal symmetrized internal coordinates. The 18 coordinates which are used to describe the normal modes are defined in Table IX for both the D_{2h} (S_0 and T_1 equilibria) and C_{2h} (S_1 equilibrium) point groups.

Table IX. Symmetrized internal coordinates for *s*-tetrazine in D_{2h} and C_{2h} symmetries. Refer to Figure 4 and footnote below[a] for definition of internal coordinates.

D_{2h} symmetry		C_{2h} symmetry	
a_g	$Q_1 = \frac{1}{\sqrt{2}}(\Delta t_1 + \Delta t_2)$	a_g	$Q_1 = \frac{1}{\sqrt{2}}(\Delta t_1 + \Delta t_2)$
a_g	$Q_2 = \frac{1}{\sqrt{2}}(\Delta s_1 + \Delta s_2)$	a_g	$Q_2 = \frac{1}{\sqrt{2}}(\Delta s_1 + \Delta s_2)$
a_g	$Q_3 = \frac{1}{2}(\Delta r_1 + \Delta r_2 + \Delta r_3 + \Delta r_4)$	a_g	$Q_3 = \frac{1}{\sqrt{2}}(\Delta r_1 + \Delta r_4)$
a_g	$Q_4 = \frac{1}{\sqrt{2}}(\Delta\alpha_1 + \Delta\alpha_2)$	a_g	$Q_4 = \frac{1}{\sqrt{2}}(\Delta r_2 + \Delta r_3)$
		a_g	$Q_5 = \frac{1}{\sqrt{2}}(\Delta\alpha_1 + \Delta\alpha_2)$
b_{2g}	$Q_5 = \frac{1}{\sqrt{2}}(\Delta\gamma_1 - \Delta\gamma_2)$	a_g	$Q_6 = \frac{1}{2}(\Delta\beta_1 - \Delta\beta_2 - \Delta\beta_3 + \Delta\beta_4)$
b_{2g}	$Q_6 = \frac{1}{\sqrt{2}}(\Delta\tau_1 - \Delta\tau_2)$	a_g	$Q_7 = \frac{1}{2}(\Delta\delta_1 - \Delta\delta_2 - \Delta\delta_3 + \Delta\delta_4)$
b_{3g}	$Q_7 = \frac{1}{2}(\Delta r_1 - \Delta r_2 - \Delta r_3 + \Delta r_4)$	b_g	$Q_8 = \frac{1}{\sqrt{2}}(\Delta\gamma_1 - \Delta\gamma_2)$
b_{3g}	$Q_8 = \frac{1}{2}(\Delta\beta_1 - \Delta\beta_2 - \Delta\beta_3 + \Delta\beta_4)$	b_g	$Q_9 = \frac{1}{\sqrt{2}}(\Delta\tau_1 - \Delta\tau_2)$
b_{3g}	$Q_9 = \frac{1}{2}(\Delta\delta_1 - \Delta\delta_2 - \Delta\delta_3 + \Delta\delta_4)$		
		a_u	$Q_{10} = \Delta\tau_3$
a_u	$Q_{10} = \Delta\tau_3$	a_u	$Q_{11} = \frac{1}{\sqrt{2}}(\Delta\gamma_1 + \Delta\gamma_2)$
		a_u	$Q_{12} = \frac{1}{\sqrt{2}}(\Delta\tau_4 - \Delta\tau_5)$
b_{1u}	$Q_{11} = \frac{1}{\sqrt{2}}(\Delta t_1 - \Delta t_2)$		
b_{1u}	$Q_{12} = \frac{1}{2}(\Delta r_1 + \Delta r_2 - \Delta r_3 - \Delta r_4)$	b_u	$Q_{13} = \frac{1}{\sqrt{2}}(\Delta t_1 - \Delta t_2)$
b_{1u}	$Q_{13} = \frac{1}{\sqrt{2}}(\Delta\alpha_1 - \Delta\alpha_2)$	b_u	$Q_{14} = \frac{1}{\sqrt{2}}(\Delta s_1 - \Delta s_2)$
		b_u	$Q_{15} = \frac{1}{\sqrt{2}}(\Delta r_1 - \Delta r_4)$
b_{2u}	$Q_{14} = \frac{1}{\sqrt{2}}(\Delta s_1 - \Delta s_2)$	b_u	$Q_{16} = \frac{1}{\sqrt{2}}(\Delta r_2 - \Delta r_3)$
b_{2u}	$Q_{15} = \frac{1}{2}(\Delta r_1 - \Delta r_2 + \Delta r_3 - \Delta r_4)$	b_u	$Q_{17} = \frac{1}{\sqrt{2}}(\Delta\alpha_1 - \Delta\alpha_2)$
b_{2u}	$Q_{16} = \frac{1}{2}(\Delta\beta_1 - \Delta\beta_2 + \Delta\beta_3 - \Delta\beta_4)$	b_u	$Q_{18} = \frac{1}{2}(\Delta\beta_1 - \Delta\beta_2 + \Delta\beta_3 - \Delta\beta_4)$
b_{3u}	$Q_{17} = \frac{1}{\sqrt{2}}(\Delta\gamma_1 + \Delta\gamma_2)$		
b_{3u}	$Q_{18} = \frac{1}{\sqrt{2}}(\Delta\tau_4 - \Delta\tau_5)$		

[a] γ_1: H_3–C_1 out of N_6–C_1–N_5 plane angle. γ_2: H_4–C_2 out of N_7–C_2–N_8 plane angle. τ_1: torsional angle between C_2–N_7–N_5 and N_7–N_5–C_1 planes. τ_2: torsional angle between C_2–N_8–N_6 and N_8–N_6–C_1 planes. τ_3: torsional angle between N_7–N_8–N_5 and N_8–N_5–N_6 planes. τ_4: torsional angle between C_1–N_5–N_8 and N_5–N_8–C_2 planes. τ_5: torsional angle between C_1–N_6–N_7 and N_6–N_7–C_2 planes.

Table X. Comparison of the DZ+P SCF harmonic vibrational frequencies with experimental fundamental frequency assignments for the $\tilde{X}\ ^1A_g$ state of *s*–tetrazine.

	Vibrational Frequencies (cm^{-1})			DZ+P SCF Potential Energy Distribution	
	DZ+P SCF[a]	Expt.	% difference[e]		
a_g	3423	3010[b]	13.7	$F_1(99)$	sym C-H stretch
a_g	1739	1415[b]	22.9	$F_2(61)\ F_3(24)\ F_4(14)$	sym N-N stretch
a_g	1171	1009[b]	16.1	$F_2(32)\ F_3(66)\ F_4(2)$	sym C-N stretch
a_g	817	736[b]	11.0	$F_3(10)\ F_4(89)$	sym N-C-N bend
b_{2g}	1087	994[b]	9.4	$F_5(90)\ F_6(10)$	out-of-plane C-H wag
b_{2g}	896	801[b]	11.9	$F_5(7)\ F_6(93)$	chair deformation
b_{3g}	1789	1525[b]	17.3	$F_7(73)\ F_8(19)\ F_9(8)$	C-N stretch
b_{3g}	1440	1291[b]	11.5	$F_7(15)\ F_8(85)$	in-plane C-H wag
b_{3g}	705	640[b]	10.2	$F_7(2)\ F_8(4)\ F_9(94)$	N-N-C bend
a_u	449	254[b]	76.8	$F_{10}(100)$	ring folding
b_{1u}	3421 (8.15)	3090[c]	10.8	$F_{11}(98)\ F_{13}(1)$	asym C-H stretch
b_{1u}	1373 (72.5)	1200[c]	14.4	$F_{12}(71)\ F_{13}(29)$	C-N stretch
b_{1u}	1183 (4.95)	...	...	$F_{12}(13)\ F_{13}(87)$	asym N-C-N bend
b_{2u}	1640 (0.414)	1435[b]	14.3	$F_{14}(20)\ F_{15}(10)\ F_{16}(70)$	in-plane C-H wag
b_{2u}	1269 (28.4)	1103[c]	15.0	$F_{14}(33)\ F_{15}(17)\ F_{16}(50)$	C-H wag+N-N stretch
b_{2u}	888 (111.)	882[d]	0.68	$F_{14}(44)\ F_{15}(54)\ F_{16}(2)$	C-N stretch+N-N stretch
b_{3u}	1022 (2.38)	904[b]	13.1	$F_{17}(94)\ F_{18}(6)$	out-of-plane C-H wag
b_{3u}	405 (53.9)	255[b]	58.8	$F_{17}(15)\ F_{18}(85)$	boat deformation

[a] Analytic infrared absorption intensities (km/mol) are noted in parentheses.

[b] Reference 103

[c] Reference 101

[d] Reference 105

[e] $\frac{|\omega_{DZ+P\ SCF} - \nu_{Expt.}|}{\nu_{Expt.}} \times 100$

In comparing the DZ+P SCF harmonic frequencies to experiment, one first notices that, in general, the agreement between theory and experiment is not very good. For most systems studied it has been found that DZ+P SCF harmonic frequencies overestimate the experimentally measured frequencies by 8%-13%;[19,162,163] this is generally attributed to the neglect of electron correlation in the SCF wavefunction and the neglect of anharmonic terms in the potential. In the case of the *s*–tetrazine

ground state, the 8%-13% error range seems to be a lower limit, and the discrepancy with experiment becomes as large as 59% and 77% for the two low frequency out-of-plane motions. For the majority of these normal modes, the source of these large differences can not be determined until a theoretical study including electron correlation and anharmonic effects is carried out; however, there are three points that can be discussed further.

The first point concerns the two b_{3u} modes on the ground state surface. In 1982 Innes investigated the vibronic coupling of S_0 to S_1 through the two b_{3u} modes.[164] The observed vibronic spectra were fit to a computer model which used the harmonic frequencies of these two modes as variable parameters. The values of these harmonics which gave the best fit between the observed spectrum and the computer generated spectrum were 411.5 cm^{-1} and 971 cm^{-1}. Comparing these two values to the harmonic frequencies predicted by DZ+P SCF theory, these being 405 cm^{-1} and 1022 cm^{-1}, respectively, one may conclude that the major contribution to the 59% discrepancy between theory and the experimental assignment in Table X for the low frequency b_{3u} mode is anharmonicity. Also the harmonized experimental value for the high frequency b_{3u} mode is now in much better agreement with the theoretical result, the error being reduced from 13% to 5%.

The second point concerns the two C-H stretching motions, a_g and b_{1u}. A point of contrast here between the present theoretical results and the results of Brumbaugh and Innes[103] is that the theoretically predicted SCF harmonic frequencies for these two modes differ by < 2 cm^{-1} with both the DZ and DZ+P basis sets. In contrast, the experimental a_g and b_{1u} fundamentals in Table X differ by 80 cm^{-1}. Experimentally, the 3090 cm^{-1} assignment for the asymmetric C-H stretch was extracted from

the gas phase infrared spectrum of *s*–tetrazine by Franks, Merer, and Innes in 1968.[101] In that same study the solid state Raman frequency for the symmetric C-H stretch was reported as 3090 cm^{-1} as well. This assignment is supported by the present theoretical study as pointed out above. More recently, however, the vapor phase fundamental for the symmetric C-H stretch was determined by Brumbaugh and Innes from vibronic fluorescence spectroscopy as 3010 cm^{-1}. Based on the present work, this revised assignment of the symmetric C-H stretch warrants further study. Additional evidence is gleaned from second derivative calculations on the benzene molecule using a DZ+d basis set[165] (polarization functions at carbon centers only). Assuming that DZ+polarization RHF theory is able to model the harmonic force field for C-H stretching motions equally well for benzene as for *s*–tetrazine, one would expect the theory vs experiment errors to be nearly equal when comparing the C-H stretching frequencies of these two aromatic rings. Making this comparison, one finds that the six theoretical DZ+d SCF C-H harmonic stretching frequencies for benzene and the DZ+P SCF asymmetric *s*–tetrazine C-H stretching harmonic are all in the range of 10%-11% greater than the experimentally determined fundamentals. Thus, the DZ+P SCF symmetric stretching harmonic for *s*–tetrazine at 13.7% greater than the 3010 cm^{-1} experimental assignment appears to be out of line.

The third point concerns the observed fundamental frequency at 882 cm^{-1}. This band was originally assigned to be of b_{1u} symmetry,[101] but recently was reassigned as b_{2u}.[105] If the original assignment is compared to theory, the error is quite large (34%). However, if the recent b_{2u} assignment is compared, the error is quite small given the approximations incorporated in the theory (< 1%). The infrared absorption intensity data in Table X is of use here. It is found that the b_{2u} mode in question should exhibit a very strong relative infrared absorption intensity, whereas the b_{1u}

band should be quite weak. The qualitative intensity data reported by Franks, Merer, and Innes[101] shows the band at 882 cm^{-1} to have a very strong absorption intensity and thus the present results support the reassignment of Thakur, Job, and Kartha.[105]

3.3.3 $\tilde{a}\ ^3B_{3u}$ State

Table XI compares the $\tilde{a}\ ^3B_{3u}$ DZ SCF and DZ+P SCF predictions with the experimental geometry. As was found for the ground state, the T_1 equilibrium is of D_{2h} symmetry. Tabulated in parentheses following each of the four unique geometrical parameters is the change in these parameters upon excitation relative from the $\tilde{X}\ ^1A_g$ ground state.

Table XI. Comparison of equilibrium theoretical geometries of the $\tilde{a}\ ^3B_{3u}$ state of *s*–tetrazine with the experimentally determined geometry. The change in geometry for each internal coordinate upon $T_1 \leftarrow S_0$ excitation is noted in parentheses. Refer to Figure 4 for definition of internal coordinates. Experimental values from reference 115.

	$\tilde{a}\ ^3B_{3u}$ Geometry (bond distances in angstroms)		
	DZ SCF	DZ+P SCF	Expt.[a]
r_1	1.3346 (– 0.0046)	1.3156 (– 0.0059)	1.35 (+ 0.01)
s_1	1.3165 (– 0.0024)	1.2915 (– 0.0008)	1.27 (– 0.06)
t_1	1.0641 (– 0.0002)	1.0730 (– 0.0013)	1.06 (– 0.01)
α_1	119.10° (– 4.93°)	120.00° (– 5.19°)	129.8° (+ 3.4°)

Unlike the generally good agreement between experiment and theory for the ground state structure, a comparison of the calculated T_1 structure with that determined spectroscopically[115] leads to several inconsistencies. First, based on previous trends established for DZ+P SCF predictions of bond angles, one expects an absolute error of 1° – 2° with respect to experiment; however the DZ+P SCF prediction for <NCN in Table XI is 9.8° smaller than the value obtained from a Franck-Condon

analysis of the vibronic intensities of a series of $T_1 \leftarrow S_0$ transitions.[115] RHF theory predicts a significant decrease in this angle upon excitation (DZ –4.93°, DZ+P –5.19°), whereas the experimental prediction is +3.4°. As noted by Livak and Innes,[115] the determination of the change in geometry from a Franck-Condon intensity profile is ambiguous as to the sign of the displacement. If one were to reverse the sign of the changes in parentheses following the experimental structural parameters, the experimental bond angle for the T_1 state would be 123.0°. This would be in much better agreement with the DZ+P SCF result.

A second problem here lies in the N-N bond distance. The DZ+P SCF vs experiment error is 1.5% for this distance, but the theoretical prediction is *longer* than that extracted from the Franck-Condon analysis. As stated above, empirical evidence has shown that DZ+P SCF bond lengths are generally 1%-2% shorter than experimental determinations. Again if one changes the sign of the experimental Δ_{geometry} with electronic excitation, the experimental prediction for the N-N bond distance becomes 1.39 angstroms and the theory vs experiment error is of the expected sign but suprisingly large in magnitude.

In general (with the exception of the NCN angle) theory predicts a very small change in geometry upon $T_1 \leftarrow S_0$ excitation whereas the analysis of Livak and Innes, when compared to the present theoretical results, predicts a somewhat greater distortion from the ground state. It is clear that further theoretical and spectroscopic studies are needed to resolve the inconsistencies with respect to the $\tilde{a}\ ^3B_{3u}$ structure.

The source of these errors for the T_1 state is not entirely clear. As comparisons of this type are very limited for molecules of this size as well as for excited triplet states, the empirical evidence gleaned from previous theory vs experiment

comparisons (primarily based on closed-shell ground states of smaller molecular systems) may not be appropriate for application here. Additionally the spectroscopic deductions of Livak and Innes[115] are ambiguous to a ± sign, and as noted in reference 115, the change in geometry determined by the Franck-Condon analysis is inconsistent with the rotational data taken in that same experiment. Concerning this the authors state,[115]

> This argument must be viewed with caution since small contributions from other normal modes could escape undetected. Indeed it is likely they have, since $\Delta\bar{B}$ calculated from the change in geometry noted above is nearly eight times that found experimentally in Section III.

The harmonic vibrational frequencies of the T_1 state predicted by DZ+P SCF theory are compared to the five experimental assignments of Livak and Innes in Table XII. The theoretical values for the low frequency a_g and b_{3u} modes agree reasonably well with experiment (10.6% and 15.7% overestimate, respectively); however, the errors for the remaining three fundamentals assigned experimentally are quite large. As was the case for the ground state, it is difficult to assess these errors without evaluating the contributions from anharmonic terms in the potential and from electron correlation; however, at this level of theory, the assigment of the 681 cm^{-1} band as b_{2u} would be more consistent with the theory (17.6% error) than the reported assignment of b_{3u}[115] (54.6% error).

Table XII. Comparison of the DZ+P SCF harmonic vibrational frequencies with experimental fundamental frequency assignments for the $\tilde{a}\ ^3B_{3u}$ state of *s*-tetrazine.

	Vibrational Frequencies (cm^{-1})			DZ+P SCF Potential Energy Distribution	
	DZ+P SCF[a]	Expt.[b]	% difference[c]		
a_g	3450	···	···	$F_1(99)$	sym C-H stretch
a_g	1792	···	···	$F_2(59)\ F_3(28)\ F_4(12)$	sym N-N stretch
a_g	1175	···	···	$F_2(37)\ F_3(62)\ F_4(1)$	sym C-N stretch
a_g	794	718	10.6	$F_3(8)\ F_4(91)$	sym N-C-N bend
b_{2g}	1068	···	···	$F_5(100)$	out-of-plane C-H wag
b_{2g}	275	···	···	$F_5(44)\ F_6(56)$	chair deformation+C-H wag
b_{3g}	1430	···	···	$F_7(2)\ F_8(98)$	in-plane C-H wag
b_{3g}	952	···	···	$F_7(97)\ F_8(3)$	C-N stretch
b_{3g}	478	370	28.9	$F_7(39)\ F_8(1)\ F_9(60)$	N-N-C bend+C-N stretch
a_u	366	284	29.2	$F_{10}(100)$	ring folding
b_{1u}	3445 (24.3)	···	···	$F_{11}(99)$	asym C-H stretch
b_{1u}	1409 (142.)	···	···	$F_{12}(90)\ F_{13}(10)$	C-N stretch
b_{1u}	652 (594.)	···	···	$F_{12}(9)\ F_{13}(91)$	asym N-C-N bend
b_{2u}	1839 (1440)	···	···	$F_{14}(90)\ F_{15}(5)\ F_{16}(5)$	asym N-N stretch
b_{2u}	1433 (156.)	···	···	$F_{14}(3)\ F_{15}(16)\ F_{16}(91)$	in-plane C-H wag
b_{2u}	801 (662.)	···	···	$F_{14}(13)\ F_{15}(87)$	C-N stretch
b_{3u}	1053 (4.91)	681	54.6	$F_{17}(92)\ F_{18}(8)$	out-of-plane C-H wag
b_{3u}	487 (34.8)	421	15.7	$F_{17}(3)\ F_{18}(97)$	boat deformation

[a] Analytic infrared absorption intensities (km/mol) are noted in parentheses.

[b] Reference 115

[c] $\frac{|\omega_{DZ+P\ SCF} - \nu_{Expt.}|}{\nu_{Expt.}} \times 100$

Table VI compares the adiabatic excitation energies theoretically predicted for this state with that obtained spectroscopically.[115] The DZ+P CISD(+Q) result should be regarded as the "best" theoretical prediction currently available in that (1) the atomic basis set is the largest employed, and (2) the most electron correlation has been accounted for within the CISD + Davidson correction approximation. The error here is 0.46 eV with the theoretical prediction being larger that that found experimentally. As can be seen in Table VI, correlation of the electrons has a much greater

energetic effect on the excited state than the ground state. One possible explanation for this is that the ground state wavefunction is dominated by a single electron configuration, while in the case of T_1, two or more configurations are important for the zeroth order description of the wavefunction. A second point to note is that the addition of polarization functions to the basis has a much greater energetic effect on the ground state than on T_1. This was also discovered for the ground state relative to 2HCN + N_2 and to the photodissociation transition state (see Section 3.3.6). This effect may arise from the fact that the *s*–tetrazine ground state equilibrium (having 4n+2 π electrons in a symmetric ring) should exhibit the greatest aromatic delocalization of any of the structures studied herein. The higher angular momentum basis functions thus seem to be important in describing this ring delocalization. While the $n \rightarrow \pi^*$ excited states also possess 4n+2 π bonding electrons, the π^* antibonding electron (to a greater or lesser extent depending on the particular excited state) destabilizes the aromatic π structure.

3.3.4 $\tilde{A}\ ^1A_u$ State

As described above, the present SCF study of the first excited singlet state of *s*–tetrazine began with a full D_{2h} geometry optimization with a double-ζ basis set. This was followed by the analytic evaluation of second derivatives which revealed two imaginary harmonic vibrational frequencies: one of b_{1u} symmetry at $1335i$ cm^{-1} and the second of b_{3g} symmetry at $963i$ cm^{-1}. The S_1 structure was relaxed along these modes corresponding to local maxima on the potential energy hypersurface and reoptimized. The b_{1u} motion leads to a structure with C_{2v} symmetry (*z*-axis as C_2 axis). This structure lies 143 cm^{-1} below the D_{2h} structure on the DZ SCF surface. Analytic energy second derivatives at this stationary point revealed a single

remaining imaginary frequency at $2069i$ cm^{-1} and of b_2 symmetry. The b_{3g} motion leads to a structure with C_{2h} symmetry (x-axis as C_2 axis) which lies 534 cm^{-1} below the D_{2h} structure. Analytic energy second derivatives revealed this structure to be a minimum on the DZ SCF S_1 surface. DZ+P optimized structures were found for these three symmetries on the S_1 surface with their relative energies being C_{2h} (0 cm^{-1}) < C_{2v} (+ 84.1 cm^{-1}) < D_{2h} (+ 132 cm^{-1}).

Figure 5 summarizes the situation on the DZ+P S_1 energy surface in the restricted space of energy vs the two unstable (with respect to the D_{2h} super-transition state) normal coordinates. It is clear that the relative energies of these three stationary points allow facile interconversion among the three. In fact the DZ SCF harmonic vibrational frequency for the motion along $Q_{b_{3g}}$ is 605 cm^{-1}; thus even at conditions of extreme rovibrational cooling, the S_1 state behaves dynamically as D_{2h} on both the DZ and DZ+P SCF surfaces. Furthermore, the energy difference between the C_{2h} minimum and the high symmetry super-transition state becomes smaller still when electron correlation is added to the energies at their SCF stationary points. In fact single point CISD theory reorders the structures as C_{2h} (0 cm^{-1}) < D_{2h} (+ 43.5 cm^{-1}) < C_{2v} (+ 362 cm^{-1}) and adding the Davidson correction yields C_{2h} (0 cm^{-1}) < D_{2h} (+ 12.3 cm^{-1}) < C_{2v} (+ 384 cm^{-1}). Given these results, dogmatic conclusions as to the topology of the true S_1 surface would be premature. Re-optimization with a CISD wavefunction (or other correlated wavefunction) and/or increasing the size of the basis set might reorder and change the character of any or all of these stationary points.

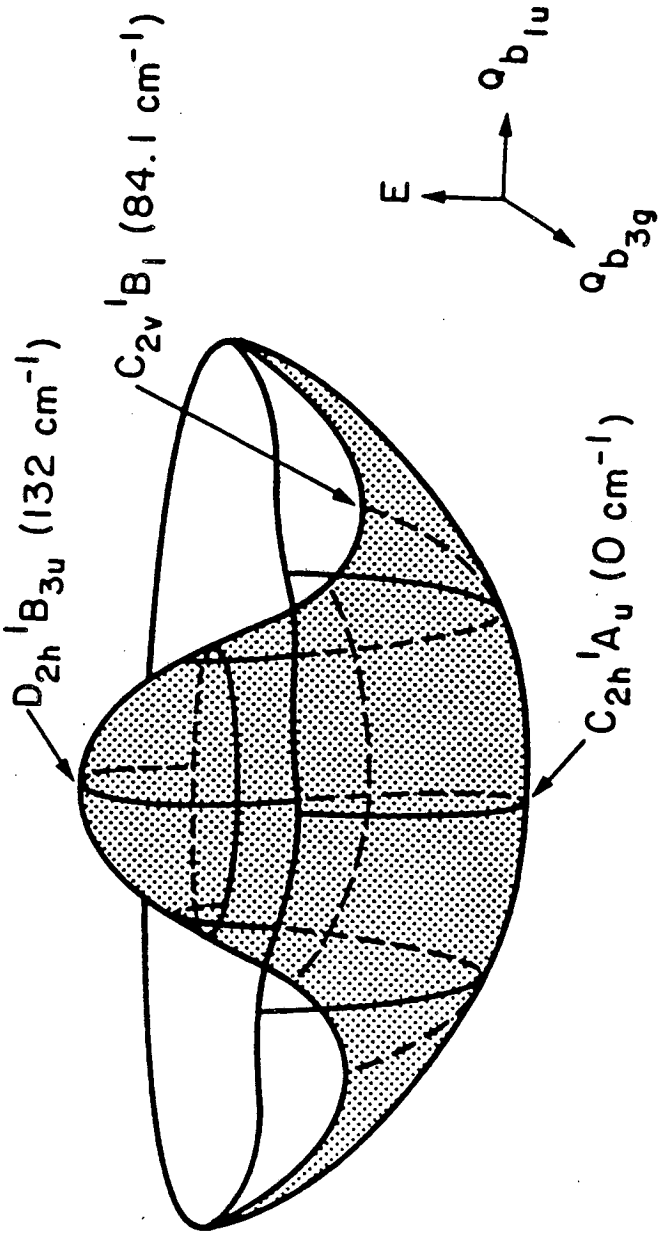

Figure 5: Cross section of the DZ+P SCF S_1 surface of *s*–tetrazine. Central local maximum corresponds to the symmetry restricted D_{2h} stationary point. The two saddle points correspond to the two equivalent C_{2v} symmetry restricted stationary points. The minimum on the surface corresponds to the C_{2h} equilibrium structure. There is a second equivalent C_{2h} minimum directly behind the D_{2h} maximum.

One additional area of concern here regarding the adequacy of a single-configuration SCF reference for qualitatively reliable equilibrium structural predictions, namely the problem of symmetry breaking,[166] has been addressed in the present study. As discussed by Engelbrecht and Liu[167] and by McLean, Lengsfield, Pacansky, and Ellinger,[168] an MCSCF treatment is needed to obtain a qualitatively correct geometry where SCF symmetry breaking occurs. In general symmetry breaking can be identified by an energy discrepancy (at the high symmetry nuclear geometry) between a calculation performed with a wavefunction constrained to be of the high symmetry of the nuclear framework and that same calculation with a wavefunction of lower symmetry. In the case of the first excited singlet state of *s*–tetrazine, DZ SCF energies were obtained at the D_{2h} saddle point with wavefunctions of both D_{2h} and C_{2h} symmetry. Both calculations were easily converged to an error of 10^{-12} in successive density matrices and both gave identical energies to 10^{-10} hartrees. It is thus concluded that the S_1 state of *s*–tetrazine does not exhibit SCF symmetry breaking.

Table XIII presents the DZ SCF, DZ+P SCF, and experimental predictions for the S_1 equilibrium geometry. Two experimental structures are displayed in Table XIII. In Experiment A (Job and Innes, 1978),[115] the $S_1 \leftarrow S_0$ 0-0 band rotational structure was analyzed for five isotopes of *s*–tetrazine ($-d_0$, $-d_1$, $-d_2$, $-1,4\ ^{15}N_2\ d_1$, and $-1,4\ ^{15}N_2\ d_2$) to determine S_0 and S_1 rotational constants for all isotopes. These five sets of rotational constants were least squares fit to obtain structural data for the S_0 (see Table VIII) and S_1 states. In Experiment B (Innes, Brumbaugh, and Franks, 1981),[114] a one-dimensional Franck-Condon analysis of the absorption intensities in the $S_1 \leftarrow S_0$ vibronic progression for the low frequency a_g mode was carried out. From the frequency and relative intensity data, the change in geometry upon

adiabatic $S_1 \leftarrow S_0$ excitation was determined (to within a ± sign), and the sign of the change was chosen to best agree with the data from Experiment A. Finally, in comparing the two experimental structures Innes, Brumbaugh, and Franks state,[114]

> Probably the Franck-Condon numbers (Experiment B) are the more accurate ones because they are rather insensitive to small changes in the relative intensities and the molecular force fields.

Additionally the optimized geometries of the D_{2h} and C_{2v} stationary points have been included in Table XIII. As pointed out above, additional theoretical studies will be necessary to determine the true shape of this surface.

Since the C_{2h} minimum exhibits significant C-N bond alternation relative to the D_{2h} stationary point, comparison of the theoretical equilibrium with the experimental structures is rendered difficult. A more meaningful comparison is experiment vs the D_{2h} theoretical structure.

Table XIII. Comparison of equilibrium theoretical geometries of the S_1 state of *s*–tetrazine with the experimentally determined geometries. The change in geometry for each internal coordinate upon $S_1 \leftarrow S_0$ excitation is noted in parentheses. Refer to Figure 4 for definition of internal coordinates.

	Geometries of the S_1 state of *s*–tetrazine (bond distances in angstroms)							
	DZ SCF			DZ+P SCF			Expt. A[a]	Expt. B[b]
	C_{2h}	C_{2v}	D_{2h}	C_{2h}	C_{2v}	D_{2h}		
r_1	1.4092	1.3383	1.3367 (–0.0025)	1.3647	1.3184	1.3168 (–0.0047)	1.3243 (–0.0163)	1.3326 (–0.0079)
r_2	1.2903	r_1	r_1	1.2832	r_1	r_1	r_1	r_1
r_4	r_1	1.3314	r_1	r_1	1.3132	r_1	r_1	r_1
s_1	1.3055	1.3287	1.3156 (–0.0033)	1.2844	1.2975	1.2908 (–0.0015)	1.3490 (+0.0234)	1.3710 (+0.0454)
t_1	1.0638	1.0647	1.0640 (–0.0003)	1.0725	1.0738	1.0729 (–0.0014)	1.0629 (–0.0097)	1.0759 (+0.0033)
t_2	t_1	1.0639	t_1	t_1	1.0724	t_1	t_1	t_1
α_1	118.91°	121.64°	118.91° (–5.12°)	119.59°	122.11°	119.87° (–5.33°)	123.17° (–3.19°)	123.61° (–2.75°)
α_2	α_1	116.83°	α_1	α_1	117.84°	α_1	α_1	α_1
β_2	123.47°	*c*	*c*	121.77°	*c*	*c*	*c*	*c*
δ_2	124.63°	*d*	*e*	124.36°	*d*	*e*	*e*	*e*

[a] Reference 113

[b] Reference 114

[c] $\frac{360° - \alpha_1}{2}$

[d] Defined by r_1, r_3, s_1, α_1, and α_2.

[e] Defined by r_1, s_1, and α_1.

The DZ+P SCF predictions for both the C-H and C-N bond distances are well within the anticipated error range; however, the N-N bond distance and NCN angle exhibit large discrepancies with the experimental predictions. These two parameters were also problematic in the DZ+P SCF vs experiment comparison for the $^3B_{3u}$ surface. In comparing the predicted change in geometry upon excitation, one finds that DZ SCF, DZ+P SCF, and the two experimental analyses all qualitatively agree that

the C-N bond distance should decrease slighty upon excitation. The N-N bond distance is found experimentally to increase significantly while both basis sets predict a slight decrease in this distance. Theory also predicts a much greater decrease in the NCN angle than appears to be shown by both the 0-0 rotational data and the Franck-Condon progression.

If the experimentally determined structures for the S_1 state are accurate, the DZ+P SCF results are rather disappointing. However based on the errors encountered here, one can extrapolate to the T_1 state where the experimental evidence is not so strong, and the choice of sign for the Franck-Condon change in geometry is not dictated by a second, independent experiment. Assuming a consistency of systematic theoretical error for the S_1 and T_1 states, it is clear that the opposite choice of sign (relative to Livak and Innes, 1971,[115] as presented in Table XI) is the better choice. This gives absolute errors (DZ+P SCF vs experiment) for the T_1 state of C-N –0.01 angstroms, N-N –0.10 angstroms, C-H –0.01 angstroms, <NCN –3.0° which are very similar to the differences found for the S_1 state C-N –0.01 angstroms, N-N –0.08 angstoms, C-H –0.01 angstroms, <NCN –3.7°.

Table XIV compares the S_1 DZ SCF harmonic vibrational frequencies with the eight S_1 vapor-phase frequencies obtained from a vibronic absorption study[102] and a SVL fluorescence study.[104] Due to the size of this calculation, only the DZ basis set could be employed for the present vibrational analysis of the S_1 state. Previous systematic comparisons of harmonic vibrational frequencies at the SCF level of theory with experimental assignments have demonstrated that the same systematic 8-13% theoretical overestimate as has generally been found using the DZ+P basis set does not hold quite as regularly for the DZ basis.[169] However, from the present DZ SCF

S_1 results, with one exception, one finds similar theory vs experiment differences as found for the DZ+P SCF ground state results. In comparing the theoretical predictions for the a_g and b_g modes with experiment, the low frequency a_g mode (b_{3g} within the D_{2h} point group) stands out (62.2% overestimate of the experimental fundamental). No other a_g or b_{3g} mode of the ground state, T_1 state, or S_1 state exhibited errors greater than 30%. This particular mode is of special significance because it represents the motion along $Q_{b_{3g}}$ in Figure 5. It is not suprising that the DZ SCF description is inadequate here since the qualitative topology of the surface in this dimension was found to depend critically on both the basis set and level of electron correlation (see above). This 62.2% error may be another reflection of the need for a better treatment of this surface for reliable qualitative and quantitative theoretical predictions. Of course, anharmonic corrections can also be substantial for such low frequency vibrations.

As discussed above, the excited state second derivative method[158,159] was employed for the $\tilde{A}\ ^1A_u$ state of *s*–tetrazine. In this particular case displacements which transform as the a_u irreducible representation of the C_{2h} point group (or as a_u and b_{3u} within the D_{2h} point group) lower the symmetry of the excited state wavefunction such that it is no longer orthogonal to that of the ground state. The three a_u harmonic frequencies obtained with the standard SCF second derivative method[157] (non-variational collapse has not been treated properly) are 986 cm^{-1}, 514 cm^{-1}, and 357 cm^{-1}. When non-variational collapse is eliminated, these frequencies are properly predicted to be (see Table XIV) 988 cm^{-1}, 533 cm^{-1}, and 402 cm^{-1}. The excited state corrections are not enormous but are significant in the case of the two low frequency modes. These corrections, however, do increase the theory vs experiment difference in all three cases. Such differences while, in general,

significantly greater than those observed for the *gerade* modes are consistent with those found both the a_u and b_{3u} modes of the ^1A_g and $^3B_{3u}$ electronic states.

Table XIV. Comparison of the DZ SCF harmonic vibrational frequencies with experimental fundamental frequency assignments for the S_1 state of *s*–tetrazine.

Vibrational Frequencies (cm^{-1})					DZ SCF Potential Energy Distribution	
	DZ SCF[a]		Expt.	% difference[d]		
a_g	3424		...	...	$F_1(99)$	sym C-H stretch
a_g	1688	a_g	1485[b]	13.7	$F_2(32)\ F_4(58)\ F_5(8)$	short C-N stretch
a_g	1404		...	...	$F_4(4)\ F_6(94)$	in-plane C-H wag
a_g	1189	a_g	1004[c]	18.4	$F_2(60)\ F_3(4)\ F_4(32)\ F_5(2)$	sym N-N stretch
a_g	952		...	...	$F_3(75)\ F_4(3)\ F_5(15)\ F_7(3)$	long C-N stretch
a_g	769	a_g	703[b]	9.4	$F_3(9)\ F_4(2)\ F_5(77)\ F_7(11)$	N-C-N bend
a_g	605	b_{3g}	373[b]	62.2	$F_3(18)\ F_4(4)\ F_5(3)\ F_7(77)$	N-N-C bend
b_g	1014		...	...	$F_8(97)\ F_9(3)$	out-of-plane C-H wag
b_g	666	b_{2g}	579[c]	15.0	$F_8(18)\ F_9(82)$	chair deformation
a_u	988 (16.2)	b_{3u}	681[b]	45.0	$F_{11}(92)\ F_{12}(8)$	out-of-plane C-H wag
a_u	535 (27.4)	b_{3u}	405[b]	32.1	$F_{10}(20)\ F_{11}(5)\ F_{12}(75)$	boat deformation
a_u	402 (6.20)	a_u	254[b]	58.3	$F_{10}(63)\ F_{12}(37)$	ring folding
b_u	3524 (0.790)		...	...	$F_{13}(98)\ F_{17}(1)$	asym C-H stretch
b_u	1769 (1400)		...	...	$F_{14}(77)\ F_{16}(4)\ F_{17}(7)\ F_{18}(11)$	asym N-N stretch
b_u	1607 (1270)		...	...	$F_{15}(18)\ F_{16}(43)\ F_{17}(21)\ F_{18}(18)$	mixed ring mode
b_u	1350 (1000)		...	...	$F_{14}(1)\ F_{15}(40)\ F_{16}(53)\ F_{18}(4)$	C-N stretch
b_u	1320 (94.6)		...	...	$F_{14}(10)\ F_{15}(12)\ F_{18}(77)$	in-plane C-H wag
b_u	795 (416.)		...	...	$F_{14}(16)\ F_{15}(37)\ F_{16}(9)\ F_{17}(37)$	mixed ring mode

[a] Analytic infrared absorption intensities (km/mol) are noted in parentheses.

[b] Reference 102

[c] Reference 104

[d] $\frac{|\omega_{DZ\ SCF} - \nu_{Expt.}|}{\nu_{Expt.}} \times 100$

The theoretical adiabatic excitation energies are compared with the experimental value in Table VI. Considering the single point DZ+P CISD(+Q) to be the best theoretical prediction, one finds the theory to overestimate the experimental value by 0.55 eV. This is reasonably consistent with the 0.46 eV overestimate observed for the T_1 state. Also, as was found for $^3B_{3u}$, polarization functions have been found to lower the energy of the ground state relative to S_1 while both CISD and the Davidson

correction have the opposite effect.

3.3.5 Higher Excited States

The DZ SCF D_{2h} stationary point structures for the remaining ten electronic states of *s*–tetrazine addressed in the present study are presented in Table XV. Unlike the equilibrium structures for S_1 and T_1 which do not distort greatly from the ground state equilibrium, the structures of these higher excited states generally show significantly more distortion. The C-N bond ranges in length from 1.326 angstroms in the $^3B_{2g}$ state to 1.449 angstroms in the $^3B_{1u}$ state. This long C-N bond distance is indicative of a pure C-N single bond rather than the "aromatic" C-N bond lengths displayed by most of the states. The N-N bond also exhibits a broad range of character with distances ranging from 1.224 angstroms in the $\tilde{B}\ ^1A_u$ state (an N=N double bond) to 1.484 and 1.481 angstroms in the $^1B_{2g}$ and $^3B_{2g}$ states, respectively (rather long N-N single bonds). It should be pointed out that this $^3B_{2g}$ surface may be purely dissociative (*s*–tetrazine $\rightarrow$ 2HCN + N_2) in that the single imaginary frequency at the D_{2h} stationary point is qualitatively similar to that found for the ground state dissociation transition state (see Section 3.3.6). The NCN angle contracts to values as small as 113.6° at the $\tilde{B}\ ^1A_u$ stationary point and opens to values as great as 128.4° at the $^3B_{2u}$ stationary point.

Table XV. DZ SCF stationary point geometries for higher excited states of *s*–tetrazine restricted to D_{2h} symmetry.

DZ SCF Geometries (bond distances in angstroms)										
	^3A_u	^1A_u	$^3B_{1u}$	$^3B_{2u}$	$^3B_{1g}$	$^3B_{2g}$	$^1B_{2g}$	$^1B_{1g}$	$^1B_{2u}$	$^1B_{1u}$
r_1	1.3938	1.3940	1.4485	1.3751	1.3265	1.3258	1.3260	1.3300	1.3871	1.4196
s_1	1.2252	1.2244	1.2476	1.3604	1.3301	1.4810	1.4842	1.3304	1.3424	1.2726
t_1	1.0580	1.0581	1.0621	1.0693	1.0651	1.0684	1.0683	1.0642	1.0667	1.0641
α_1	113.73°	113.55°	123.10°	128.39°	122.51°	124.00°	123.75°	122.70°	127.11°	125.90°

Table XVI presents the DZ SCF harmonic vibrational frequencies for the higher excited electronic states investigated in this study. These frequencies were evaluated at the DZ SCF D_{2h} stationary points, and, as illustrated in Table XVI, all but the $^3B_{1g}$ state are symmetry restricted saddle points with at least one imaginary harmonic vibrational frequency at the D_{2h} optimized geometries, i.e. these are stationary points of higher (than 1) Hessian index. As was the case with the optimized geometries of these higher excited states, the harmonic frequencies show large deviations from the corresponding ground state values and among themselves. Additionally, the instabilities with respect to the D_{2h} stationary points appear in a variety of forms. The $^3B_{1u}$, $^3B_{2u}$, $^1B_{1g}$, $^1B_{2g}$, $^1B_{2u}$, and $^1B_{1u}$ states are unstable with respect to one or two out-of-plane distortions while the ^3A_u, ^1A_u, and $^3B_{2g}$ states are unstable with respect to one or two distortions in the plane of the molecule. No state is unstable with respect to both an in-plane and an out-of-plane distortion. As mentioned above one or more of these states could be purely dissociative from their D_{2h} saddle points, although this has not yet been explicitly investigated.

Finally, it should be noted that many of the non-totally symmetric motions on these higher excited surfaces lead to non-variational collapse to single configuration RHF states of lower energy within any of the symmetry sub-groups of D_{2h}. Thus the harmonic vibrational frequencies corresponding to these motions are not properly

treated here. As discussed above, this non-variational collapse did not greatly change the harmonic frequencies in the case of the S_1 state, but there are cases where such changes are quite large.[170]

Table XVI. DZ SCF harmonic vibrational frequencies for the higher excited states of *s*–tetrazine restricted to D_{2h} symmetry.

	DZ SCF Harmonic Vibrational Frequencies[a] (cm^{-1})									
	^3A_u	^1A_u	$^3B_{1u}$	$^3B_{2u}$	$^3B_{1g}$	$^3B_{2g}$	$^1B_{2g}$	$^1B_{1g}$	$^1B_{2u}$	$^1B_{1u}$
a_g	3586	3587	3536	3474	3492	3454	3456	3503	3498	3536
a_g	1943	1952	1828	1528	1667	1484	1480	1658	1538	1768
a_g	1076	1077	972	1025	1111	891	883	1098	1027	1023
a_g	703	703	673	757	800	711	710	782	751	679
b_{2g}	720	722	603	931	1106	1095	1069	1093	857	833
b_{2g}	406	435	355*i*	457*i*	761	725	720*i*	737	1360*i*	1047*i*
b_{3g}	1361	1360	1434	1996	1593	1641	1582	1488	1975	1491
b_{3g}	748	781	1057	1450	1434	1474	1477	1015	1420	1182
b_{3g}	1816*i*	575*i*	649	599	661	820	1081	746	754	733
a_u	595	592	474	227	541	267	254	569*i*	118	431
b_{1u}	3570	3574	3533	3473	3493 (35.2)	3456	3548	3503	3509	3534
b_{1u}	982	986	1150	1139	1523 (1130)	1358	1357	1333	1473	1184
b_{1u}	997*i*	807*i*	857	1010	1343 (58.5)	1157	1107	1274	1065	932
b_{2u}	2323	2414	1765	1571	1566 (10.5)	1543	1525	1571	1572	1600
b_{2u}	1341	1350	1423	1486	1313 (83.4)	910	893	1209	1487	1298
b_{2u}	889	878	1090	1013	871 (411.)	634*i*	309	731	1174	1071
b_{3u}	509	524	75	1037	1075 (2.83)	1070	1065	1068	895	2260
b_{3u}	94	208	362*i*	69	542 (32.0)	369	371	429	234*i*	375

[a] Analytic infrared absorption intensities (km/mol) are noted in parentheses for $^3B_{1g}$ state only (genuine minimum within the restriction to D_{2h} symmetry).

The relationship between the S_1 and S_2 surfaces is quite interesting. The previous theoretical study by Ha[151] reported a vertical ΔE for $\tilde{B}\ ^1A_u$ of 4.78 eV, nearly 2 eV above that found for $\tilde{A}\ ^1B_{3u}$. The present theoretical study predicts $\Delta E_{0\text{–}0} \leq 2.90$ eV for the $\tilde{B}$ state, just 0.41 eV above the minimum on the S_1 surface. Due to the

energetic proximity of these two surfaces, the previously suggested[102,111,157] spin allowed vibronic coupling between S_1 and S_2 may be important in analysis of the vibronic spectrum of $S_1 \leftarrow S_0$. In fact, at the S_2 stationary point, the S_1 energy is above that of S_2, and thus the global $\tilde{B}$ state is the local $\tilde{A}$ state at its D_{2h} stationary point. Within D_{2h} symmetry these two electronic states are orthogonal (S_1 transforms as $^1B_{3u}$ and S_2 transforms as ^1A_u) and thus a curve crossing is implied. This situation is illustrated in Figure 6 with the excited state DZ SCF energies expressed in kcal/mol relative to the ground state DZ SCF energy at equilibrium. The horizontal axis represents a generalized D_{2h} coordinate which leads from the ground state equilibrium to the $^1B_{3u}$ and ^1A_u stationary points (structures I, II, and III in Figure 6, repsectively), while retaining D_{2h} symmetry throughout.

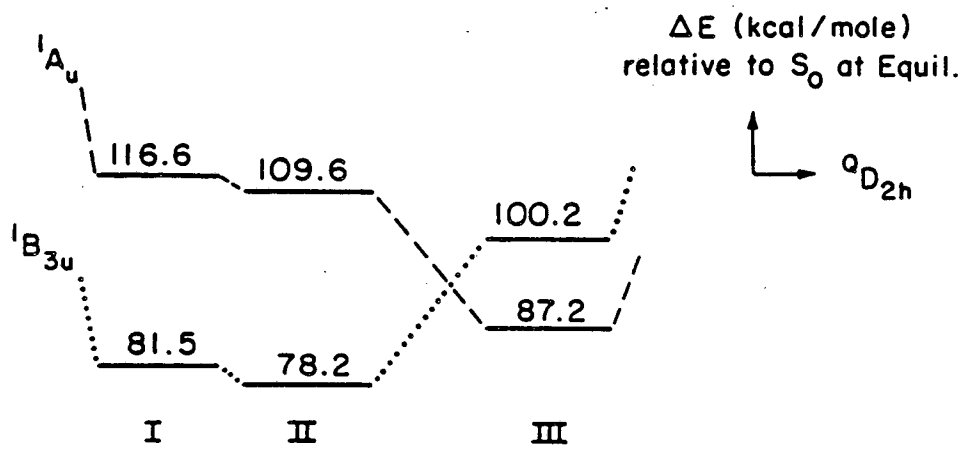

Figure 6: Relative DZ SCF energies (kcal/mol relative to the $\tilde{X}\ ^1A_g$ DZ SCF equilibrium) on the S_1 ($\tilde{A}\ ^1B_{3u}$) and S_2 ($\tilde{B}\ ^1A_u$) surfaces. The horizontal axis corresponds to a general D_{2h} coordinate which takes the nuclear framework through the DZ SCF ground state equilibrium (structure I), and the DZ SCF D_{2h} restricted stationary points on the $^1B_{3u}$ and ^1A_u surfaces (structures II and III, respectively).

As discussed previously, RHF theory predicts that the S_1 equilibrium is of C_{2h} symmetry and thus the wavefunction transforms as ^1A_u for S_1. Furthermore, the DZ SCF D_{2h} stationary point for S_2 is characterized by two imaginary harmonic frequencies: a b_{3g} mode at $575i$ cm^{-1} and a b_{1u} mode at $807i$ cm^{-1}. These two motions are qualitatively identical to the two imaginary modes at the D_{2h} stationary point on the DZ SCF S_1 surface, and thus they lead to structures of C_{2h} and C_{2v} symmetry. Within these two subgroups of D_{2h}, the S_2 state wavefunction transforms as ^1A_u and $^1A_2$, respectively. If one now considers Figure 6 within C_{2h} symmetry, the S_1 and S_2 surfaces are no longer orthogonal and exhibit an avoided crossing. Thus S_1 is a lower ^1A_u surface and S_2 is an upper ^1A_u surface. Within conventional Hartree-Fock theory only the lower surface can be examined. Attempts have been made to locate a second C_{2h} stationary point on the lower ^1A_u surface by carefully distorting the S_2 D_{2h} stationary point geometry along the b_{3g} imaginary mode, but none has been found. All attempts have led to the C_{2h} structure described in Table XIV.

3.3.6 *s*-Tetrazine Photodissociation

The spectroscopic investigations into the mechanism and thermochemistry of the photodissociation of *s*–tetrazine were discussed in detail in Section 3.1.3. Perhaps most fascinating among the various photochemical findings for *s*–tetrazine is the appearance of very simple dissociation products, namely, molecular nitrogen and hydrogen cyanide. Clearly the mechanism for this decomposition of a medium-sized molecule into three small molecules is of interest, and a number of experimental studies have addressed just this.[123–133]

Of particular interest is the 1977 study of King, Denny, Hochstrasser, and Smith[125] in which experiments were performed which appeared to eliminate all but three mechanisms for the photochemical decomposition of *s*–tetrazine. The three remaining plausible mechanisms are shown below.

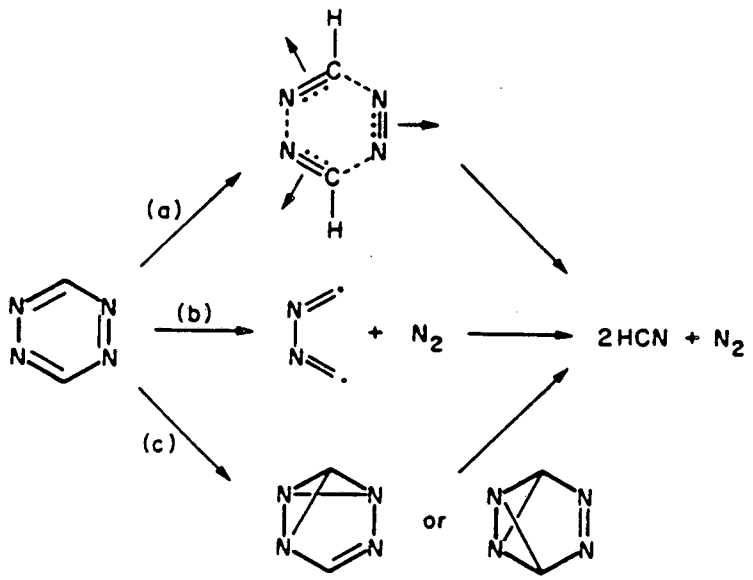

Of these the triple dissociation [path (a)] is perhaps the most intriguing, although, as discussed in Section 3.1.3, Glownia and Riley suggest that it is an unlikely process.[129] Unimolecular reactions ABC → A + B + C involving a single transition state are quite rare, although just such a mechanism has recently been established[171] for the photodissociation of glyoxal.

In the photochemical experiments the first step is the electronic excitation $S_1 \leftarrow S_0$. S_1 lies at 18 128 cm^{-1}, or 51.8 kcal/mol.[97] This is followed by a radiationless transition to the higher vibrational manifold of the ground state potential energy hypersurface. As noted by Karl and Innes,[122] the ensuing ground state unimolecular reaction must proceed with an activation energy less than or equal to 51.8 kcal/mol. Accordingly, one of the goals of this study was to ask whether the one-

step triple dissociation does indeed have such a lower energy barrier.

The triple dissociation pathway can in principle maintain C_{2v} symmetry throughout. In light of the massive rearrangement of bonds [two aromatic (bond order 1.5) CN bonds and one aromatic NN bond broken; two aromatic CN bonds and one aromatic NN bond become triple bonds in the reaction products], it seems at first glance unlikely that such a high-symmetry process would be allowed by orbital symmetry. However, as Figure 7 illustrates, the orbitals of *s*–tetrazine, resolved into C_{2v} symmetry, have precisely the same numbers of a_1, a_2, b_1, and b_2 occupied orbitals as do HCN + HCN + N_2 in the same dissociated C_{2v} arrangement. Thus the triple dissociation is allowed by orbital symmetry in the sense of Woodward and Hoffmann.[172]

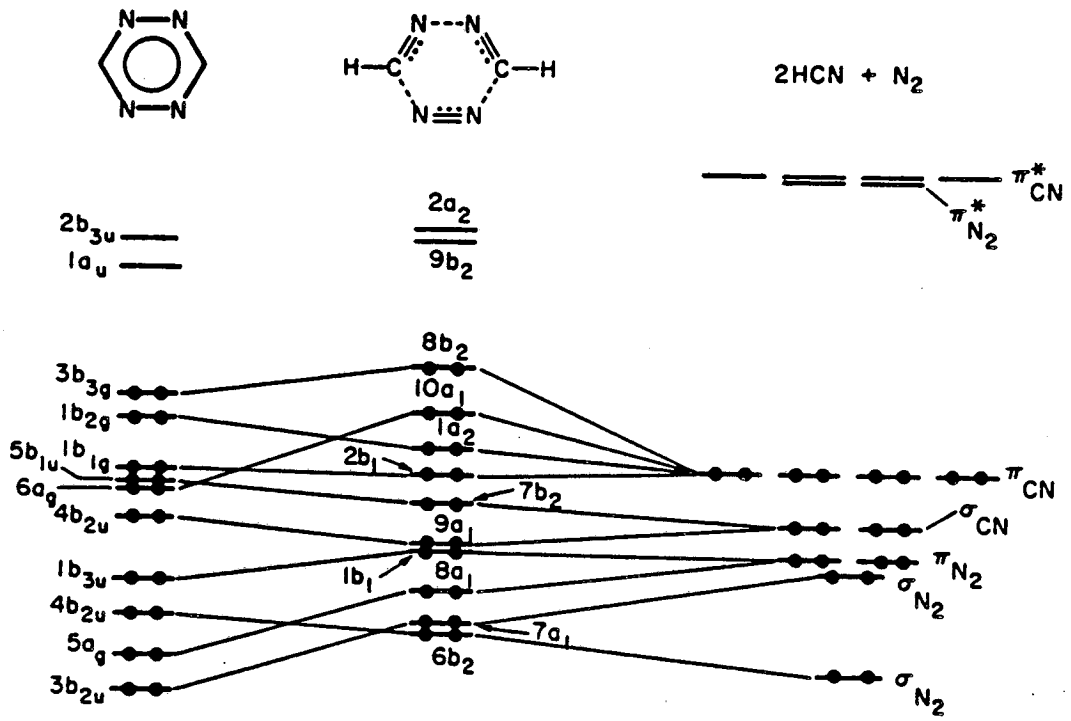

Figure 7: Orbital correlation diagram for the dissociation of *s*–tetrazine.

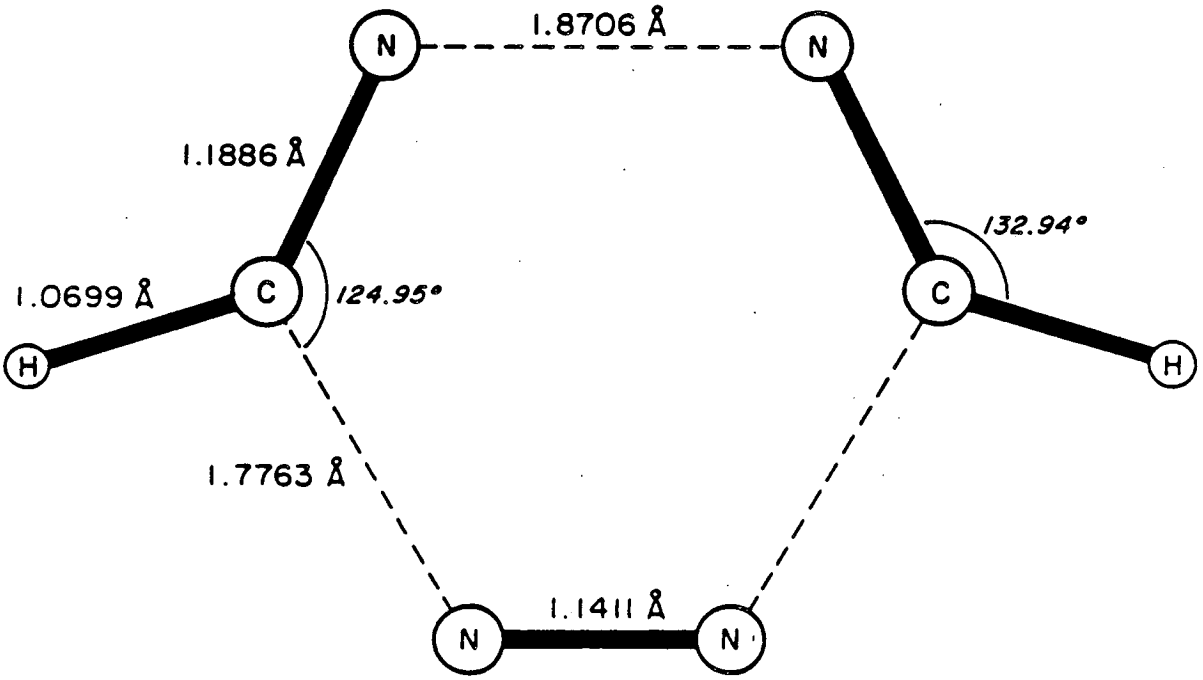

Figure 8: DZ+P SCF geometry for the dissociation transition state of *s*–tetrazine.

A stationary point geometry for the C_{2v} transition state was located using a DZ+P SCF wavefunction. This structure is illustrated in Figure 8. Harmonic vibrational analysis showed that this stationary point is in fact a true transition state with a single imaginary vibrational frequency of $1267i$ cm^{-1}, and the corresponding normal mode vibrational eigenvector does indeed connect the transition state to the HCN + HCN + N_2 products.

In order to more accurately predict the classical barrier height for the triple dissociation, single-point correlated energies were obtained at the SCF geometries for the *s*–tetrazine equilibrium and the transiton state structure. To this end, CCSD, CISD, and CISD(+Q) energies were calculated and these are summarized in Table XVII.

Table XVII. Theoretical predictions (in kcal/mol) of the classical barrier height for the triple dissociation of *s*–tetrazine. A standard DZ+P one-electron basis set was employed. The correlated energies were obtained at the SCF stationary points. ZPVE ≡ zero point vibrational energy.

	Classical Barrier Height
SCF	79.4
CISD	67.8
CISD(+Q)	60.1
CCSD	52.8
SCF ZPVE correction	– 5.8
exptl. activation energy	≤ 51.8

The important point to note here is that both the CISD and CISD(+Q) barriers when corrected for zero point vibrational energy predict barrier heights above the experimental activation enrgy (62.0 and 54.3 kcal/mol, respectively), and based on these results alone, conclusions as to the operablility of the triple dissociation pathway would be tentative. However, with the highest level of theory, CCSD with ZPVE correction, the activation energy for the triple dissociation is predited to be 47.0 kcal/mol. This prediction is 4.8 kcal/mol lower than the experimental upper limit. Furthermore, it is well established that such levels of theory yield activation energies above available observed experimental values (i.e. more complete correlation of the electrons will reduce the theoretical prediction slightly, a reasonable estimate would be 3 kcal/mol). Thus, one may conclude that the unimolecular triple dissociation proceeds with an energy below the $S_1 \leftarrow S_0$ electronic excitation of *s*–tetrazine.

Clearly, CISD and even Davidson corrected CISD are inadequate to properly describe the energetics of the photodynamics of *s*–tetrazine. Only by rigorously including the higher-order disconnected terms in the CCSD expansion does the theory predict a barrier height below the experimental activation energy. In this context both CISD and CISD(+Q) neglect contributions to the correlation energy which are of chemical importance.

Finally, the question of the overall exothermicity of the dissociation has not yet been resolved. The two previous estimates of – 1 kcal/mol[123] and – 51 kcal/mol[127] are clearly incompatible, and an accurate quantitative prediction of this value is certainly of interest and of importance in understanding the energies available to the products. Table XVIII presents the present theoretical predictions for the total exoergicity of dissociation. At the highest level of theory, single point DZ+P CCSD including the DZ+P SCF zero point vibrational energy correction,

$\Delta E_{dissociation} = -57.4$ kcal/mol. Thus a sizeable downhill energy gap is found between the reactant and product molecules, in concurrence with Coulter *et. al.*[127] Of course, the previous estimates were based on the total enthalpy change, $\Delta H_{dissociation}$, which includes a contribution from $+\Delta(PV)$. This contribution is most probably positive for this particular chemical process, but it could not possibly be as great as 56 kcal/mol. As a rough estimate, one can assume ideal gas behavior for the products and constant temperature and pressure at STP to give a $\Delta(PV) = +1.6$ kcal/mol. Thus one finds a rough prediction for $\Delta H_{dissociation}$ of -56.2 kcal/mol.

Table XVIII. Total exoergicity (in kcal/mol) for the dissociation of *s*–tetrazine to 2HCN + N_2. A standard DZ+P one-electron basis set was employed. Correlation energies were obtained at the SCF stationary points. ZPVE ≡ zero point vibrational energy.

	$\Delta E_{dissociation}$
SCF	− 56.9
CISD	− 44.3
CISD(+Q)	− 43.9
CCSD	− 48.1
ZPVE correction	− 9.3

An Efficient Formulation of the Closed-Shell CCSD Energy Gradient Equations

4.1 Introduction

Theoretical methods for the analytic evaluation of derivatives of the electronic energy with respect to nuclear displacements have proven to be powerful tools in the field of modern quantum chemistry.[49] Such methods greatly facilitate the location of stationary points on energy hypersurfaces for all but the most simple of molecular frameworks. When the nuclear dimensionality of these hypersurfaces exceeds three or four, the search for equilibrium chemical structures and transition states becomes impractical, if not impossible, without analytic energy derivatives.

Analytic energy gradients are now routinely obtained for both Hartree-Fock[173] and configuration interaction (CI)[174–177] wavefunctions. Additionally, the formulation and implementation of analytic energy gradients for multi-configuration SCF (MCSCF)[178–182], MCSCF-CI[183,184] wavefunctions, and second-[185] and third-order[186] many-body (or Møller-Plesset) perturbation theory (MP2 and MP3, respectively) wavefunctions has also been achieved. With the exception of MP theories, the energy obtained from the wavefunctions of the aforementioned methods is an expectation value in terms of a set of variationally optimized parameters. On the other hand, for MP2 and MP3 along with higher levels of many-body perturbation theory (MBPT), the energy is non-variationally obtained from a perturbation expansion of the wavefunction; and in truncated coupled cluster theory (CC), the energy is non-variationally obtained as $\langle\Psi_0| e^{-\hat{T}} \hat{H} e^{\hat{T}} |\Psi_0\rangle$, where Ψ_0 represents the one-particle reference function and $e^{\hat{T}}$ is the standard CC wave operator.

The theory of analytic derivatives for coupled cluster wavefunctions has taken shape very recently with the initial groundwork laid out by Jørgensen and Simons in 1983[187] who presented second quantized matrix/operator expressions for the gradient and Hessian of a general coupled cluster wavefunction. In 1984 Adamowicz, Laidig, and Bartlett presented initial algebraic expressions for the CCSD gradient.[188] Additionally, these authors proposed a computational strategy for implementing these expressions using the Z-vector method of Handy and Schaefer.[189] Following this, Fitzgerald, Harrison, Laidig, and Bartlett (1985) reported DZ CCD geometries and finite difference harmonic frequencies for H_2O and the $^1A_1$ state of CH_2.[190] Most recently, Bartlett[191] and Fitzgerald, Harrison, and Bartlett (FHB)[192] presented general diagrammatic and algebraic expressions for the analytic derivatives of CC and MBPT wavefunctions. FHB cast this energy gradient expression into a density matrix form (analogous to the efficient CI gradient approach[177]), and it is this idea upon which the present work is based.

In terms of formulating an analytic derivative theory, the energy gradients for these non-variational methods, $\frac{\partial E}{\partial \lambda}$, (where λ represents a generalized nuclear displacement) include a contribution from the derivative of the energy with respect to the configuration coefficients, $\frac{\partial E}{\partial C_i}$. This contribution is, by construction, zero for any variational method as the energy is stationary with respect to these coefficients. In principle, this makes the evaluation of the analytic energy gradient for the non-variational methods more difficult.[193] However, as shall be presented herein, analytic energy gradients for CC theory, or, in general, any non-variational theory, can be designed to be as computationally efficient as in the variational case.

As stressed above, the analytic evaluation of energy derivatives is an essential tool for the prediction of chemical structures and molecular harmonic vibrational frequencies. Additionally properties such as molecular dipole moments (gradient of the energy with respect to an external electric field), infrared absorption intensities (proportional to the square of the derivative of the dipole moment with respect to internal coordinates), molecular polarizabilities (second derivative of the energy with respect to an external electric field), and Raman absorption intensities (proportional to the square of the derivative of the polarizability with respect to internal coordinates) may be obtained from energy derivatives. Thus, in order to begin to fully assess the value of CCSD for general chemical applications, the theory and results of applications of a closed-shell RCCSD analytic gradient method are presented herein.

In what follows are presented (1) detailed formulas and implementational details for the efficient evaluation of analytic closed-shell CCSD energy gradients; (2) application of this method to the water and formaldehyde molecules; and (3) discussion of these results with particular emphasis on comparisons to analogous CI results and to experiment.

4.2 Derivation of the CCSD Gradient Equations

Recall from Eq. (2.28) that the total CCSD energy for a closed-shell system may be written

$$E_{CCSD} = E_0 + 2\sum_{i,a} f_a^i \, t_i^a + \sum_{\substack{i,j \\ a,b}} (2v_{ab}^{ij} - v_{ba}^{ij}) \, \tau_{ij}^{ab} \, . \tag{4.1}$$

Also recall that in order to determine the RCCSD cluster coefficients, a set of coupled, non-linear equations is solved [Eqs. (2.32) and (2.33)]. Here these two

equations will be written in a compact form, namely

$$W_u^\beta (t_1, t_2, F, V) = 0 \tag{4.2}$$

$$W_{uv}^{\beta\gamma} (t_1, t_2, F, V) = 0 \tag{4.3}$$

for the unique set of W_u^β and $W_{uv}^{\beta\gamma}$. The indices $u,v/\beta,\gamma$ are special occupied/unoccupied indices used to label the set of independent external indices for W_1 (W_u^β) and W_2 ($W_{uv}^{\beta\gamma}$). t_1 and t_2 represent the vectors of one-electron and two-electron cluster coefficients, respectively. Additionally, V and F are used here to represent the vectors of two-electron MO integrals and fock matrix, respectively.

As detailed in Section 2.2, there are NM unique elements of W_1 and t_1 and $\frac{1}{2}NM\times(NM + 1)$ unique elements of W_2 and t_2 where $NM = NO \times NV$ (# of doubly occupied orbitals × # of unoccupied MOs).

The primary goal of the present CCSD gradient study is to obtain an explicit analytic expression for $\frac{\partial E_{CCSD}}{\partial\lambda} \equiv E_{CCSD}^{(\lambda)}$ for each of the $3N_\alpha$ (where N_α represents the number of atomic centers) nuclear degrees of freedom. In the spirit of efficient gradient theories for correlated wavefunctions,[177,189,192,194] one would like to arrive at a final expression for $E_{CCSD}^{(\lambda)}$ in the form

$$E_{CCSD}^{(\lambda)} = \sum_{p,q} Q_{pq}\, h_{pq}^{(\lambda)} + \sum_{\substack{p,q\\r,s}} G_{pqrs}\, v_{qs}^{pr(\lambda)} \tag{4.4}$$

where the one- and two-electron derivative integrals, $h_{pq}^{(\lambda)} \equiv \frac{\partial h_{pq}}{\partial\lambda}$ and $v_{qs}^{pr(\lambda)} \equiv \frac{\partial v_{qs}^{pr}}{\partial\lambda}$, respectively, have been introduced along with Q and G the *effective* CCSD one- and

two-particle density matrices (1PDM and 2PDM), respectively. It is important to note the difference between these effective CCSD density matrices and the CI 1PDM and 2PDM. In the case of truncated CI theory, the density matrices are denstiy matrices in the usual sense, in that they define the CI energy

$$E_{CI} = \sum_{p,q} Q^{CI}_{pq}\, h_{pq} + \sum_{\substack{p,q \\ r,s}} G^{CI}_{pqrs}\, v^{pr}_{qs} \,. \tag{4.5}$$

The CCSD effective 1- and 2-PDMs are density matrices constructed in the context of Eq. (4.4) only, i.e. there is no CC expression analogous to Eq. (4.5) based on these effective density matrices.

Differentiating Eq. (4.1) with respect to λ yields

$$E^{(\lambda)}_{CCSD} = E^{(\lambda)}_0 + 2\sum_{i,a} f^{i(\lambda)}_a\, t^a_i + \sum_{\substack{i,j \\ a,b}} (2v^{ij}_{ab}{}^{(\lambda)} - v^{ij}_{ba}{}^{(\lambda)})\, \tau^{ab}_{ij} \tag{4.6}$$

$$+ 2\sum_{i,a} f^i_a\, t^{a(\lambda)}_i + \sum_{\substack{i,j \\ a,b}} (2v^{ij}_{ab} - v^{ij}_{ba})(2t^b_j t^{a(\lambda)}_i + t^{ab(\lambda)}_{ij}) \,.$$

Defining the vectors

$$\mathbf{t} \equiv \begin{bmatrix} t^a_i \\ t^{ab}_{ij} \end{bmatrix} \tag{4.7}$$

and

$$\mathbf{J} \equiv \begin{bmatrix} 2f^i_a + 2\sum_{j,b} (2v^{ij}_{ab} - v^{ij}_{ba})\, t^b_j \\ 2v^{ij}_{ab} - v^{ij}_{ba} \end{bmatrix} \tag{4.8}$$

Eq. (4.6) can be rewritten as

$$E^{(\lambda)}_{CCSD} = E^{(\lambda)}_0 + 2\sum_{i,a} f^{i(\lambda)}_a\, t^a_i + \sum_{\substack{i,j \\ a,b}} (2v^{ij}_{ab}{}^{(\lambda)} - v^{ij}_{ba}{}^{(\lambda)})\, \tau^{ab}_{ij} + \mathbf{J}^T \cdot \mathbf{t}^{(\lambda)} \,. \tag{4.9}$$

Note that the dot product defined in Eq. (4.9) runs over all i,j,a,b for the two-electron term as prescribed by Eq. (4.6)

In order to evaluate the $\mathbf{J}^T \cdot \mathbf{t}^{(\lambda)}$ contribution to the gradient, expressions for the linear response of $\mathbf{t}_1$ and $\mathbf{t}_2$ with respect to λ are needed. Considering the set of Eqs. (4.2) and (4.3) at some perturbed nuclear geometry, $\lambda = \lambda_0 + \Delta\lambda$, one can write the expansion

$$\mathbf{W}_i[\lambda] = \mathbf{W}_i[\lambda_0] + \left[\frac{\partial \mathbf{W}_i}{\partial \lambda}\right]_{\lambda=\lambda_0} \cdot \Delta\lambda + \left[\frac{\partial^2 \mathbf{W}_i}{\partial \lambda^2}\right]_{\lambda=\lambda_0} \cdot (\Delta\lambda)^2 + \cdots \qquad (4.10)$$

$$i = 1,2 \text{ for CCSD,}$$

and since Eqs. (4.2) and (4.3) must be satisfied at both λ and λ_0, i.e. $\mathbf{W}_i[\lambda] = 0$ and $\mathbf{W}_i[\lambda_0] = 0$, then to first order in $\Delta\lambda$

$$\left[\frac{\partial \mathbf{W}_i}{\partial \lambda}\right]_{\lambda=\lambda_0} = 0 \qquad i = 1, 2 \text{ for CCSD.} \qquad (4.11)$$

Now using the chain rule,

$$\frac{\partial \mathbf{W}_i}{\partial \lambda} = 0 = \frac{\partial \mathbf{W}_i}{\partial \mathbf{t}_1} \cdot \frac{\partial \mathbf{t}_1}{\partial \lambda} + \frac{\partial \mathbf{W}_i}{\partial \mathbf{t}_2} \cdot \frac{\partial \mathbf{t}_2}{\partial \lambda} + \frac{\partial \mathbf{W}_i}{\partial \mathbf{F}} \cdot \frac{\partial \mathbf{F}}{\partial \lambda} + \frac{\partial \mathbf{W}_i}{\partial \mathbf{V}} \cdot \frac{\partial \mathbf{V}}{\partial \lambda} \qquad (4.12)$$

and writing this in matrix form

$$\begin{bmatrix} \frac{\partial \mathbf{W}_1}{\partial \mathbf{t}_1} & \frac{\partial \mathbf{W}_1}{\partial \mathbf{t}_2} \\ \frac{\partial \mathbf{W}_2}{\partial \mathbf{t}_1} & \frac{\partial \mathbf{W}_2}{\partial \mathbf{t}_2} \end{bmatrix} \cdot \begin{bmatrix} \mathbf{t}_1^{(\lambda)} \\ \mathbf{t}_2^{(\lambda)} \end{bmatrix} = - \begin{bmatrix} \mathbf{B}_1^{(\lambda)} \\ \mathbf{B}_2^{(\lambda)} \end{bmatrix} \qquad (4.13)$$

or in compact notation

$$\mathbf{A} \cdot \mathbf{t}^{(\lambda)} = - \mathbf{B}^{(\lambda)} \qquad (4.14)$$

where

$$\mathbf{B}_i^{(\lambda)} = \frac{\partial \mathbf{W}_i}{\partial \mathbf{F}} \cdot \mathbf{F}^{(\lambda)} + \frac{\partial \mathbf{W}_i}{\partial \mathbf{V}} \cdot \mathbf{V}^{(\lambda)}. \tag{4.15}$$

The explicit expressions for elements of the $\mathbf{B}_i^{(\lambda)}$ vector were derived in a much simpler fashion than that implied by Eq. (4.15). An equivalent (and much less tedious) approach is to perturb the Fock matrix elements and two-electron integrals in the zeroth order CCSD equations, Eqs. (2.32) and (2.33). In other words, one simply writes the elements of the $\mathbf{B}_i^{(\lambda)}$ vector by replacing all f_q^p by $f_q^{p(\lambda)}$ and all v_{qs}^{pr} by $v_{qs}^{pr(\lambda)}$ in Eqs. (2.32) and (2.33).

This linear system, Eqs. (4.13) or (4.14), is the first-order coupled perturbed coupled cluster (CPCC) set of equations. The analogous CI contribution, first-order CPCI, does not contribute to the CI gradient since the energy is stationary with respect to the configuration coefficients. The above analysis, Eqs. (4.10)-(4.15), is not unique to the closed-shell CCSD method. As shown by Bartlett[191] and FHB,[192] analogous sets of linear CP equations will be necessary for analytic evaluation of gradients for a general coupled cluster wavefunction. However, there is no need to evaluate this contribution when considering finite orders of MBPT.[192] Of course, for higher levels of CC truncation, the A matrix, $\mathbf{t}^{(\lambda)}$, and $\mathbf{B}^{(\lambda)}$ will be of larger dimension, and, similarly, for a UCC method, the size of these will depend on the number of independent *spin* orbitals as opposed to spatial MOs used in the present implementation.

The CPCC equations depend on the nuclear perturbation through $\mathbf{t}^{(\lambda)}$ and $\mathbf{B}^{(\lambda)}$. The A matrix is independent of the perturbation however, and if explicitly constructed, may be utilized in the solution of higher order CPCC systems (needed for analytic evaluation of higher derivatives). As shown by Monkhorst,[58] all orders of

CPCC systems are defined by this same perturbation independent A matrix.

From Eq. (4.14) it appears that one must solve for $\mathbf{t}^{(\lambda)}$ for each of the $3N_\alpha$ nuclear perturbations. However, one can introduce the *Z*–vector method of Handy and Schaefer[189] such that only one perturbation independent solution to Eq. (4.14) is required. Let

$$\mathbf{Z} = \begin{bmatrix} \mathbf{Z}_1 \\ \mathbf{Z}_2 \end{bmatrix} \tag{4.16}$$

be a vector of length $NM + \frac{1}{2}NM\times(NM + 1)$ defined such that

$$\mathbf{A}^T * \mathbf{Z} = -\mathbf{J} \tag{4.17}$$

with **A** and **J** defined in Eqs. (4.14) and (4.8) respectively. Note that the *star* product defined in Eq. (4.17) is distinct from the *dot* product used in Eqs. (4.9), (4.13), and (4.14). The star product runs over the the reduced/independent set of two-particle CPCC coefficients, while the dot product includes all i,j,a,b. Taking the transpose of Eq. (4.17) and right-multiplying (using the *dot* product) with $t^{(\lambda)}$ yields the result

$$\mathbf{J}^T \cdot \mathbf{t}^{(\lambda)} = \mathbf{Z}^T * \mathbf{B}^{(\lambda)} . \tag{4.18}$$

Eq. (4.18) is the CPCC contribution to the total energy gradient [see Eq. (4.9)]. Thus, one only need solve Eq. (4.17), which is perturbation independent, once, and this solution is contracted with $\mathbf{B}^{(\lambda)}$ for each of the nuclear degrees of freedom.

The explicit form of Eq. (4.17) is presented in Section 4.3, however, several important points regarding details of its solution and construction will be discussed here.

First, if one attempts to construct the $\mathbf{A}^T$ matrix explicitly, terms arise which scale at best as $\begin{cases} NV^4\,NO^3 \\ NO^4\,NV^3 \end{cases} \approx N^7$: an order of N more costly than both CI gradients and the CCSD equations themselves. A process with such an N^7 computational requirement is very expensive and not tractable for application to most systems of chemical interest given the present state of computational technology. However, if $\mathbf{A}^T$ is never explicitly constructed, and an iterative procedure is used to seek the solution $\mathbf{Z}$, then the process remains proportional to N^6. For example, in explicit construction of $\mathbf{A}^T$ (from $\frac{\partial W_{\mu\nu}^{\beta\gamma}}{\partial t_{kl}^{cd}}$), one must evaluate

$$\delta_{uk} \sum_i (v_{cd}^{li} - 2v_{dc}^{li})\, t_{iv}^{\beta\gamma} \tag{4.19}$$

which is an unavoidable $NV^4\,NO^3$ process. Conversely, when $\mathbf{A}^T * \mathbf{Z}$ is formed, this term becomes

$$\sum_{\substack{i,v \\ \beta,\gamma}} (v_{cd}^{li} - 2v_{dc}^{li})\, t_{iv}^{\beta\gamma}\, Z_{kv}^{\beta\gamma} \tag{4.20}$$

which scales as $2\,NO^3\,NV^2$. Similarly, all N^7 type terms appearing in $\mathbf{A}^T$ can be reduced to, at worst, N^6 processes after contraction with $\mathbf{Z}$. The preferred method for solution of Eq. (4.17) is, therefore, explicit evaluation of the product

$$\begin{bmatrix} \frac{\partial \mathbf{W}_1}{\partial \mathbf{t}_1} & \frac{\partial \mathbf{W}_2}{\partial \mathbf{t}_1} \\ \frac{\partial \mathbf{W}_1}{\partial \mathbf{t}_2} & \frac{\partial \mathbf{W}_2}{\partial \mathbf{t}_2} \end{bmatrix} * \begin{bmatrix} \mathbf{Z}_1 \\ \mathbf{Z}_2 \end{bmatrix} \tag{4.21}$$

or equivalently,

$$\sum_{u,\beta} \frac{\partial W_u^{\beta}}{\partial t_k^c}\, Z_u^{\beta} + \sum_{\left\{\substack{u,v \\ \beta,\gamma}\right\}} \frac{\partial W_{uv}^{\beta\gamma}}{\partial t_k^c}\, Z_{uv}^{\beta\gamma} \tag{4.22a}$$

$$\sum_{u,\beta} \frac{\partial W_u^\beta}{\partial t_{kl}^{cd}} Z_u^\beta + \sum_{\substack{u,v \\ \beta,\gamma}} \frac{\partial W_{uv}^{\beta\gamma}}{\partial t_{kl}^{cd}} Z_{uv}^{\beta\gamma} \tag{4.22b}$$

Eqs. (4.22a) and (4.22b) are then set equal to $-J_k^c$ and $-J_{kl}^{cd}$ respectively.

$$\sum_{u,\beta} \frac{\partial W_u^\beta}{\partial t_k^c} Z_u^\beta + \sum_{\substack{u,v \\ \beta,\gamma}} \frac{\partial W_{uv}^{\beta\gamma}}{\partial t_k^c} Z_{uv}^{\beta\gamma} = -2 f_c^k - \sum_{j,b} 2(v_{cb}^{kj} - v_{bc}^{kj})\, t_j^b \tag{4.23a}$$

$$\sum_{u,\beta} \frac{\partial W_u^\beta}{\partial t_{kl}^{cd}} Z_u^\beta + \sum_{\substack{u,v \\ \beta,\gamma}} \frac{\partial W_{uv}^{\beta\gamma}}{\partial t_{kl}^{cd}} Z_{uv}^{\beta\gamma} = -2 v_{cb}^{kj} + v_{bc}^{kj} \tag{4.23b}$$

Eqs. (4.23a) and (4.23b) are then cast into an iterative form for Z_u^β and $Z_{uv}^{\beta\gamma}$ (see Section 4.3) and solved to within a chosen tolerance. Here as with the CCSD equations themselves, the DIIS convergence scheme[195] has proven to be valuable.

The notation $\sum_{\substack{u,v \\ \beta,\gamma}}$ has been used to designate that these summations be carried out only over the independent $\frac{1}{2}NM\times(NM+1)$ elements of $Z_{uv}^{\beta\gamma}$: all u, v for $\beta > \gamma$ and $u \geq v$ for $\beta = \gamma$. The explicit iterative expressions for Eqs. (4.23a) and (4.23b) were obtained by using the relationship

$$\sum_{\substack{u,v \\ \beta,\gamma}} '\ldots' = \frac{1}{2}\left[\sum_{\substack{u,v \\ \beta,\gamma}} '\ldots' + \sum_{\substack{u=v \\ \beta=\gamma}} '\ldots'\right] = \frac{1}{2}\sum_{\substack{u,v \\ \beta,\gamma}} (1 + \delta_{uv}\delta_{\beta\gamma})\, '\ldots' \tag{4.24}$$

Thus, if the $\mathbf{Z}_2$ terms are rescaled by defining

$$\tilde{Z}_{uv}^{\beta\gamma} \equiv Z_{uv}^{\beta\gamma}\,(1 + \delta_{uv}\delta_{\beta\gamma})\,, \tag{4.25}$$

Eqs. (4.23a) and (4.23b) can be expressed as

$$\sum_{u,\beta} \frac{\partial W_u^\beta}{\partial t_k^c} Z_u^\beta + \frac{1}{2}\sum_{\substack{u,v \\ \beta,\gamma}} \frac{\partial W_{uv}^{\beta\gamma}}{\partial t_k^c} \tilde{Z}_{uv}^{\beta\gamma} = -2 f_c^k - \sum_{j,b} 2(v_{cb}^{kj} - v_{bc}^{kj})\, t_j^b \tag{4.26a}$$

$$\sum_{u,\beta} \frac{\partial W_u^\beta}{\partial t_{kl}^{cd}} Z_u^\beta + \frac{1}{2} \sum_{\substack{u,v \\ \beta,\gamma}} \frac{\partial W_{uv}^{\beta\gamma}}{\partial t_{kl}^{cd}} \tilde{Z}_{uv}^{\beta\gamma} = -2v_{cb}^{kj} + v_{bc}^{kj} \tag{4.26b}$$

which greatly simplifies the derivation of these expressions.

Along these same lines, the indices labeling Eq. (4.26b) may be chosen to be either the independent $\frac{1}{2}NM\times(NM+1)$ set or the complete/redundant set of all $NO^2 \times NV^2$ $\mathbf{t}_2$'s provided an iterative scheme is employed. If, however, explicit formation and inversion of $\mathbf{A}^T$ is used, then only the independent set of Eqs. (4.26b) is adequate since for the complete/redundant set, $\det \mathbf{A}^T = 0$.

Another mathematical point of note arises when evaluating the derivatives $\frac{\partial \mathbf{W}_i}{\partial \mathbf{t}_2}$. Recall from the symmetry of $\mathbf{t}_2$ that $t_{uv}^{\beta\gamma} = t_{vu}^{\gamma\beta}$. Thus,

$$\frac{\partial t_{uv}^{\beta\gamma}}{\partial t_{kl}^{cd}} = \begin{cases} \delta_{uk}\delta_{vl}\delta_{\beta c}\delta_{\gamma d} & \text{if } u = v \text{ and } \beta = \gamma \\ \delta_{uk}\delta_{vl}\delta_{\beta c}\delta_{\gamma d} + \delta_{ul}\delta_{vk}\delta_{\beta d}\delta_{\gamma c} & \text{otherwise} \end{cases} \tag{4.27}$$

The actual derivations of $\frac{\partial \mathbf{W}_i}{\partial \mathbf{t}_2}$, therefore, required two separate procedures: (1) for $u \neq v$ or $\beta \neq \gamma$ and (2) for $u = v$ and $\beta = \gamma$. With the definition of $\tilde{\mathbf{Z}}$ [Eq. (4.25)], however, and because of the action of the permutation operator on the $\mathbf{W}_2$ equation (Section 2.2), it is possible to write a final expression for Eq. (4.26b) in a general form as presented in Section 4.3. Finally, the contraction $\mathbf{Z}^T * \mathbf{B}^{(\lambda)}$ (spanning the independent terms) is evaluated for its contributions to the effective one- and two-particle density matrices of Eq. (4.4).

The remaining contributions to Eq. (4.9), namely

$$E_0^{(\lambda)} + 2\sum_{i,a} f_a^{i(\lambda)} t_i^a + \sum_{\substack{i,j \\ a,b}} (2v_{ab}^{ij\,(\lambda)} - v_{ba}^{ij\,(\lambda)})\, \tau_{ij}^{ab} , \tag{4.28}$$

where in the present implementation

$$E_0^{(\lambda)} = E_{RHF}^{(\lambda)} = 2\sum_i h_{ii}^{(\lambda)} + \sum_{i,j} (2v_{ij}^{ij(\lambda)} - v_{ji}^{ij(\lambda)}), \tag{4.29}$$

are straightforward to evaluate, and the final expressions for **Q** and **G** are presented in Section 4.3. Additionally, the construction of **G** can be designed to scale as no worse than N^6 and that of **Q** as no worse than N^5.

Now the contributions from the total MO derivative integrals $h_{pq}^{(\lambda)}$ and $v_{qs}^{pr(\lambda)}$ are addressed. At this stage, the methodology employed exactly parallels the CI gradient approach of Rice and co-workers[187] of which an outline is presented here.

From standard coupled perturbed Hartree-Fock (CPHF) theory,[196]

$$h_{pq}^{(\lambda)} = h_{pq}^{\lambda} + \sum_t (U_{tp}^{\lambda} h_{tq} + U_{tq}^{\lambda} h_{pt}) \tag{4.30}$$

$$v_{qs}^{pr(\lambda)} = v_{qs}^{pr\,\lambda} + \sum_t (U_{tp}^{\lambda} v_{qs}^{tr} + U_{tq}^{\lambda} v_{ts}^{pr} + U_{tr}^{\lambda} v_{qs}^{pt} + U_{ts}^{\lambda} v_{qt}^{pr}) \tag{4.31}$$

where h_{pq}^{λ}, $v_{qs}^{pr\,\lambda}$ are the AO derivative integrals rotated into the MO basis

$$h_{pq}^{\lambda} = \sum_{\mu,\omega} c_{\mu p}\, c_{\omega q}\, h_{\mu\omega}^{\lambda} \tag{4.32}$$

$$v_{qs}^{pr\,\lambda} = \sum_{\substack{\mu,\omega \\ \rho,\sigma}} c_{\mu p}\, c_{\omega q}\, c_{\rho r}\, c_{\sigma s}\, v_{\omega\sigma}^{\mu\rho\,\lambda} \tag{4.33}$$

and U_{pq}^{λ} are the first-order CPHF coefficients which represent the linear response of the MO coefficients to the perturbation λ. The greek indices μ, ω, ρ, σ have been used to label atomic orbitals in Eqs. (4.32) and (4.33). Additionally, the total derivative Fock matrix can be expressed explicity in terms of derivative integrals and CPHF coefficients by differentiating Eq. (2.31) with respect to λ and using Eqs. (4.30) and (4.31)

$$f_q^{p(\lambda)} = f_q^{p\,\lambda} + \sum_r (U_{rp}^\lambda f_q^r + U_{rq}^\lambda f_p^r) + \sum_{r,i} U_{ri}^\lambda (4v_{qi}^{pr} - v_{ri}^{pq} - v_{ir}^{pq}) \tag{4.34}$$

where

$$f_q^{p\,\lambda} = h_{pq}^\lambda + \sum_i (2v_{qi}^{pi\,\lambda} - v_{ii}^{pq\,\lambda}) \,. \tag{4.35}$$

As per reference 187, the total electronic energy gradient is now expressed as

$$E_{CCSD}^{(\lambda)} = 2 \sum_{p,q} U_{pq}^\lambda X_{qp} + \sum_{p,q} Q_{pq} h_{pq}^\lambda + \sum_{\substack{p,q \\ r,s}} G_{pqrs} v_{qs}^{pr\,\lambda} \,. \tag{4.36}$$

Note that in going from Eq. (4.4) to Eq. (4.36), the CPHF contributions have been separated, and now the MO density matrices are contracted with the AO derivative integrals rotated into the MO basis. X_{pq} represents the CC Langrangian matrix with elements

$$X_{pq} = \sum_r Q_{pr} h_{qr} + 2 \sum_{r,s,t} G_{prst} v_{rt}^{qs} \,. \tag{4.37}$$

Furthermore, by back transforming the effective one- and two-particle density matrices into the AO basis and, thus, writing Eq. (4.36) as

$$E_{CCSD}^{(\lambda)} = 2 \sum_{p,q} U_{pq}^\lambda X_{qp} + \sum_{\mu,\omega} Q_{\mu\omega} h_{\mu\omega}^\lambda + \sum_{\substack{\mu,\omega \\ \rho,\sigma}} G_{\mu\omega\rho\sigma} v_{\omega\sigma}^{\mu\rho\,\lambda} \tag{4.38}$$

only a single four index transformation (of the 2PDM) is required rather than $3N_\alpha$ of such transformations (of two-electron derivative integrals) as implied by Eq. (4.36). In this way, the derivative integrals $v_{\omega\sigma}^{\mu\rho\,\lambda}$ require no permanent disk storage; rather each is formed in core memory and immediately contracted with the appropriate 2PDM elements.

Further simplifications to the method result from consideration of redundancies in the CPHF solution U_{pq}^λ. Essentially, by recognizing that the energy is invariant to

a unitary transformation among MOs of the same type (active doubly occupied, active unoccupied, frozen core, frozen virtual, and various open-shell orbitals), one need only solve the CPHF equations for matrix elements which connect MOs of different type, the so-called non-redundant pairs. The remaining matrix elements (representing redundant pairs) can simply be evaluated by using the orthonormality condition of the MOs: $U^{\lambda}_{pq} + U^{\lambda}_{qp} + S^{\lambda}_{pq} = 0$ where S^{λ}_{pq} is the derivative overlap matrix rotated into the MO basis. In the present implementation of the CCSD gradient method with the restriction to closed-shell systems and with all orbitals active in the correlation procedure, the CC non-redundant pairs are simply the SCF non-redundant pairs: a doubly occupied orbital paired with an unoccupied orbital. The Z-vector method[189] (see above discussion of CPCC solution) was also applied to the solution of the CPHF equations. With these additional implementations, the final working expression for the analytic gradient of the CCSD electronic energy with respect to λ is

$$E^{(\lambda)}_{CCSD} = \sum_{p>q}^{\substack{CC \\ nonred}} z_{pq}\, b^{\lambda}_{pq} - \sum_{p,q} X_{pq}\, S^{\lambda}_{pq} + \sum_{\mu,\omega} Q_{\mu\omega}\, h^{\lambda}_{\mu\omega} + \sum_{\substack{\mu,\omega \\ \rho,\sigma}} G_{\mu\omega\rho\sigma}\, v^{\mu\rho\ \lambda}_{\omega\sigma} \qquad (4.39)$$

where $\mathbf{z}$ is the solution of the perturbation independent CPHF equation

$$\mathbf{a}^T \cdot \mathbf{z} = -\Delta\mathbf{X} \qquad (4.40)$$

with $\Delta X_{pq} = X_{pq} - X_{qp}$. Explicit formulas for the general CPHF $\mathbf{a}^T$ matrix and $\mathbf{b}^{\lambda}$ vector are given in reference 187. In the present implementation, these reduce to the closed-shell RHF expressions:

$$a_{pqrs} = 4v^{pr}_{qs} - v^{pq}_{rs} - v^{pq}_{sr} \qquad (4.41)$$

$$b_{pq}^{\lambda} = h_{pq}^{\lambda} + \sum_{k} (2v_{qk}^{pk\,\lambda} - v_{kk}^{pq\,\lambda}) - S_{pq}^{\lambda} \left\{ h_{qq} + \sum_{k} (2v_{qk}^{qk} - v_{kk}^{qq}) \right\} \qquad (4.42)$$

$$- \sum_{k,l} S_{kl}^{\lambda} (2v_{jl}^{ik} - v_{kl}^{ij}) \, .$$

The final gradient of the total energy with respect to perturbation must, of course, include the nuclear-nuclear repulsion terms which are trivially evaluated within the Born-Oppenheimer approximation.

The overall process of evaluating the analytic CCSD gradient is as follows:

[1] The one- and two-electron integrals are evaluated in the basis of symmetrized atomic orbitals.

[2] The SCF procedure is carried out to obtain a closed-shell independent-particle reference determinant.

[3] The one- and two-electron integrals are transformed into the MO basis, and the two-electron MO integrals are then sorted in preparation for the CCSD program.

[4] The $\mathbf{t}_1$ and $\mathbf{t}_2$ amplitudes are evaluated by iteratively solving the set of Eqs. (2.32) and (2.33).

[5] The linear system of CPCCSD equations is solved (see Eqs. (4.44) and (4.45) below) iteratively for $\mathbf{Z}_1$ and $\tilde{\mathbf{Z}}_2$.

[6] The effective CCSD one- and two-particle density matrices are constructed (see Eqs. (4.62)-(4.70) below).

[7] The Lagrangian X_{pq} is constructed.

[8] Q and G are back transformed into the AO basis.

[9] Molecular dipole moments are evaluated analytically as

$$\mu_x = \frac{dE}{d\varepsilon_x} = -\sum_{p,q} Q_{pq} \langle p|x|q\rangle - 2 \sum_{p>q}^{nonred} z_{pq} \langle p|x|q\rangle. \tag{4.43}$$

The first term in this expression is evaluated here while the second term is evaluated in step [11] following solution of the CPHF equations.

[10] The derivative integrals in the AO basis are formed and immediately contracted with the back-transformed one- and two-particle density matrices. Additionally, the AO derivative overlap integrals are transformed into the MO basis and contracted with the Langrangian.

[11] Using the Langrangian as a perturbation, the CPHF equations are solved for **z**, and this vector is then contracted with each of the $\mathbf{b}^{\lambda}$ as prescribed by Eq. (4.39).

Summarizing this section, the important aspects of the present formulation of the analytic CC gradient should be re-emphasized. First, in order to keep this method computationally tractable (N^6 dependence), explicit formation of the $\mathbf{A}^T$ matrix must be avoided, and the CPCC equations must be solved in an iterative fashion. Second, the *Z*-vector method allows the perturbation dependent linear response equations (both CPCC and CPHF) to be reformulated such that these systems be solved only once in a perturbation independent scheme. Furthermore, in this same spirit of efficient algorithms for analytic gradient evaluation of correlated wave functions, AO two-electron derivative integrals are contracted with the appropriate back transformed effective CCSD 2PDM elements upon construction. In this way, there is no need to rotate or store these derivative integrals for later use. Finally, it is worth noting that although the specific equations presented herein were formulated within the closed-

shell CC singles and doubles approach, the extension of the general ideas of the present formalism to cover both UCC wave functions and higher levels of CC truncation is clearly possible.

4.3 Implementational Details

In this section the explicit form of the iterative CPCC equations and the effective CCSD one- and two-particle density matrices are presented. In a manner analogous to the reformulation of the CCSD equations into iterative expressions for t_u^β and $t_{uv}^{\beta\gamma}$, Eqs. (4.26a) and (4.26b) are cast into iterative forms for Z_u^β and $\tilde{Z}_{uv}^{\beta\gamma}$, respectively

$$(f_\beta^\beta - f_u^u)\, Z_u^\beta = -2I_u^\beta + \sum_a g_a^\beta\, Z_u^a + \sum_i k_u^i\, Z_i^\beta + \sum_{i,a} (r-2q)_{ua}^{\beta i}\, Z_i^a + \sum_{\substack{i,j \\ a}} E_{ua}^{ij}\, \tilde{Z}_{ij}^{\beta a} \qquad (4.44)$$

$$+ \sum_{\substack{i \\ a,b}} F_{ab}^{\beta i}\, \tilde{Z}_{ui}^{ab} + \sum_i f_i^\beta\, (t\tilde{Z}_2)_{iu} + \sum_a f_u^a\, (t\tilde{Z}_2)^{a\beta} + \sum_{i,j} j_{iu}^{j\beta}\, (t\tilde{Z}_2)_{ij} + \sum_{a,b} H_{bu}^{a\beta}\, (t\tilde{Z}_2)^{ab}$$

$$(f_\beta^\beta + f_\gamma^\gamma - f_u^u - f_v^v)\, \tilde{Z}_{uv}^{\beta\gamma} = \sum_{i,j} a_{uv}^{ij}\, \tilde{Z}_{ij}^{\beta\gamma} + \sum_{a,b} b_{ab}^{\beta\gamma}\, \tilde{Z}_{uv}^{ab} + \hat{P}\Big\{ - I_{uv}^{\beta\gamma} + I_u^\gamma\, Z_v^\beta \qquad (4.45)$$

$$- 2I_v^\gamma\, Z_u^\beta + \sum_b I_{uv}^{b\gamma}\, (t\tilde{Z}_2)^{b\beta} + \sum_j I_{jv}^{\beta\gamma}\, (t\tilde{Z}_2)_{ju} + \sum_a g_a^\gamma\, \tilde{Z}_{uv}^{\beta a} + \sum_i k_v^i\, \tilde{Z}_{ui}^{\beta\gamma} + \sum_a H_{av}^{\beta\gamma}\, Z_u^a$$

$$+ \sum_i f_{uv}^{i\gamma}\, Z_i^\beta + \sum_{i,a} r_{ua}^{\gamma i}\, \tilde{Z}_{iv}^{\beta a} + \sum_{i,a} q_{ua}^{\gamma i}\, \tilde{Z}_{vi}^{\beta a} + \sum_{i,a} (r-2q)_{va}^{\gamma i}\, \tilde{Z}_{ui}^{\beta a}\Big\}$$

where

$$\tilde{Z}_{ij}^{ab} = Z_{ij}^{ab}\,(1 + \delta_{ij}\delta_{ab}) \qquad (4.46)$$

and the following intermediate products have been defined to facilitate computational

efforts

$$I_u^{\beta} = f_u^{\beta} + \sum_{i,a} (2v_{ua}^{\beta i} - v_{iu}^{\beta a})\, t_i^a \,, \tag{4.47}$$

$$I_{uv}^{\beta\gamma} = 2v_{uv}^{\beta\gamma} - v_{vu}^{\beta\gamma} \,, \tag{4.48}$$

$$g_a^{\beta} = -f_a^{\beta}\,(1 - \delta_{\beta a}) + \sum_i f_i^{\beta}\, t_i^a - \sum_{i,b} (2v_{ai}^{\beta b} - v_{ia}^{\beta b})\, t_i^b + \sum_{\substack{i,j \\ b}} (2v_{ij}^{\beta b} - v_{ji}^{\beta b})\, \tau_{ij}^{ab} \,, \tag{4.49}$$

$$k_u^i = f_u^i\,(1 - \delta_{ui}) + \sum_a f_u^a\, t_i^a + \sum_{j,a} (2v_{ji}^{au} - v_{ui}^{aj})\, t_j^a + \sum_{\substack{j \\ a,b}} (2v_{uj}^{ab} - v_{ju}^{ab})\, \tau_{ij}^{ab} \,, \tag{4.50}$$

$$r_{ua}^{\beta i} = v_{au}^{\beta i} + \sum_b v_{ab}^{\beta u}\, t_i^b - \sum_j v_{ju}^{\beta i}\, t_j^a - \sum_{j,b} v_{ju}^{\beta b}\, \tau_{ji}^{ab} \,, \tag{4.51}$$

$$q_{ua}^{\beta i} = v_{ua}^{\beta i} + \sum_b v_{ua}^{\beta b}\, t_i^b - \sum_j v_{uj}^{\beta i}\, t_j^a - \sum_{j,b} v_{ju}^{\beta b}\, t_{ij}^{ab} + \sum_{j,b} v_{uj}^{\beta b}\, (2t_{ij}^{ab} - \tau_{ji}^{ab}) \,, \tag{4.52}$$

$$H_{av}^{\beta\gamma} = v_{va}^{\beta\gamma} - 2v_{av}^{\beta\gamma} + \sum_i (2v_{iv}^{\beta\gamma} - v_{vi}^{\beta\gamma})\, t_i^a \,, \tag{4.53}$$

$$j_{uv}^{i\gamma} = 2v_{vu}^{\gamma i} - v_{uv}^{\gamma i} + \sum_a (2v_{vu}^{\gamma a} - v_{uv}^{\gamma a})\, t_i^a \,, \tag{4.54}$$

$$(t\tilde{Z}_2)^{ab} = \sum_{\substack{i,j \\ c}} t_{ij}^{ac}\, \tilde{Z}_{ij}^{bc} \,, \tag{4.55}$$

$$(t\tilde{Z}_2)_{ij} = \sum_{\substack{k \\ a,b}} t_{ik}^{ab}\, \tilde{Z}_{jk}^{ab} \,, \tag{4.56}$$

$$E_{ua}^{ij} = v_{ua}^{ij} + \sum_{k} a_{uk}^{ij}\, t_k^a + \sum_{k,b} j_{uk}^{ib}\, t_{jk}^{ab} + \sum_{b,c} v_{ua}^{bc}\, \tau_{ij}^{bc} + \sum_{b} (v_{ua}^{bj}\, t_i^b + v_{ua}^{ib}\, t_j^b) \tag{4.57}$$

$$- \sum_{k,b} (v_{uk}^{bj}\, t_{ki}^{ab} + v_{ub}^{ik}\, t_{kj}^{ab}) - \sum_{\substack{k \\ b,c}} (v_{uk}^{bc}\, t_{kj}^{ac}\, t_i^b + v_{uk}^{cb}\, t_{ki}^{ac}\, t_j^b) + \sum_{\substack{k \\ b,c}} (2v_{uk}^{cb} - v_{ku}^{cb})\, t_{ji}^{ac}\, t_k^b \,,$$

$$F_{ab}^{\beta i} = - v_{ab}^{\beta i} + \sum_{c} b_{ab}^{\beta c}\, t_i^c + \sum_{j,c} H_{aj}^{\beta c}\, t_{ij}^{bc} - \sum_{j,k} v_{kj}^{\beta i}\, \tau_{jk}^{ba} + \sum_{j} (v_{aj}^{\beta i}\, t_j^b + v_{ji}^{\beta b}\, t_j^a) \tag{4.58}$$

$$+ \sum_{j,c} (v_{aj}^{\beta c}\, t_{ji}^{bc} + v_{jc}^{\beta b}\, t_{ij}^{ca}) - \sum_{\substack{j,k \\ c}} (v_{jk}^{\beta c}\, t_{ki}^{bc}\, t_j^a + v_{kj}^{\beta c}\, t_{ki}^{ac}\, t_j^b) + \sum_{\substack{j,k \\ c}} (2v_{kj}^{\beta c} - v_{jk}^{\beta c})\, t_{ik}^{ba}\, t_j^c \,,$$

$$a_{uv}^{ij} = - v_{uv}^{ij} - \sum_{a,b} v_{uv}^{ab}\, \tau_{ij}^{ab} - \sum_{a} (v_{uj}^{av}\, t_i^a + v_{vi}^{au}\, t_j^a) \,, \tag{4.59}$$

$$b_{ab}^{\beta\gamma} = - v_{ab}^{\beta\gamma} - \sum_{i,j} v_{ij}^{\beta\gamma}\, \tau_{ij}^{ab} + \sum_{i} (v_{ib}^{\beta\gamma}\, t_i^a + v_{ia}^{\gamma\beta}\, t_i^b) \,. \tag{4.60}$$

Also, the permutation operator $\hat{P}$ as defined by Eq. (2.35) is utilized in Eq. (4.45) to reduce the size of the algebraic expression.

It was decided, based on both derivational and computational grounds, to break the construction of the one- and two-particle density matrices into a sequence of steps in which blocks of these matrices are formed separately and then placed into their appropriate locations in the full one- and two-PDMs. In the case of the 1PDM, the blocks occupied-occupied, virtual-occupied, and virtual-virtual have been constructed

separately; while for the 2PDM the six blocks *oooo*, *vvvv*, *vvoo*, *vovo*, *vooo*, and *vovv* were constructed separately. In the case of the 2PDM, these blocks have been labeled G^A, G^B, G^C, G^D, G^E, and G^F, respectively. This notation has been chosen to correspond to the nomenclature for the two-electron integrals employed in the solution of the CCSD equations (see Section 2.3). Furthermore, if one considers the one-particle density matrix term in Eq. (4.36), one may rewrite the sum

$$\sum_{p,q} Q_{pq}\, h^{\lambda}_{pq} = \sum_{p \geq q} (Q_{pq} + Q_{qp})\, h^{\lambda}_{pq} \times \begin{Bmatrix} \frac{1}{2} & \text{for } p = q \\ 1 & \text{otherwise} \end{Bmatrix} = \sum_{p \geq q} \tilde{Q}_{pq}\, h^{\lambda}_{pq}\,, \tag{4.61}$$

where the symmetrized 1PDM $\tilde{\mathbf{Q}}$ has been defined with the appropriate factor of $\frac{1}{2}$ in the diagonal terms. In this way, the one-particle density matrix has been symmetrized such that $\tilde{Q}_{pq} = \tilde{Q}_{qp}$. A similar analysis for the 2PDM has been carried out to obtain expressions for a symmetrized 2PDM, $\tilde{\mathbf{G}}$, such that $\tilde{G}_{pqrs} = \tilde{G}_{qprs} = \tilde{G}_{pqsr} = \tilde{G}_{qpsr} = \tilde{G}_{rsqp} = \tilde{G}_{srqp} = \tilde{G}_{rspq} = \tilde{G}_{srpq}$. In what follows, the tilde notation is dropped, and Q and G refer to the symmetrized one- and two-PDMs, respectively. The expressions for these effective RCCSD symmetrized density matrices are

$$Q_{ij} = -\frac{1}{2}\, \hat{P}_{ij} \left\{ \sum_{a} Z^{a}_{i}\, t^{a}_{j} + \sum_{\substack{k \\ a,b}} \tilde{Z}^{ab}_{ik}\, t^{ab}_{jk} \right\} + 2\delta_{ij}\,, \tag{4.62}$$

$$Q_{ab} = \frac{1}{2}\, \hat{P}_{ab} \left\{ \sum_{i} Z^{a}_{i}\, t^{a}_{j} + \sum_{\substack{i,j \\ c}} \tilde{Z}^{ac}_{ij}\, t^{bc}_{ij} \right\}, \tag{4.63}$$

$$Q_{ia} = \frac{1}{2}\left[2t_i^a + Z_i^a + \sum_{j,b} Z_j^b \, (2t_{ij}^{ab} - \tau_{ji}^{ab}) - \sum_{\substack{j,k \\ b,c}} (t_i^b \, t_{jk}^{ac} + t_j^a \, t_{ik}^{bc}) \, \tilde{Z}_{jk}^{bc} \right], \tag{4.64}$$

$$G_{ijkl}^{A} = \frac{1}{8} \, \hat{P}_{ijkl} \left\{ \frac{1}{2} \, (\tau \tilde{Z}_2)_{ikjl} - 2\delta_{kl} \left[(t_1 Z_1)_{ij} + \sum_a [\Omega_1]_{ij}^{aa} \right] \right. \tag{4.65}$$

$$\left. + \, \delta_{jl} \left[(t_1 z_1)_{ik} + \sum_a [\Omega_1]_{ik}^{aa} \right] \right\} + 2\delta_{ij}\delta_{kl} - \delta_{ik}\delta_{jl} \, ,$$

$$G_{abcd}^{B} = \frac{1}{8} \, \hat{P}_{abcd} \left\{ \frac{1}{2} \, (\tau \tilde{Z}_2)^{acbd} \right\}, \tag{4.66}$$

$$G_{abij}^{C} = \frac{1}{8} \, \hat{P}_{ij} \, \hat{P}_{ab} \left\{ - Z_i^a \, t_j^b - [\Omega_1]_{ij}^{ab} - [\Omega'_3]_{ij}^{ab} \right\}, \tag{4.67}$$

$$G^D_{aibj} = \frac{1}{8}\,\hat{P}_{ai,bj}\Bigg\{\frac{1}{2}\,\tilde{Z}^{ab}_{ij} + 2\tau^{ab}_{ij} - \tau^{ab}_{ji} + 2t^a_i\,Z^b_j + 2[\Omega_1]^{ab}_{ij} - [\Omega'_2]^{ab}_{ij} \tag{4.68}$$

$$+ (4[\omega_1]^a_i - 2[\omega'_2]^a_i)\,t^b_j - (2[\omega_1]^a_j - [\omega'_2]^a_j)\,t^b_i$$

$$- \sum_k (2t^{ab}_{ik} - t^{ab}_{ki})\,(t_1Z_1)_{jk} - \sum_c (2t^{ac}_{ij} - t^{ac}_{ji})\,(t_1Z_1)^{bc}$$

$$+ \sum_{l,d} ([\Omega_1]^{ad}_{il} - [\Omega_2]^{ad}_{il})\,t^{bd}_{jl} - \sum_{l,d} ([\Omega_1]^{ad}_{jl} - [\Omega_2]^{ad}_{jl})\,t^{bd}_{il}$$

$$- \frac{1}{2}\sum_{l,d} ([\Omega_1]^{ad}_{il} - [\Omega_2]^{ad}_{il})\,(t^{db}_{jl} - t^{db}_{lj}) + \frac{1}{2}\sum_{l,d} [\Omega_1]^{ad}_{il} t^{bd}_{jl}$$

$$- \sum_{l,d} (2[\Omega_1]^{ad}_{il} - [\Omega_2]^{ad}_{il})\,t^b_l\,t^d_j + \sum_{l,d} ([\Omega_1]^{ad}_{jl} + [\Omega_3]^{ad}_{jl})\,t^b_l\,t^d_i$$

$$+ \sum_{l,d} [\Omega_1]^{dd}_{jl}\,(\tau^{ab}_{li} - 2\tau^{ba}_{li}) + \sum_{l,d} [\Omega_1]^{bd}_{il}\,(\tau^{da}_{ij} - 2\tau^{da}_{ji}) + \frac{1}{2}\sum_{l,d} [\Omega_3]^{bd}_{il}\,t^{ad}_{lj}$$

$$+ \frac{1}{2}\sum_{c,d} (\tau\tilde{Z}_2)^{abcd}\,\tau^{cd}_{ij} - \delta_{ij}\left[(t_1Z_1)^{ab} + \sum_k [\Omega_1]^{ab}_{kk}\right]\Bigg\},$$

$$G^E_{aijk} = \frac{1}{8}\,\hat{P}_{jk}\Bigg\{ -\sum_b (2\tau^{ab}_{ij} - \tau^{ab}_{ji})\, Z^b_k - \sum_b t^b_j\, \tilde{Z}^{ab}_{ik} - 2\sum_b [\Omega_1]^{bb}_{jk}\, t^a_i \tag{4.69}$$

$$+ \sum_b [\Omega_1]^{bb}_{ik}\, t^a_j - \sum_b (2[\Omega_1]^{ab}_{ik} - [\Omega_2]^{ab}_{ik})\, t^b_j$$

$$+ \sum_b ([\Omega_1]^{ab}_{jk} + [\Omega_3]^{ab}_{jk})\, t^b_i + \sum_l (\tau\tilde{Z}_2)_{ijlk}\, t^a_l$$

$$+ 2\delta_{jk}\left[2t^a_i + Z^a_i + 2[\omega_1]^a_i - [\omega'_2]^a_i - \sum_{l,b} [\Omega_1]^{bb}_{il}\, t^a_l - \sum_{l,b} [\Omega_1]^{ab}_{il}\, t^b_i \right]$$

$$- \delta_{ik}\left[2t^a_j + Z^a_j + 2[\omega_1]^a_j - [\omega'_2]^a_j - \sum_{l,b} [\Omega_1]^{bb}_{jl}\, t^a_l - \sum_{l,b} [\Omega_1]^{ab}_{il}\, t^b_j \right]\Bigg\},$$

$$G^F_{aibc} = \frac{1}{8}\,\hat{P}_{bc}\Bigg\{ \sum_j 2(\tau^{ab}_{ij} - \tau^{ab}_{ji})\, Z^c_j + \sum_j t^b_j\, \tilde{Z}^{ac}_{ij} - \sum_d (\tau\tilde{Z}_2)^{abdc}\, t^d_i \tag{4.70}$$

$$+ 2\sum_j [\Omega_1]^{bc}_{jj}\, t^a_i - \sum_j [\Omega_1]^{ac}_{jj}\, t^b_i$$

$$+ \sum_j (2[\Omega_1]^{ac}_{ij} - [\Omega_2]^{ac}_{ij})\, t^b_j - \sum_j ([\Omega_1]^{bc}_{ij} + [\Omega_3]^{bc}_{ij})\, t^a_j \Bigg\}$$

Here, as above, several intermediate products and a set of permutation operators have been defined;

$$[\Omega_1]^{ac}_{jk} = \sum_{l,d} t^{ad}_{jl}\, \tilde{Z}^{cd}_{kl}\,, \tag{4.71}$$

$$[\Omega_2]^{ac}_{jk} = \sum_{l,d} t^{ad}_{lj}\, \tilde{Z}^{cd}_{kl}\,, \tag{4.72}$$

$$[\Omega_3]^{ac}_{jk} = \sum_{l,d} t^{ad}_{lj}\, \tilde{Z}^{cd}_{lk}\,, \tag{4.73}$$

$$[\omega_1]^{a}_{i} = \sum_{k,c} t^{ac}_{ik}\, Z^{c}_{k}\,, \tag{4.74}$$

$$[\omega_2]^{a}_{i} = \sum_{k,c} t^{ac}_{ki}\, Z^{c}_{k}\,, \tag{4.75}$$

$$(t_1 Z_1)_{ij} = \sum_{a} t^{a}_{i}\, Z^{a}_{j}\,, \tag{4.76}$$

$$(t_1 Z_1)^{bc} = \sum_{i} t^{b}_{i}\, Z^{c}_{i}\,, \tag{4.77}$$

$$(\tau \tilde{Z}_2)_{ijkl} = \sum_{a,b} \tau^{ab}_{ij}\, \tilde{Z}^{ab}_{kl}\,, \tag{4.78}$$

$$(\tau \tilde{Z}_2)^{abcd} = \sum_{i,j} \tau^{ab}_{ij}\, \tilde{Z}^{cd}_{ij}\,, \tag{4.79}$$

$$\hat{P}_{pqrs} f(p, q, r, s) = f(p, q, r, s) + f(q, p, r, s) + f(p, q, s, r) \tag{4.80}$$
$$+ f(q, p, s, r) + f(r, s, p, q) + f(s, r, p, q)$$
$$+ f(r, s, q, p) + f(s, r, q, p) ,$$

$$\hat{P}_{pq} f(p, q) = f(p, q) + f(q, p) , \tag{4.81}$$

$$\hat{P}_{pq,rs} f(p, q, r, s) = f(p, q, r, s) + f(r, s, p, q) . \tag{4.82}$$

Finally, in Eqs. (4.67) and (4.68), the notation [Ω˜] and [ω˜] is used to indicate that τ is to be substituted for t_2 in Eqs. (4.71)-(4.75).

The computational approach to the solution of Z_1 and $\tilde{Z}_2$ is (1) read in the converged cluster amplitudes and MO integrals (in separate reads of the A, B, C, D, E, and F two-electron integral blocks) and form the intermediate products defined in Eqs. (4.47)-(4.60). Of these, the intermediate products of large dimension ($H_{av}^{\beta\gamma}$, $F_{ab}^{\beta i}$, and $b_{ab}^{\beta\gamma}$) are held in core when possible, but for most cases these have to be formed and written to disk in a series of steps, and similarly, read back into core as needed for each iteration of the Z-vector program; (2) contract these intermediate arrays with the appropriate elements of Z_1 and $\tilde{Z}_2$ as prescribed by Eqs. (4.44) and (4.45); (3) repeat step (2) until the iterative solutions for Z_1 and $\tilde{Z}_2$ have reached a chosen convergence. An error of 1×10^{-10} in succesive Z-vectors has been found to be sufficiently accurate for the energy gradient.

Next the one- and two-particle density matrices are calculated by (1) reading in the converged cluster amplitudes, Z amplitudes, and MO integrals (as desribed above); (2) forming each of the blocks of these density matrices as prescribed by

Eqs. (4.62)-(4.70). Note that the intermediate products $[\Omega_i]$, $[\omega_i]$, $(\tau\tilde{Z}_2)$, and $(t_1 Z_1)$ are never explicitly constructed; instead, columns of these arrays are formed within loops as needed. In smaller cases, all blocks of the 2PDM are held in core. However, for most cases, they must be calculated and written to disk separately.

4.4 Application to the H_2O and H_2CO Molecules

In this section, the CCSD analytic gradient method presented in Section 4.2 and 4.3 is applied to the water and formaldehyde molecules. In particular, the optimized DZ+P CCSD geometry for both the water and formaldehyde molecules are reported here along with their analytically evaluated molecular dipole moments, and, via finite differences of gradients, the harmonic vibrational frequencies and infrared absorption intensities for these same systems. These results are compared to analogous CISD (for both H_2O and H_2CO), and CISDT, CISDQ, & CISDTQ (for H_2O only) calculations along with results from experiment.

The standard contracted Gaussian DZ+P basis set of Dunning and Hay[12,15] was employed for this study. It is designated as C,O(9s5p1d/4s2p1d) with $\alpha_d = 0.75$ for carbon and 0.85 for oxygen, H(4s1p/2s1p) with $\alpha_p = 0.75$ for H_2O and $\alpha_p = 1.0$ for H_2CO. Additionally, the hydrogen *s* functions were scaled by a factor of 1.2. For the H_2O molecule, this basis set consisted of 26 contracted Gaussian orbitals, while for H_2CO, 42 contracted Gaussians were employed. The molecular structures were fully optimized at all levels of theory, and, with the exception of the CISD formaldehyde results (Lengsfield *et. al.*, 1987[197]) for which the two lowest energy occupied SCF molecular orbitals were held doubly occupied in all configurations, all electrons and all orbitals were active in the correlation procedures. The number of

configurations included in each H_2O CI calculation were 1,636 (CISD), 36,694 (CISDT), 461,177 (CISDQ), and 496,235 (CISDTQ), and for the H_2CO CISD calculation 21,115 configurations were included.

Table XIX. Comparison of DZ+P CCSD, DZ+P CI, DZ+P SCF, and experimental predictions for molecular constants of H_2O. The O-H bond distances and HOH bond angles are equilibrium values.

	SCF	CISD	CISDT	CISDQ	CISDTQ	CCSD	Expt.
E (hartrees)	-76.046807	-76.257507	-76.260391	-76.267091	-76.269799	-76.266874	
r_{OH} (angstroms)	0.9457	0.9585	0.9592	0.9621	0.9629	0.9649	0.9572[a]
< HOH (degrees)	106.16	104.86	104.74	104.59	104.45	103.90	104.52[a]
Harmonic Frequencies (cm^{-1})							
ω_1 (a_1)	4152	3967	3953	3908	3892	3889	3834[b]
ω_2 (a_1)	1750	1693	1689	1681	1677	1679	1647[b]
ω_3 (b_2)	4267	4090	4077	4037	4022	4008	3943[b]
Infrared Intensities ($km \cdot mol^{-1}$)							
A_1	21.90	6.58	5.48	4.44	3.46	4.95	2.24[c]
A_2	101.47	83.18	81.09	79.23	77.36	72.22	53.6[c]
A_3	76.28	37.42	34.30	31.44	28.33	31.79	44.6[c]
μ (debye)	2.133	2.144	2.136	2.138	2.130	2.087	1.855[d]

[a] Reference 198
[b] Reference 199
[c] Reference 200
[d] Reference 201

Table XIX summarizes the present CCSD predictions for water. Although the experimental parameters are included in Table XIX, the better comparison in terms of evaluating the CCSD results (with a relatively small basis set such as DZ+P) is with the CISDTQ predictions. The latter CI results are quite close to the (unknown) full CI predictions for a well-behaved/one reference system of 10 electrons. Additionally, as discussed in Section 1.3.3, the CCSD results may be closer to CISDQ than to CISD, thus the comparison with the SDQ variational results is timely.

The predicted CCSD O-H bond distance is indeed closer to CISDQ (Δr = 0.0028 angstroms) than to CISD (Δr = 0.0064 angstroms). In fact the CCSD bond distance is closer yet (Δr = 0.0020 angstroms) to the CISDTQ prediction, which should be very close to full CI for water. Furthermore the same trend holds for the theoretical bond angles. There the CCSD value of θ_e differs by 0.96° from that predicted by CISD while the difference $\Delta\theta_e$ between CCSD and CISDQ is 0.69°. Again the CCSD prediction is closest to CISDTQ, the difference being 0.55°. However, the latter difference is larger than $\Delta\theta_e$ (CISD – CISDTQ) = 0.41°. In addition the CISDQ bond angle is significantly closer (within 0.14°) to the high-level CISDTQ prediction.

The predicted CCSD harmonic vibrational frequencies in Table XIX are notably superior to the analogous CISD predictions. Specifically, the differences [CCSD – CISDTQ] are -3 cm^{-1} (ω_1), $+2$ cm^{-1} (ω_2), and -14 cm^{-1} (ω_3). The comparable differences [CISD – CISDTQ] are an order of magnitude greater, namely $+75$ cm^{-1} (ω_1), $+16$ cm^{-1} (ω_2), and $+68$ cm^{-1} (ω_3). This would appear to be strong evidence that CCSD is doing a good job of bridging the gap between CISD and full CI. Perhaps suprisingly, CCSD even does a bit better for this small number of electrons with respect to CISDTQ than does CISDQ. The differences [CISDQ – CISDTQ] are $+16$ cm^{-1} (ω_1), $+4$ cm^{-1} (ω_2), and $+15$ cm^{-1} (ω_3).

A good discussion of theoretical infrared intensities for the water molecule has recently been given by Swanton, Bacskay, and Hush.[202] The experimental data have been carefully analyzed by Ziles and Person in their 1973 paper.[200] Generally speaking the DZ+P basis set used in the present study is inadequate for quantitative predictions of IR intensities.[19] Nevertheless, comparison with the work of Swanton,

Bacskay, and Hush[202] (who employed CI methods with larger basis sets) suggests that the DZ+P basis is reasonable for the case of water. Remaining errors with respect to experiment may be inherent in the double harmonic approximation.

The CCSD IR intensities are in significantly better agreement with CISDTQ than are the analogous CISD predictions. For the CCSD – CISDTQ comparison, the differences are 1.49, –5.14, and 4.46 km/mole, respectively, for the three normal modes. The CISD – CISDTQ differences are 3.12, 5.54, and 9.09 km/mole, respectively.

It would be instructive to press on with all the methods included in Table XIX using much larger basis sets. However, given that the CISDTQ includes 496,235 configurations, this does not seem likely in the immediate future. Yet it will soon be possible to employ much larger basis sets with the CCSD analytic gradient method. At that time it will certainly be of interest to compare basis set limit CCSD results with experiment. From the limited comparisons presented herein, the CCSD analytic gradient method is expected to become an attractive approach to post-CISD theoretical studies. Currently, Lee and coworkers are preparing a report of CISDT and CISDTQ studies of several other small molecular systems.[203] These results will also be of importance in evaluating the performance of CCSD theory for chemical applications.

Table XX. Comparison of DZ+P CCSD, DZ+P CISD, DZ+P SCF, and experimental predictions for molecular constants of H_2CO. The bond distances and bond angles are equilibrium values.

	SCF[a]	CISD[b]	CCSD	Expt.
E (hartrees)	-113.895328	-114.195568	-114.249798	
r_{CO} (angstroms)	1.1888	1.2116	1.2187	1.203 ± 0.003[c]
r_{CH} (angstroms)	1.0943	1.0998	1.1027	1.099 ± 0.009[c]
< HCH (degrees)	116.22	116.27	116.35	116.5 ± 1.2[c]
Harmonic Frequencies (cm^{-1})				
ω_1 (a_1)	3149	3074	3011	2944[d]
ω_2 (a_1)	2006	1868	1754	1764[d]
ω_3 (a_1)	1656	1596	1581	1563[d]
ω_4 (b_1)	1335	1272	1211	1191[d]
ω_5 (b_2)	3226	3173	3110	3009[d]
ω_6 (b_2)	1367	1305	1287	1287[d]
Infrared Intensities ($km \cdot mol^{-1}$)				
A_1	72.7	66.1	48.8	75[e]
A_2	157.9	93.1	99.2	74[e]
A_3	14.0	7.6	0.0	11[e]
A_4	1.7	3.9	4.3	6.5[e]
A_5	112.1	106.2	109.65	87[e]
A_6	19.3	14.8	11.4	9.9[e]
μ (debye)	2.781	2.506	2.441	2.33[f]

[a] Energy, geometry, and harmonic vibrational frequencies from reference 163; infrared absorption intensities from reference 197.

[b] Reference 197; the two lowest energy SCF molecular orbitals were held doubly occupied in all configurations.

[c] Reference 204

[d] Reference 205

[e] Reference 206

[f] Reference 207

The DZ+P CCSD predictions for formaldehyde are compared with DZ+P SCF and DZ+P CISD results along with the experimental predictions in Table XX. Critical assessment of the CCSD method is not possible here because the higher excitation CISDTQ method is not computationally tractable for a problem of this size; an all electron calculation using the CISDTQ method would involve 102,579,225

configurations. There are, however, two trends which may be noted based on the CISD vs CCSD vs experiment comparison in Tables XIX and XX. First, one finds that for both H_2O and H_2CO the DZ+P CISD method generally gives better agreement with the experimental geometries than does the DZ+P CCSD method. The CCSD method, when coupled with such a relatively modest one-particle basis, predicts equilibrium bond distances which are significantly greater than experimental predictions, and, based on these limited results, one may conclude that basis sets of better than DZ+P quality are needed for CCSD geometries which accurately reflect experiment. Systematic CCSD basis set studies are in progress to investigate this further. The second trend which is evident from Tables XIX and XX is that the DZ+P CCSD harmonic frequencies are in significantly better agreement with experiment than are the analogous CISD results. The range of discrepancies for the DZ+P CCSD H_2CO harmonic frequencies with those from experiment is 0.0-3.4% (ave. = 1.5%) while that for DZ+P CISD is 2.1-6.8% (ave. = 4.4%). In particular, the CCSD description of the potential surface is most important for the C=O stretching motion, ω_2, and the out-of-plane oxygen wag, ω_4. This observation is in accord with the general belief that the higher order correlation effects incorporated by CCSD (and higher excitation CI methods) are important in properly describing the harmonic vibrational frequency of multiply bonded systems.

Finally, the computational requirements for these particular calculations and projections for still larger calculations are discussed below. Following the computational outline presented above, near the end of Section 4.2, the timings for each step of the CCSD gradient calculation (in total cpu seconds on an IBM 3090-200 processor) are as follows.

	H_2O	H_2CO
[1]	4.7 sec.	29.7 sec.
[2]	3.2 sec.	17.2 sec.
[3]	10.0 sec. (2%)	71.7 sec. (1%)
[4]	289.7 sec. (53%)	6240 sec. (62%)
[5]	185.6 sec. (34%)	3250 sec. (32%)
[6]	20.0 sec. (4%)	322.0 sec. (3%)
[7] + [8]	10.4 sec. (2%)	75.6 sec. (1%)
[9]	0.2 sec.	0.5 sec.
[10]	15.8 sec. (3%)	88.8 sec. (1%)
[11]	1.0 sec.	6.6 sec.

The horizontal line has been placed to demarcate those steps required for the CCSD energy alone (steps [1]-[4]) from the additional work necessary for the CCSD energy gradient. For DZ+P H_2O, the former group accounted for 57% of the cpu requirement while the latter made up the remaining 43%, and for DZ+P H_2CO, the breakdown was 63% for steps [1]-[4] + 37% for the remainder. In other words, the additional work for analytic evaluation of the gradient once the CCSD equations were solved was only 75% of the CCSD overhead in the case of water and 59% in the larger formaldehyde case. Focusing only on the N^6 steps ([5] + [6] vs [4]) which will dominate as N increases, the additional work for the CCSD gradient compared to that required for the CCSD energy for the two examples studied herein is very similar: 58% for DZ+P H_2O and 57% for DZ+P H_2CO.

It is important to note that the timings listed above correspond to calculations which did not take advantage of molecular symmetry. By taking advantage of such symmetry considerations, significant savings in cpu requirements can be achieved (see Section 2.4). In fact, the time for solution of the CCSD equations (step [4]) for H_2CO is reduced by more than one order of magnitude (to 560 sec.) by taking advantage of the proper C_{2v} symmetry of formaldehyde. Currently, these symmetry reductions are being implemented in the CPCCSD and density matrix codes, and similar reductions in the timings for steps [5] and [6] are anticipated as well.

Even without making use of molecular symmetry, the relative timings ([5] + [6] vs [4]) listed above are certainly encourgaing for further CCSD gradient studies, and, if the number of N^6 loops are analyzed for the various steps of the calculation, one may anticipate timing comparisons as larger systems are investigated. The N^6 requirement for solution of the closed-shell CCSD equations [Eqs. (2.32) and (2.33)] breaks down as

$$\frac{13}{2}\, NO^4\, NV^2 + 12\, NO^3\, NV^3 + \frac{1}{2}\, NO^2\, NV^4 \qquad \text{per CCSD iteration.} \quad (4.83)$$

Comparing this to the analogous analysis for the CCSD gradient equations, one finds

$$\frac{11}{2}\, NO^4\, NV^2 + 7\, NO^3\, NV^3 + \frac{7}{2}\, NO^2\, NV^4 \quad (4.84)$$

for the one-time formation of the intermediate products for the CPCCSD equations [Eqs. (4.47)-(4.60)], plus

$$\frac{1}{2}\, NO^4\, NV^2 + 3\, NO^3\, NV^3 + \frac{1}{2}\, NO^2\, NV^4 \qquad \text{per CPCCSD iteration.} \quad (4.85)$$

[Eqs. (4.44)-(4.45)], plus

$$NO^4\, NV^2 + 10\, NO^3\, NV^3 + 2\, NO^2\, NV^4 \quad (4.86)$$

for the one-time formation of G [Eqs. (4.65)-(4.70)]. Thus, the ratio of steps [5] +[6] vs step [4] depends on the ratio of *NV* to *NO* along with the number of CCSD and CPCCSD iterations required for convergence. In preliminary analyses (assuming # CPCCSD iterations = # CCSD iterations = 15), this ratio is found to increase monotonically as $\frac{NV}{NO}$ increases with a very workable value of 0.85 at a large value of $\frac{NV}{NO} = 20$.

Concluding Remarks

It has been evident since the general implementation of the UCCSD method of Purvis and Bartlett in 1982[42] that, as a single-determinant based many-electron method, the CCSD approximation is of great value to quantum chemistry. By including disconnected contributions to the wavefunction to all levels of excitation (made up of products of one- and two-electron cluster operators) yet remaining proportional to N^6 in computational cost, CCSD provides a tractable, size-extensive, accurate approach to the electron correlation problem. This property of size-extensivity provides a realistic and consistent means of treating the electron correlation problem as quantum chemical methods are applied to larger systems.

As documented in Chapter 2, these higher-order disconnected excitations incorporated by CCSD result in an additional and *inherent* computational cost relative to the variational CISD method. More precisely, it has been found that the ratio $\frac{\alpha_{CCSD}}{\alpha_{CISD}}$ (Section 1.3.3) ranges from 4-20, and that this ratio depends critically on the molecular symmetry that one is able to exploit for the particular molecular system being studied. In general the higher the symmetry, the smaller the $\frac{\alpha_{CCSD}}{\alpha_{CISD}}$ ratio (see Table II). A somewhat discouraging result, however, is that the $\frac{\alpha_{CCSD}}{\alpha_{CISD}}$ ratio increases with NV (# of unoccupied orbitals in the reference determinant) for a given molecular system.

While CCSD energies are, in general, significantly more accurate than those predicted by CISD, it has been found that for the majority of the small to medium-sized molecules studied herein, Davidson corrected CISD does a good job of approximating the disconnected excitations. Relative to CCSD, CISD(+Q) overestimates the

CCSD correlation energy for the smaller cases (where small refers to the number of electrons being correlated) investigated in the present study [N_2 (14 e^-), H_2O ($10e^-$ and $8e^-$), and H_3O^+ ($10e^-$ and $8e^-$)] and underestimates the CCSD result for the larger cases [$H_5O_2^+$ ($20e^-$ and $16e^-$), HSOH ($26e^-$), and $C_2N_4H_2$ ($30e^-$)]. For the H_3O^+ and $H_5O_2^+$ molecules, the exclusion of the oxygen 1*s* electrons decreases the Davidson correction errors slightly. It thus appears that as the number of electrons being correlated increases, the fraction of the higher excitation correlation energy accounted for by the Davidson correction decreases, and thus, as larger molecular systems are investigated, the rigorously size-extensive CCSD method is clearly preferable. With the exception of *s*–tetrazine, the CISD(+Q) and CCSD results agree to within ± 5 mhartrees. However, for *s*–tetrazine, a serious bifurcation occurs. Moreover, this total energy difference appears to have chemical consequences in that the barrier height for the one-step triple dissociation pathway of *s*–tetrazine to HCN + HCN + N_2 predicted by both CISD and CISD(+Q) is above the experimental activation energy for the photodissociation process from the S_1 state. On the other hand, CCSD reduces the CISD(+Q) barrier by an additional 7 kcal/mol (4.8 kcal/mol below the experimental activation energy) and thus the one-step, unimolecular process is predited to be energetically operable.

Further details of the present *s*–tetrazine study have been presented herein, and there are several questions of chemical and physical interest which are now definitively resolved while other such questions require further study both theoretically and spectroscopically.

First, as described above, much insight has been gained into the mechanism and thermochemistry of the *s*–tetrazine photodissociation. The present theoretical results

clearly indicate that a one-step, concerted mechanism is operable under experimental conditions. Furthermore, this reaction has been found to be significantly exoergic (by 57.4 kcal/mol).

A second new result reported here is the discovery of the proximity of the S_1 and S_2 electronic states. While these results are not quantitative at present, it is evident that these two surfaces ($^1B_{3u}$ and ^1A_u within the D_{2h} symmetry group; both ^1A_u within the C_{2h} symmetry group) are near enough in energy that interaction between vibronic levels may be significant. DZ SCF theory predicts a crossing (avoided crossing in C_{2h}) of these two surfaces.

The present theoretical characterization of the ground state is, in general, satifactory when compared to the spectroscopic results. The one area where large differences with ground state experimental results are found within the DZ+P SCF description encompasses several of the vibrational frequencies. Unusually large overestimates have been found for the two low frequency out-of-plane ring distortions, and the discrepancies associated with many of the remaining normal modes are somewhat greater than those found for analogous theory vs experiment comparisons of smaller molecular systems. It was discovered, however, that the 59% discrepancy reported for the low frequency b_{3u} mode is due to neglect of anharmonicity on the ground state potential energy hypersurface in the present theoretical treatment.

While the experimental data is less abundant for the T_1 and S_1 states, here one finds less satisfactory agreement between the DZ+P SCF structures and those deduced from spectroscopic analyses. In the case of the $\tilde{a}\ ^3B_{3u}$ state, where only one experimental geometry has been reported to date,[115] the present theoretical results tend to suggest that the sign chosen for the Franck-Condon change in geometry upon

excitation be reversed, although neither choice yields a highly satisfactory comparison. In the case of the S_1 state, the best theoretical prediction at present gives an equilibrium structure not of D_{2h} symmetry but of C_{2h} symmetry. However, the subtle nature of this problem, as exhibited by the near degeneracy of these two structures when single point CISD energies are obtained at the RHF stationary points, demands that a more complete theoretical treatment be applied before any firm conclusions are reached. The comparison of the theoretical harmonic vibrational frequencies with the experimental assignments for the T_1 and S_1 states shows similar discrepancies as exhibited by the ground state.

Finally, concerning the higher excited states, with the present characterization of the D_{2h} stationary points employing DZ SCF theory, a wide variety of structures, harmonic vibrational frequencies, responses to relaxation from a vertical excitation, and responses to basis set and electron correlation has been found. The relative energies of several of these states ($T_3 - T_6$, $S_3 - S_5$) are not yet well converged with respect to basis set nor electron correlation, and thus the energetic ordering of these states is not yet firmly established. This question, along with those mentioned above which are still not well resolved, will most likely require studies involving a more complete treatment of electron correlation, larger basis sets, and the determination of correlated structures and frequencies to arrive at definitive theoretical answers. It is hoped that this study has laid the foundation for those that follow. It is also very much hoped that this study will provide the impetus for new experimental studies of the spectroscopy of *s*–tetrazine.

Up until very recently, one of the major limitations associated with the CCSD method (and CC methods in general) has been the lack of a theory for analytic energy derivatives, and while CCSD appeared to be a highly accurate and reasonably

efficient method for approximate solution of the electronic Schrödinger equation, the success of any theoretical method must be measured by its ability to solve problems and make predictions of general chemical interest. The efficient analytic evaluation of energy derivatives is an essential tool for such an ability. As reported here, analytic CCSD gradients can be handled efficiently by (1) constructing a density matrix expression for the gradient;[177,192,194] (2) employing the Z-vector method[189] for the solution of the first-order CPCCSD equations; and (3) casting these equations into an iterative scheme so that the process scales as no worse than N^6.

From the present results for the structures and molecular properties of H_2O and H_2CO, CCSD appears to be bridging the gap between CISD and full CI. In particular, the CCSD harmonic vibrational frequencies are in significantly better agreement with experiment than are the analogous CISD predictions. In terms of cpu timings, while the present CCSD analytic gradient codes are not yet optimized, the initial results are encouraging in that the additional work required for the gradient is roughly 60% of that required for the CCSD energy alone.

One area which has not been addressed in the present study is that of multi-reference based methodology. While to a certain extent, the need for multi-reference approaches with a size-extensive method for dynamical electron correlation is not as great as with non size-extensive CI techniques, the lack of a generally applicable theory for multi-reference schemes remains the one major limitation to non-variational approaches to the electron correlation problem. While some initial work has been done in the area of multi-reference coupled cluster (MR-CC) theory,[208–211] there is not yet one clear solution to this problem. At present MR-CI methods represent the most accurate (short of full CI) state of the art methods of electron correlation, and in the near future, MR-CC should prove to be as accurate if not more

so.

References

[1] H. F. Schaefer, *Quantum Chemistry* (Clarendon, Oxford, 1984).

[2] W. A. Goddard, Science **227**, 917 (1985).

[3] H. F. Schaefer, Science **231**, 1100 (1986).

[4] By treating the electrons non-relativisticly, effects such as spin-spin and spin-orbit hyperfine coupling terms are not taken into account. While the effect of relativistic corrections is an area of active interest in theoretical chemistry, it will not be addressed herein. The molecular systems studied in the present work most certainly exhibit negligible relativistic effects. For a treatment of relativistic quantum mechanics, see P. A. M. Dirac, *The Principles of Quantum Mechanics* 4th Edition, (Clarendon, Oxford, 1958), pp. 253-275. For a review of the methods employed in relativistic quantum chemistry, see P. Pyykkö, Adv. Quantum Chem. **11**, 353 (1978).

[5] M. Born and J. R. Oppenheimer, Ann. Physik. **84**, 457 (1927).

[6] By separating the nuclear and electronic coordinates, the electronic energy becomes a parametric function of the nuclear coordinates. This function constitutes a potential energy surface on which the nuclei move. There are cases where the Born-Oppenheimer approximation results in non-negligible errors in quantum chemical calculations; see P. Saxe, B. H. Lengsfield, and D. R. Yarkony, Chem. Phys. Lett. **113**, 159 (1985); N. C. Handy, Y. Yamaguchi, and H. F. Schaefer, J. Chem. Phys. **84**, 4481 (1986).

[7] C. C. J. Roothan, Rev. Mod. Phys. **23**, 69 (1951); **32**, 179 (1960).

[8] I. Shavitt, in *Modern Theoretical Chemistry*, edited by H. F. Schaefer (Plenum, New York, 1977), Vol. 3, pp. 189-275.

[9] R. J. Bartlett and G. D. Purvis, Int. J. Quantum Chem. **14**, 561 (1978).

[10] R. Ahlrichs, P. Scharf, and C. Ehrhardt, J. Phys. Chem. **82**, 890 (1984).

[11] S. F. Boys, Proc. Roy. Soc. (London) **A200**, 542 (1950).

[12] S. Huzinaga, J. Chem. Phys. **42**, 1293 (1965).

[13] J. L. Whitten, J. Chem. Phys. **44**, 359 (1966).

[14] R. P. Hostery, R. R. Gilman, T. H. Dunning, A. Pipano, and I. Shavitt, Chem. Phys. Lett. **7**, 325 (1970).

[15] T. H. Dunning, J. Chem. Phys. **53**, 2823 (1970).

[16] R. C. Raffenetti, J. Chem. Phys. **59**, 1872 (1973).

[17] J. Almlöf and P. R. Taylor, J. Chem. Phys. **86**, 4070 (1987).

[18] K. Jankowski, R. Becherer, P. Scharf, H. Schiffer, and R. Ahlrichs, J. Chem. Phys. **82**, 1413 (1985).

[19] Y. Yamaguchi, M. Frisch, J. Gaw, H. F. Schaefer, and J. S. Binkley, J. Chem. Phys. **84**, 2262 (1986).

[20] T. J. Lee and H. F. Schaefer, J. Chem. Phys. **83**, 1784 (1985).

[21] E. A. McCullough, Chem. Phys. Lett. **24**, 55 (1974); J. Chem. Phys. **62**, 3991 (1975); J. Chem. Phys. **63**, 5050 (1975).

[22] L. R. Kahn, P. Baybutt, and D. Truhlar, J. Chem. Phys. **65**, 3826 (1976); L. R. Kahn and W. A. Goddard, Chem. Phys. Lett. **2**, 667 (1968); J. Chem. Phys. **58**, 2686 (1972).

[23] C. F. Melius and W. A. Goddard, Phys. Rev. A **10**, 1528 (1974).

[24] S. Topiol, M. A. Ratner, and J. W. Moskowitz, Chem. Phys. **70**, 1 (1977); Chem. Phys. Lett. **46**, 256 (1977).

[25] C. S. Ewig, P. Coffey, and J. R. Van Wazer, Inorg. Chem. **14**, 1848 (1976); R. Osman, C. S. Ewig, and J. R. Van Wazer, Chem. Phys. Lett. **39**, 27 (1976).

[26] R. Osman and H. Weinstein, Chem. Phys. Lett. **49**, 69 (1977).

[27] K. Szalewicz, B. Jeziorski, H. J. Monkhorst, and J. G. Zabolitzky, J. Chem. Phys. **78**, 1420 (1983); **79**, 5543 (1983); **81**, 368 (1984); **81**, 2723 (1984).

[28] A. C. Hurley, Proc. Roy. Soc. (London) **A226**, 170, 176, 193 (1954).

[29] P. O. Löwdin, Adv. Chem. Phys. **2**, 207 (1959).

[30] O. Sinanoglu, Proc. U. S. Natl. Acad. Sci. **47**, 1217 (1961).

[31] H. Sivlerstone and O. Sinanoglu, J. Chem. Phys. **44**, 1899 (1966).

[32] J. Cizek, J. Chem. Phys. **45**, 4256 (1966); Adv. Chem. Phys. **14**, 32 (1969).

[33] B. Roos, Chem. Phys. Lett. **15**, 153 (1972).

[34] J. Paldus, J. Chem. Phys. **61**, 5321 (1974).

[35] R. Ahlrichs, H. Lischka, V. Staemmler, and W. Kutnelnigg, J. Chem. Phys. **62**, 1225 (1975).

[36] C. E. Dykstra, H. F. Schaefer, and W. Meyer, J. Chem. Phys. **65**, 2740 (1976).

[37] I. Shavitt, Int. J. Quantum Chem. Symp. **11**, 131 (1977).

[38] B. R. Brooks and H. F. Schaefer, J. Chem. Phys. **70**, 5092 (1979).

[39] P. E. M. Siegbahn, J. Chem. Phys. **70**, 5391 (1979).

[40] B. O. Roos, P. R. Taylor, and P. E. M. Siegbahn, Chem. Phys. **48**, 157 (1980).

[41] R. Krishnan, M. J. Frisch, and J. A. Pople, J. Chem. Phys. **72**, 4244 (1980).

[42] G. D. Purvis and R. J. Bartlett, J. Chem. Phys. **76**, 1910 (1982).

[43] V. R. Saunders and J. H. van Lenthe, Mol. Phys. **48**, 923 (1983).

[44] D. P. Chong and S. R. Langhoff, J. Chem. Phys. **84**, 5606 (1986).

[45] Y. S. Lee, S. A. Kucharski, and R. J. Bartlett, J. Chem. Phys. **81**, 5906 (1984).

[46] R. S. Grev and H. F. Schaefer, J. Chem. Phys. **80**, 3552 (1984).

[47] M. J. Frisch, A. C. Scheiner, H. F. Schaefer, and J. S. Binkley, J. Chem. Phys. **82**, 4194 (1985).

[48] J. A. Pople, J. S. Binkley, and R. Seeger, Int. J. Quantum Chem. Symp. **10**, 1 (1976); J. A. Pople, M. H. Gordon, and K. Raghavachari, submitted to J. Chem. Phys.

[49] J. F. Gaw and N. C. Handy, "Derivatives of the Potential Energy Hypersurface by Analytic Techniques", in *Annual Reports C, The Royal Society of Chemistry*, (London, 1984), pp. 291-323; H. F. Schaefer and Y. Yamaguchi, J. Mol. Struct. (Theochem) **135**, 369 (1986).

[50] P. Jørgensen and J. Simons, *Second Quantization-Based Methods in Quantum Chemistry* (Academic, New York, 1981) pp. 1-13.

[51] F. Coester, Nucl. Phys. **7**, 421 (1958); F. Coester and H. Kümmel, Nucl. Phys. **17**, 477 (1960); H. Kümmel, Nucl. Phys. **22**, 177 (1961).

[52] J. Cizek and J. Paldus, Int. J. Quantum Chem. **5**, 359 (1971).

[53] J. Paldus, J. Cizek, and I. Shavitt, Phys. Rev. A **5**, 50 (1972).

[54] J. Paldus and J. Cizek, Adv. Quantum Chem. **9**, 105 (1975).

[55] R. F. Bishop and H. G. Kümmel, Physics Today, March, 1987, pp. 52-60.

[56] A. C. Hurley, *Electron Correlation in Small Molecules*, (Academic, London, 1976); P. R. Taylor, G. B. Backsay, N. S. Hush, and A. C. Hurley, J. Chem. Phys.

69, 1971 (1977).

[57] F. E. Harris, Int. J. Quantum Chem Symp. **11**, 403 (1977); F. E. Harris, *Electrons in Finite and Infinite Structures*, edited by P. Phariseau and L. Scheive (Plenum, New York, 1977).

[58] H. J. Monkhorst, Int. J. Quantum Chem., Symp. **11**, 421 (1977).

[59] J. A. Pople, R. Krishnan, H. B. Schlegel, and J. S. Binkley, Int. J. Quantum Chem. **14**, 545 (1978).

[60] I. Lindgren, Int. J. Quantum Chem. Symp. **12**, 33 (1978).

[61] J. Paldus, J. Cizek, M. Saute, and L. Laforgue, Phys. Rev. A **17**, 805 (1978); M. Saute, J. Paldus, and J. Cizek, Int. J. Quantum Chem. **15**, 463 (1979).

[62] H. Nakatsuki, Chem. Phys. Lett. **59**, 362 (1978); *ibid* **67**, 329 (1979).

[63] D. Mukherjee and P. K. Mukherjee, Chem. Phys. **39**, 325 (1979).

[64] H. Reitz and W. Kutzelnigg, Chem. Phys. Lett. **66**, 111 (1979); W. Kutzelnigg, J. Chem. Phys. **77** 3081 (1981); *ibid* **80**, 822 (1984).

[65] R. A. Chiles and C. E. Dykstra, J. Chem. Phys. **74**, 4544 (1981); C. E. Dykstra, Chem. Phys. Lett. **88**, 202 (1982); P. G. Jasien and C. E. Dykstra, Int. J. Quantum Chem., Symp. **17**, 289 (1983).

[66] A. Banerjee and J. Simons, Int. J. Quantum Chem. **19**, 207 (1981).

[67] R. J. Bartlett, Annu. Rev. Phys. Chem. **32**, 359 (1981).

[68] J. Paldus, in *New Horizons of Quantum Chemistry*, edited by P. O. Löwdin and B. Pullman (Reidel, Dodrecht, 1983) pp. 31-60.

[69] G. D. Purvis, R. Sheppard, F. B. Brown, and R. J. Bartlett, Int. J. Quantum Chem. **23**, 835 (1983).

[70] R. J. Bartlett, C. E. Dykstra and J. Paldus, in *Advanced Theories and Computational Approaches to the Electronic Structure of Molecules*, edited by C. E. Dykstra (Reidel, Dodrecht, 1984) pp. 127-159.

[71] A. Hague and D. Mukherjee, J. Chem. Phys. **80**, 5058 (1984).

[72] M. Urban, J. Noga, S. J. Cole, and R. J. Bartlett, J. Chem. Phys. **83**, 4041 (1985).

[73] W. D. Laidig, G. D. Purvis, and R. J. Bartlett, J. Phys. Chem. **89**, 2161 (1985).

[74] S. J. Cole, G. D. Purvis, and R. J. Bartlett, Chem. Phys. Lett. **113**, 271 (1985).

[75] M. R. Hoffmann and H. F. Schaefer, J. Chem. Phys. **83**, 703 (1985).

[76] J. Geertsen and J. Oddershede, J. Chem. Phys. **85**, 2112 (1986).

[77] A. Haque and U. Kaldor, Int. J. Quantum Chem. **29**, 425 (1986).

[78] G. Fitzgerald, S. J. Cole, and R. J. Bartlett, J. Chem. Phys. **85**, 1701 (1986).

[79] M. Urban, V. Kello, I. Cernusak, J. Noga, and G. H. F. Dierksen, Chem. Phys. Lett., *in press*.

[80] S. J. Cole and R. J. Bartlett, J. Chem. Phys. **86**, 873 (1987).

[81] N. H. March, W. H. Young, and S. Sampanthar, *The Many Body Problem in Quantum Mechanics* (Cambridge, London, 1967).

[82] R. J. Bartlett and I. Shavitt, Int. J. Quantum Chem. Symp. **11**, 165 (1977); R. J. Bartlett and G. D. Purvis, Ann. N. Y. Acad. Sci. **367**, 62 (1981).

[83] R. Ahlrichs, Theor. Chim. Acta **35**, 59 (1974).

[84] F. Keil and R. Ahlrichs J. Am. Chem. Soc. **98**, 4787 (1976).

[85] E. R. Davidson, in *The World of Quantum Chemistry*, edited by R. Daudel and B. Pullman (Reidel, Dodrecht, 1974), pp. 17-30.

[86] J. Paldus, in *The Unitary Group*, Lecture Notes in Chemistry 22, eidted by J. Hinze (Springer, Berlin, 1981), pp. 1-50.

[87] P. Pulay and S. Saebo, J. Chem. Phys. **81**, 1904 (1984).

[88] C. W. Bauschlicher, S. R. Langhoff, P. R. Taylor, and H. Partridge, Chem. Phys. Lett. **126**, 436 (1986).

[89] R. J. Harrison and N. C. Handy, Chem. Phys. Lett. **95**, 386 (1983).

[90] P. Saxe, D. J. Fox, H. F. Schaefer, and N. C. Handy, J. Chem. Phys. **77**, 5584 (1982).

[91] R. B. Remington and H. F. Schaefer, unpublished work on H_2O, H_3O^+, $H_5O_2^+$, $H_7O_3^+$, and $H_9O_4^+$. Presented at the American Chemical Society National Meeting, Miami Beach, May 1, 1985; Symposium on Gas Phase Ions, Abstract #103, Division of Physical Chemistry.

[92] C. R. Moylan and J. I. Brauman, Annu. Rev. Phys. Chem. **34**, 187 (1983).

[93] A. J. Cunningham, J. D. Payzant, and P. Kebarle, J. Am. Chem. Soc. **94**, 7627 (1972).

[94] T. J. Lee, N. C. Handy, J. E. Rice, A. C. Scheiner, and H. F. Schaefer, J. Chem. Phys. **85**, 3930 (1986).

[95] T. Curtius, A. Darapsky, and F. Muller, Chem. Ber. **40**, 84 (1907).

[96] J. Koenigsberger and K. Vogt, Phys. Z. **14**, 1269 (1913).

[97] S. F. Mason, J. Chem. Soc., 1263 (1959).

[98] G. H. Spencer, Jr., P. C. Cross, and K. B. Wiberg, J. Chem. Phys. **35**, 1925 (1961); **35**, 1939 (1961).

[99] V. I. Berezin, Opt. Spectry. (USSR) (English Transl.) **16**, 131 (1964); **16**, 167 (1964).

[100] K. K. Innes, J. P. Byrne, and I. G. Ross, J. Mol. Spectrosc. **22**, 125 (1967).

[101] L. A. Franks, A. J. Merer, and K. K. Innes, J. Mol. Spectrosc. **26**, 458 (1968).

[102] K. K. Innes, L. A. Franks, A. J. Merer, G. K. Vemulapalli, T. Cassen, and J. Lowry, J. Mol. Spectrosc. **66**, 465 (1977).

[103] D. V. Brumbaugh and K. K. Innes, Chem. Phys. **59**, 413 (1981).

[104] D. V. Brumbaugh, C. A. Haynam, and D. H. Levy, J. Mol. Spectrosc. **94**, 316 (1982).

[105] K. B. Thakur, V. A. Job, and V. B. Kartha, J. Mol. Spectrosc. **107**, 373 (1984); **112**, 340 (1985).

[106] S. F. Mason, J. Chem. Soc., 1269 (1959).

[107] A. J. Merer and K. K Innes, Proc. R. Soc. London, Ser. A **302**, 271 (1968).

[108] J. M. Brown, Can. J. Phys. **47**, 233 (1969).

[109] K. K. Innes, A. Y. Khan, and D. T. Livak, J. Mol. Spectrosc. **40**, 177 (1971).

[110] K. K. Innes, A. H. Kalantar, A. Y. Khan, and T. J. Durnick, J. Mol. Spectrosc. **43**, 477 (1972).

[111] J. H. Meyling, R. P. van der Werf, and D. E. Wiersma, Chem. Phys. Lett. **28**, 364 (1974).

[112] R. E. Smalley, L. Wharton, D. H. Levy, and D. W. Chandler, J. Mol. Spectrosc. **66**, 375 (1977).

[113] V. A. Job and K. K. Innes, J. Mol. Spectrosc. **71**, 299 (1978).

[114] K. K. Innes, D. V. Brumbaugh, and L. A. Franks, Chem. Phys. **59**, 439 (1981).

[115] D. T. Livak and K. K. Innes, J. Mol. Spectrosc. **39**, 115 (1971).

[116] M. Chowdhury and L. Goodman, J. Chem. Phys. **36**, 548 (1962).

[117] M. Chowdhury and L. Goodman, J. Chem. Phys. **38**, 2979 (1963).

[118] G. K. Vemulapalli and T. Cassen, J. Chem. Phys. **56**, 5120 (1972).

[119] J. R. McDonald and L. E. Brus, J. Chem. Phys. **59**, 4966 (1973).

[120] R. M. Hochstrasser and D. S. King, Chem. Phys. **5**, 439 (1974).

[121] R. M. Hochstrasser and D. S. King, J. Am. Chem. Soc. **97**, 4760 (1975).

[122] R. R. Karl, Jr. and K. K. Innes, Chem. Phys Lett. **36**, 275 (1975).

[123] R. M. Hochstrasser and D. S. King, J. Am. Chem. Soc. **98**, 5443 (1976).

[124] B. Dellinger, D. S. King, R. M. Hochstrasser, and A. B. Smith, J. Am. Chem. Soc. **99**, 7138 (1977).

[125] D. S. King, C. T. Denny, R. M. Hochstrasser, and A. B. Smith, J. Am. Chem. Soc. **99**, 271 (1977).

[126] R. M. Hochstrasser, D. S. King, and A. B. Smith, J. Am. Chem. Soc. **99**, 3923 (1977).

[127] D. Coulter, D. Dows, H. Reisler, and C. Wittig, Chem. Phys. **32**, 429 (1978).

[128] D. M. Burland, F. Carmona, and J. Pacansky, Chem. Phys. Lett. **56**, 221 (1978).

[129] J. H. Glownia and S. J. Riley, Chem. Phys. Lett. **71**, 429 (1980).

[130] P. F. Barbara, L. E. Brus, and P. M. Rentzepis, Chem. Phys. Lett. **69**, 447 (1980).

[131] T. J. Aartsma, W. H. Hesselink, and D. A. Wiersma, Chem. Phys. Lett. **71**, 424 (1980).

[132] M. Paczkowski, R. Pierce, A. B. Smith, and R. M. Hochstrasser, Chem. Phys. Lett. **72**, 5 (1980).

[133] A. Kiermeier, K. Dietrich, E. Riedle, and H. J. Neusser, J. Chem. Phys. **85**, 6983 (1986).

[134] R. E. Smalley, L. Wharton, D. H. Levy, and D. W. Chandler, J. Chem. Phys. **68**, 2487 (1978).

[135] D. V. Brumbaugh, J. E. Kenny, and D. H. Levy, J. Chem. Phys. **78**, 3415 (1983).

[136] J. J. F. Ramakers, H. K. van Dijk, J. Langelaar, and R. P. H. Rettschnick, Faraday Discuss. Chem. Soc. **75**, 183 (1983).

[137] C. A. Haynam, D. V. Brumbaugh, and D. H. Levy, J. Chem. Phys. **79**, 1581 (1983).

[138] L. Young, C. A. Haynam, and D. H. Levy, J. Chem. Phys. **79**, 1592 (1983).

[139] C. A. Haynam, D. V. Brumbaugh, and D. H. Levy, J. Chem. Phys. **80**, 2256 (1984).

[140] C. A. Haynam and D. H. Levy, J. Phys. Chem. **87**, 2091 (1983).

[141] C. A. Haynam, D. V. Brumbaugh, and D. H. Levy, J. Chem. Phys. **81**, 2270 (1984); **81**, 2282 (1984).

[142] L. Paoloni, J. Chem. Phys. **25**, 1277 (1956).

[143] N. Mataga, Bull. Chem. Soc. Jpn. **31** 453 (1958).

[144] R. L. Flurry, Jr., E. W. Stout, and J. J. Bell, Theor. Chim. Acta **8**, 203 (1967).

[145] G. W. Pukanic, D. R. Forshey, J. D. Wegener, and J. B. Greenshields, Theor. Chim. Acta **10**, 240 (1968).

[146] M. Sundbom, Acta Chem. Scand. **25** 487 (1971).

[147] J. Ridley and M. Zerner, Theor. Chim. Acta **32**, 111 (1973).

[148] M. J. S. Dewar, Pure Appl. Chem. **44**, 767 (1975).

[149] J. Almlöf, B. Roos, U. Wahlgren, and H. Johansen, J. Elec. Spect. Rel. Phen. **2**, 51 (1973).

[150] M. H. Palmer, A. J. Gaskell, R. H. Findlay, J. Chem. Soc. Perkin Trans. 2 **7**, 778 (1974).

[151] T. K. Ha, Mol. Phys. **29**, 1829 (1975).

[152] H. Ito and Y. J. I'Haya, Bull Chem. Soc. Jpn. **49**, 940 (1976).

[153] J. Leclercq, P. Yvan, and J. M. Leclercq, Chem. Phys. **22**, 233 (1977).

[154] W. von Niessen, W. P. Kraemer, and G. H. F. Diercksen, Chem. Phys. **41**, 113 (1979).

[155] B. Dick and B. Nickel, Chem. Phys. **78**, 1 (1983).

[156] E. W. Knight and C. S. Parmenter, Chem. Phys. **15**, 85 (1976).

[157] Y. Osamura, Y. Yamaguchi, P. Saxe, M. A. Vincent, J. F. Gaw, and H. F. Schaefer, Chem. Phys. **72**, 131 (1982).

[158] G. Fitzgerald and H. F. Schaefer, J. Chem. Phys. **83**, 1162 (1985).

[159] E. R. Davidson and L. Z. Stenkamp, Int. J. Quantum Chem., Symp. **10**, 21 (1976).

[160] E. B. Wilson, Phys. Rev. **43**, 760 (1934).

[161] S. Ghosh and M. Chowdhury, Chem. Phys. Lett. **85**, 233 (1982).

[162] M. M. Frank, W. J. Pietro, W. J. Hehre, J. S. Binkley, M. S. Gordon, D. J. Defrees, and J. A. Pople, J. Chem. Phys. **77**, 3654 (1982).

[163] Y. Yamaguchi and H. F. Schaefer, J. Chem. Phys. **73**, 2310 (1980).

[164] K. K. Innes, J. Chem. Phys. **76**, 2100 (1982).

[165] D. A. Clabo and H. F. Schaefer, private communication.

[166] For a detailed discussion of symmetry breaking see R. Murphy, H. F. Schaefer, R. H. Nobes, L. Radom, and R. M. Pitzer, Int. Rev. Phys. Chem., Vol. 5, Nos. 2 & 3, 229 (1986) and references cited therein.

[167] L. Engelbrecht and B. Liu, J. Chem. Phys. **78**, 3097 (1983).

[168] A. D. McLean, B. H. Lengsfield, J. Pacansky, and Y. Ellinger, J. Chem. Phys. **83**, 3567 (1985).

[169] See, for example, the HCNO results of A. Kormornicki, J. D. Goddard, and H. F. Schaefer, J. Am. Chem. Soc. **102**, 1763 (1980).

[170] W. D. Allen and H. F. Schaefer, J. Chem. Phys. **84**, 2212 (1986).

[171] Y. Osamura, and H. F. Schaefer, J. Chem. Phys. **74**, 4576 (1981); Y. Osamura, H. F. Schaefer, M. Dupuis, W. A. Lester, J. Chem. Phys. **75**, 5828 (1981); J. W. Hepburn, R. J. Buss, L. J. Butler, Y. T. Lee, J. Phys. Chem. **87**, 3638 (1983).

[172] R. B. Woodward and R. Hoffmann, *The Conservation of Orbital Symmetry* (Academic, New York, 1970).

[173] P. Pulay, in *Applications of Electronic Structure Theory*, edited by H. F. Schaefer (Plenum, New York, 1977) Vol. 4, pp. 153-185.

[174] B. R. Brooks, W. D. Laidig, P. Saxe, J. D. Goddard, Y. Yamaguchi, and H. F. Schaefer, J. Chem. Phys. **72**, 4652 (1980).

[175] R. Krishnan, H. B. Schlegel, and J. A. Pople, J. Chem. Phys. **72**, 4654 (1980).

[176] Y. Osamura, Y. Yamaguchi, and H. F. Schaefer, J. Chem. Phys. **77**, 383 (1982).

[177] J. E. Rice, R. D. Amos, N. C. Handy, T. J. Lee, and H. F. Schaefer, J. Chem. Phys. **85**, 963 (1986).

[178] S. Kato and K. Morokuma, Chem. Phys. Lett. **65**, 19 (1979).

[179] J. D. Goddard, N. C Handy, and H. F. Schaefer, J. Chem. Phys. **71**, 1525 (1979).

[180] H. B. Schlegel and M. A. Robb, Chem Phys. Lett. **92**, 43 (1982).

[181] P. J. Knowles, G. J. Sexton, and N. C. Handy, Chem. Phys. **72**, 337 (1982).

[182] P. R. Taylor, J. Comput. Chem. **5**, 589 (1984).

[183] M. Page, P. Saxe, G. F. Adams, and B. H. Lengsfield, J. Chem. Phys. **81**, 434 (1984).

[184] T. J. Lee, W. D. Allen, and H. F. Schaefer, submitted to J. Chem. Phys.

[185] J. A. Pople, R. Krishnan, H. B. Schlegel, and J. S. Binkley, Int. J. Quantum Chem., Symp. **13**, 225 (1979).

[186] G. Fitzgerald, R. J. Harrison, W. D. Laidig, and R. J. Bartlett, J. Chem. Phys. **82**, 4379 (1985).

[187] P. Jørgensen and J. Simons, J. Chem. Phys. **79**, 334 (1983).

[188] L. Adamowicz, W. D. Laidig, and R. J. Bartlett, Int. J. Quantum Chem., Symp. **18**, 245 (1984).

[189] N. C. Handy and H. F. Schaefer, J. Chem. Phys. **81**, 5031 (1984).

[190] G. Fitzgerald, R. J. Harrison, W. D. Laidig, and R. J. Bartlett, Chem. Phys. Lett. **117**, 433 (1985).

[191] R. J. Bartlett, in *Geometrical Derivatives of Energy Surfaces and Molecular Properties*, edited by P. Jørgensen and J. Simons (Reidel, Dodrecht, 1986) pp. 35-61.

[192] G. Fitzgerald, R. J. Harrison, and R. J. Bartlett, J. Chem. Phys. **85**, 5143 (1986).

[193] P. Pulay, J. Mol. Struct. (Theochem) **103**, 57 (1983).

[194] J. E. Rice and R. D. Amos, Chem. Phys. Lett. **122**, 585 (1986).

[195] P. Pulay, Chem Phys. Lett. **73**, 393 (1980).

[196] J. Gerratt and I. M. Mills, J. Chem. Phys. **49**, 1719 (1968).

[197] B. H. Lengsfield, S. Havriliak, M. E. Colvin, and H. F. Schaefer, Chem. Phys. Lett. **135**, 340 (1987).

[198] A. R. Hoy, I. M. Mills, and G. Strey, Mol. Phys. **24**, 1265 (1972).

[199] M. G. Bucknell and N. C. Handy, Mol. Phys. **28**, 777 (1974).

[200] B. A. Ziles and W. B. Person, J. Chem. Phys. **79**, 65 (1983).

[201] S. A. Clough, Y. Beers, G. P. Klein, and L. S. Rothman, J. Chem. Phys. **59**, 2254 (1973).

[202] D. J. Swanton, G. B. Bacskay, and N. S. Hush, J. Chem. Phys. **84**, 5715 (1986).

[203] T. J. Lee, R. B. Remington, Y. Yamaguchi, and H. F. Schaefer, in preparation.

[204] K. Yamada, T. Nakagawa, K. Kuchitsu, and Y. Morino, J. Mol. Spectrosc. **38**, 70 (1971).

[205] J. L. Duncan and P. D. Mallinson, Chem. Phys. Lett. **23**, 597 (1973).

[206] T. Nakanaga, S. Kondo, and S. Saeki, J. Chem. Phys. **76**, 3860 (1982).

[207] R. D. Nelson, D. R. Lide, and A. A. Maryott, *Selected Values of Electric Dipole Moments for Molecules in the Gas Phase*, U. S. National Bureau of Standards, Washington D. C., 1967.

[208] W. D. Laidig and R. J. Bartlett, Chem. Phys. Lett. **104**, 424 (1984).

[209] W. D. Laidig, P. Saxe, and R. J. Bartlett, J. Chem. Phys. **86**, 887 (1987).

[210] S. Pal, M. Rittby, R. J. Bartlett, D. Sinha, and D. Mukherjee, submitted to Chem. Phys. Lett.

[211] M. R. Hoffmann and J. Simons, submitted to J. Chem. Phys.

LAWRENCE BERKELEY LABORATORY
TECHNICAL INFORMATION DEPARTMENT
UNIVERSITY OF CALIFORNIA
BERKELEY, CALIFORNIA 94720